ABSTRACT

STUDY OF CONTROLLED RELEASE OF ACTIVE PHARMACEUTICAL INGREDIENTS FROM FUNCTIONALIZED NANOCLAYS AND POLYMER MATRICES

by
Jin Uk Ha

This dissertation contains the results of three related novel investigations in the field of structure-property-processing relationships of pharmaceutical polymer-based products. They are: a) modification of a pharmaceutical anionic nanoclay with two different Active Pharmaceutical Ingredients (APIs) to produce nanohybrid API carriers intended to be used alone or in acrylic polymer matrices, b) comparison of binary systems containing the above APIs in the selected acrylic polymers in terms of their miscibilities with the polymer, but in the absence of nanoclay, and c) comparison of the polymer/API binary systems with ternary polymer/API/Clay systems.

For the first study, the calcination method which can be directly applied to carbonated hydrotalcite was used and successfully achieved API intercalations. During reconsitution of the clay, the crystalline APIs in the clay interlayer was apparently transformed in an amorphous state, and as a result it showed increased apparent solubility in the simulated body fluids.

The second study dealt with API-polymer miscible or immiscible systems prepared by different mixing methods. The selected APIs have low solubility at the low pH of the aqueous medium and different solubility parameters by comparison with the polymer. The Eudragit® E100/ DIK-Na^+ mixture produced by batch melt mixing showed an API solid dispersion whereas the Eudragit® E100/ IND system produced an API solid solution. These different morphologies were anticipated by calculating API and polymer

solubility parameters and were confirmed by several analytical methods. The miscible API-polymer system showed better apparent solubility in the aqueous media. In order to confirm the effect on apparent solubility of the different API physical states differing in particle size or crystallinity, solvent casting and twin screw extruder mixing were also compared with batch mixing. The amorphous API in the polymer matrix showed improved apparent solubility as compared to its crystalline state. This confirmed that the state of API in the polymer matrix is the most important factor to increase its apparent aqueous solubility.

The third segment of this research focused on the API release from the ternary system (API/clay/polymer) produced by hot melt mixing. A novel approach in order to have a sustained API release by utilizing the nanoclays was attempted. Since the API present in the clay interspacing may experience one more step in its release by diffusion as compared to the binary system, the API from the ternary system showed a slower and more controlled release than the one from the binary system. Controlled API release from such a ternary system produced by hot melt mixing, to the best of our knowledge, has not been reported in the literature.

The mechanisms of APIs release in solution from the aforementioned systems were identified by using the Korsmeyer-Peppas (Power law) and Peppas-Sahlin models.

STUDY OF CONTROLLED RELEASE OF ACTIVE PHARMACEUTICAL INGREDIENTS FROM FUNCTIONALIZED NANOCLAYS AND POLYMER MATRICES

by
Jin Uk Ha

A Dissertation
Submitted to the Faculty of
New Jersey Institute of Technology
In Partial Fulfillment of the Requirements for the Degree of
Doctor of Philosophy in Chemical Engineering

Otto H. York Department of
Chemical, Biological and Pharmaceutical Engineering

January 2011

APPROVAL PAGE

STUDY OF CONTROLLED RELEASE OF ACTIVE PHARMACEUTICAL INGREDIENTS FROM FUNCTIONALIZED NANOCLAYS AND POLYMER MATRICES

Jin Uk Ha

Dr. Marino Xanthos, Dissertation Advisor — Date
Professor of Chemical, Biological and Pharmaceutical Engineering, NJIT

Dr. Costas G. Gogos, Committee Member — Date
Distinguished Research Professor of Chemical, Biological and Pharmaceutical Engineering, NJIT

Dr. Boris Khusid, Committee Member — Date
Professor of Chemical, Biological and Pharmaceutical Engineering, NJIT

Dr. Laurent Simon, Committee Member — Date
Associate Professor of Chemical, Biological and Pharmaceutical Engineering, NJIT

Dr. Ecevit A. Bilgili, Committee Member — Date
Assistant Professor of Chemical, Biological and Pharmaceutical Engineering, NJIT

Dr. Kun Sup Hyun, Committee Member — Date
Research Professor of Chemical, Biological and Pharmaceutical Engineering, NJIT

Dr. Michael C. Y. Huang, Committee Member — Date
Principal Scientist, Pfizer, Pearl River, NY

Dr. Peng Wang, Committee Member — Date
Assistant Professor of Chemical Engineering and Department of Biomedical and Pharmaceutical Sciences, University of Rhode Island, RI

BIOGRAPHICAL SKETCH

Author: Jin Uk Ha

Degree: Doctor of Philosophy

Date: January 2011

Undergraduate and Graduate Education:

- Doctor of Philosophy in Chemical Engineering,
  New Jersey Institute of Technology, Newark, NJ, 2011

- Master of Science in Chemical Engineering,
  New Jersey Institute of Technology, Newark, NJ, 2007

- Bachelor of Science in Chemical Engineering,
  Inha University, Incheon, Republic of Korea, 2004

Major: Chemical Engineering

Book Chapter:
Xanthos, M. and Ha, J. U. "Clays Modified with Thermally Stable Ionic Liquids with Applications in Thermoplastic Nanocomposites" Chapter 6 in Mittal V. ed., *Thermally stable and flame retardant polymer nanocomposites*, Cambridge University Press, UK (*In Press*) Submitted on May 2010.

Publications:

Ha, J. U.; Xanthos, M., Sequential Modification of Cationic and Anionc Nanoclay with Ionic Liquids, *Green Chemistry letters and reviews*, 2010 *In press.* Approved on Aug 2010.

Ha, J. U.; Xanthos, M., "Studies on Novel Anionic/Cationic Modified Nanoclays and their Effects on the Properties of the Polylactic Acid Composites", *Applied Clay Science*, 2010, **27**, 303-310.

Park, K. I.; Ha, J. U.; Xanthos, M., "Ionic Liquids as Plasticizers/Lubricants for Polylactic Acid" *Polymer Engineering and Science*, 2010, **50**, 1105-1110.

Ha, J. U.; Xanthos, M., "Functionalization of Nanoclays with Ionic Liquids for Polypropylene Composites" *Polymer Composites,* 2008, **30** 534 - 542.

Ha, J. U.; Kim M.; Lee, J.; Choe, S.; Cheong, I. W.; Shim, S. E., "A Novel Synthesis of Polymer Brush on Multiwall Carbon Nanotubes Bearing Terminal Monomeric Unit" *J. Polym. Sci. A: Polym. Chem,* 2006, ***44***, 6394-6401.

Lee, J.; Ha, J. U.; Choe, S.; Lee C. S.; Shim S. E., "Synthesis of Highly Monodisperse Polystyrene Microspheres via Dispersion Polymerization using an Amphoteric Initiator" *J. Colloid Interface Sci.,* 2006, ***298***, 663-671.

Presentations:

Ha, J. U.; Xanthos, M. "Melt Mixing Studies of Miscible and Immiscible Drug-Polymer Systems", Proc. Polymer Processing Society *PPS-26* conf., Banff, Canada July 2010.

Yoon, H.; Ha, J. U.; Xanthos, M.; Yamaguchi, M. "Nanofillers Transfer between Sheets of Immiscible Polymers", Proc. Polymer Processing Society *PPS-26* conf., Banff, Canada, July 2010.

Ha, J. U.; Xanthos, M. "Novel Delivery Systems by Melt Compounding Polymers with Drug Functionalized Nanoclays", Proc Society of Plastics Engineers (SPE) *ANTEC 2010*, Orlando FL, May 2010.

Ha, J. U.; Xanthos, M. "Nevel Drug Delivery Method by utilizing API Functionalized Nanoclay.", *The 19th KSEA Northeast Regional Conference 2010*, Somerset, NJ.

Xanthos, M.; Ha, J. U.; Zhou, Q. "Nanoclays and Polmyer Nanocomposites for Biomedical and Pharmaceutical Applications", *Advanced Technologies for New Materials, Mold Design/Analysis, Molding Process, Equipment and Inspection 2009 Workshop*, Chung Yuan University, Taiwan, July 2009.

Ha, J. U.; Xanthos, M., "Polylactic Acid Composites based on Ionic Liquid Modified Cationic and Anionic Clay", Proc Society of Plastics Engineers (SPE) *ANTEC 2009*, Chicago, IL.

Ha, J. U.; Xanthos, M., "Nanoclay Modification with Thermally Stable Ionic Liquids for PP", *The 18th KSEA Northeast Regional Conference 2009*, Somerset, NJ.

Ha, J. U.; Xanthos, M., "The Study of Polymer Nannocomposites Functionalized by Phosphonium based Ionic Liquids", *UKC 2008*, San Diego, CA.

Ha, J. U.; Xanthos, M., "UV Curable Top Coat System for Depot and in-field Repair Use" *US Corrosion Summits 2008*, Clearwater, FL.

Xanthos, M.; Kim, N. H.; Ha, J. U.; Malhotra, S. V., "Nanocomposites based on Ionic Liquids Modified Clays" Proc Society of Plastics Engineers (SPE) *ANTEC 2007*, Cincinnati, OH.
Ha, J. U.; Xanthos, M., "Functionalization of Nanoclays through Ionic Liquid Exchange Reactions" *Polymer Nanocomposites Conference 2007*, Lehigh University, PA.

Patent Application:

Ha, J. U.; Kim M.; Lee, J.; Choe, S.; Cheong, I. W.; Shim, S. E., "Synthesis of Vinyl Group Carrying Reactive Multiwall Carbon Nanotubes for Development of CNT/ Polymer Nanocomposites" *Korean Patent* No. 10-0689866 (2007).

"But he knows the way that I take; when he has tested me, I will come forth as gold"
Job 23:10

ACKNOWLEDGMENTS

First and foremost, I wish to express my deepest appreciation to my advisor, Professor Marino Xanthos, not only for his professional advice but also his encouragement, patience and support throughout this research. He gave me many opportunities to learn and strengthen my background in polymer science. I also would like to thank him for the many hours spent in revising my dissertation and the lessons for the wisdom of life. It was a great honor to have him as my advisor.

I would like to thank Professor Costas G. Gogos, not only for his novel advice and encouragement but also for timely financial support when I did not have research fund.

I would like to thank my committee members Professor Boris Khusid, Professor Laurent Simon, Professor Kun Sup Hyun, Professor Ecevit A. Bilgili, Dr.Michael C. Y. Huang and Professor Peng Wang for providing me insightful comments and their priceless support.

I would also like to thank the staff of the Polymer Processing Institute (PPI), Newark, NJ for providing a friendly and productive environment. Their invaluable cooperation and advice is greatly appreciated.

In addition, I would like to thank Dr. Huiju Liu of NJIT, Dr. Kuan Yin Lin, and Dr. John H. Suwardie of PPI, for providing me valuable advice.

I would like to thanks Mr. Qian Zheng, Ms. Min Yang and Dr. Kwang Seok Kim for particle size analysis and dissolution fitting analysis. Also, Mr. Young Gil Yoon of KIST, Republic of Korea, for providing SEM images of modified nanoclays. I would like to thank Mr. Byung Soo Ham of Texas A&M for his help with my literature searches.

I would like to express my gratitude to Professor Sang Eun Shim of Inha University in Incheon, S. Korea, for his encouragement during difficult times.

Lastly, I take this opportunity to sincerely thank my parents (Sung Gi Ha and Ok Hwa Ahn) and parents-in-law (Ik Tae Kim and Jung Hee Oh), my beloved daughters, Noel Songju, and Nadia Hyoju and my companion for life, Hee Jun Kim for their patience, understanding and endless support.

TABLE OF CONTENTS

TABLE OF CONTENTS
(Continued)

Chapter **Page**

TABLE OF CONTENTS
(Continued)

Chapter **Page**

TABLE OF CONTENTS
(Continued)

TABLE OF CONTENTS
(Continued)

Chapter **Page**

TABLE OF CONTENTS
(Continued)

Chapter **Page**

TABLE OF CONTENTS
(Continued)

Chapter **Page**

LIST OF TABLES

LIST OF FIGURES

LIST OF FIGURES
(Continued)

Figure **Page**

LIST OF FIGURES
(Continued)

Figure **Page**

LIST OF FIGURES
(Continued)

Figure **Page**

LIST OF FIGURES
(Continued)

Figure **Page**

LIST OF FIGURES
(Continued)

Figure **Page**

LIST OF FIGURES
(Continued)

Figure **Page**

LIST OF FIGURES
(Continued)

Figure **Page**

LIST OF ACRONYMS

API	Active pharmaceutical ingredient
CHT	Calcined hydrotalcites
DIK/Clay	Calcined hydrotalcite modified with diclofenac sodium
DIK-Na^+	Diclofenac sodium
DSC	Differential scanning calorimetry
EDX	Energy dispersive X-ray analysis
Eudragit ®E100	Butyl/ methyl methacrylate-dimethylaminoethyl methacrylate terpolymer (1:1:2)
Eudragit® E100/ DIK-Na^+	Eudragit® E100 mixed with diclofenac sodium
Eudragit® E100- DIK/Clay	Eudragit® E100 mixed with DIK/Clay
Eudragit® E100/ IND	Eudragit® E100 mixed with indomethacin
Eudragit® E100- IND/Clay	Eudragit® E100 mixed with IND/Clay
Eudragit® S100	Methacrylic acid-methyl methacrylate (1:2) copolymer
Eudragit® S100/TEC	Eudragit® S100 premixed with triethyl citrate
Eudragit® S100/TEC/DIK-Na^+	Eudragit® S100/TEC mixed with diclofenac sodium
Eudragit® S100/TEC-DIK/Clay	Eudragit® S100/TEC mixed with DIK/Clay
FTIR	Fourier transform infrared spectroscopy
HT	Hydrotalcite
IND	Indomethacin
IND/Clay	Calcined hydrotalcite modified with indomethacin

LDH	Layered double hydroxides
MMT	Montmorillonite
MW	Molecular weight
PLM	Polarized light microscopy
SEM	Scanning electron microscopy
TEC	Triethyl citrate
TGA	Thermogravimetric analysis
XRD	Wide-angle X-ray diffraction

CHAPTER 1

INTRODUCTION

One big challenge currently facing the pharmaceutical industry is that as many as 40% of new drug molecular entities have poor bioavailability, related to a large extent to their low aqueous solubility.[1-3] In addition to size reduction of the Active Pharmaceutical Ingredient (API) powders, a promising solution to this widespread issue is to mix the API with one or more highly aqueous soluble polymeric excipients using the novel Hot-Melt Extrusion process (HME). HME involves continuously mixing the APIs, commonly available in a crystalline form, with polymeric excipients by means of one or more rotating screws at elevated temperatures. Consequently, depending on the polymer and the API chemical structures, the API may be fully dissolved, or dispersed to very fine particle sizes in the polymer matrix, leading to a dramatically increased API dissolution rate in the body fluids.[1, 2] In contrast to traditional processes such as fluidized bed granulation, HME can significantly reduce the API size during mixing. HME also offers other advantages such as continuous processing, ease of automation and process control, better product consistency, and environmental friendliness by eliminating or minimizing solvent usage.

In addition to increased bioavailability of the API, controlled drug release is also a very important issue in the pharmaceutical industry. Since all drugs for oral administration need to get through the gastrointestinal tract this means that the drug may experience an acid environment for a few hours (1 ~ 2 hours) in the stomach, and a neutral pH in the small intestine (3~4 hours) and the large intestine for several hours (7~

10 hours). Therefore, delivering the drug to the target organ is not easily accomplished. In order to overcome this barrier, enteric polymer coated API is commonly used for transferring the drug into the intestinal tracts.[4, 5]

Nanoclays are well known as high performance functional fillers for polymers in order to increase their mechanical, thermal, and barrier properties.[6, 7] However, their broader applications in the pharmaceutical industry are less known. In addition to the therapeutic attributes of some unmodified nanoclays, their hybrids with ionic APIs that may be intercalated in the nanoclay interlayer space[8] in an amorphous state can also increase the apparent API solubility. As a result,[8-12] it is hypothesized that the addition of nanoclay platelets may improve the overall API stability by providing a tortuous path that would slow down the API's diffusion to the body fluids in the presence or absence of a polymeric excipient. The decrease of the API's mobility inside the polymeric excipient would also help to prevent or slow down the aggregation of the API molecules. Thus, the crystallization of the API molecules that may lead to their delayed dissolution could be minimized and the long term drug stability improved. It should be noted that hydrophilic polymers are, in general, chosen as excipients for the purpose of improving the APIs' dissolution rate. It folllows, then, that hydrophilic pharmaceutical nanoclays such as montmorillonite and hydrotalcite, would tend to disperse better in hydrophilic polymers due to their improved affinity. Among the primary objectives of this research is to increase the aqueous solubility of API released from immiscible API/polymer systems produced by melt mixing. Emphasis is placed on the role of nanoclays in such systems.

From a thermodynamic point of view, each substance has only one solubility value at a specific temperature, pressure and volume. This value is defined as the

saturated concentration of the substance in solution when it is in equilibrium with its most stable solid state structure. In this research, the term solubility is often used loosely to mean the metastable or kinetic solubility rather than the solubility at this thermodynamically stable state. In most cases, metastable apparent solubility decreases to the level of the true or thermodynamically stable solubility, after an infinite equilibrium time.

In this dissertation, three different types of binary and ternary drug delivery systems prepared by different methods are investigated and compared in order to address the aforementioned issues of solulibility and rates of API release.

In the first part of the dissertation on organic API-inorganic clay binary systems, named also hybrids, the fundamentals of intercalation of cationic API molecules of different sizes and chemical structures into the anionic nanoclay interlayer are investigated. In the absence of a polymer matrix, the nanoclay acts both as an API carrier and inorganic matrix. Intercalating API molecules into the interlayers of a nanoclay such as hydrotalcite is not an easy task,[13] unless a co-precipitation method is used for the preparation of the API/Clay complex. To the best of our knowledge, there are only few reports on the direct intercalation of the API molecules into the interlayer space of commercially available hydrotalcite by ion exchange methods. Thus, in this research, the experimental conditions for achieving intercalation of the API, preferably in its amorphous state, were firstly investigated with particular emphasis on possible physiochemical interactions between API and nanoclays that could adversely affect the functionality of the drug. API release from the clay/API hybrids in simulated gastric and

intestinal fluids was subsequently investigated in order to understand and identify potential pharmaceutical applications for sustained drug delivery.

In the second part of the dissertation on organic binary systems (API/polymer), different combinations of polymer matrices with miscible or immiscible APIs prepared from solution or melt mixing are compared. By calculating solubility parameters, the solubility of the API in polymer matrices of different chemical compositions can be predicted and subsequently confirmed, the differences in the properties between the miscible and immiscible systems are then examined, particularly, in terms of drug morphology and rate of API dissolution.

The third part of the dissertation refers to ternary systems containing components of parts one and two above, i.e. API intercalated anionic nanoclays (hybrids) dispersed in a polymer matrix. For drug delivery applications, polymer/API intercalated nanoclay composites are anticipated to have interesting advantages as compared to polymer/API systems. It may be possible to achieve more controllable API release pattern as compared to polymer/API systems since the ternary system involves one more additional step, which is the API release from the clay. Furthermore, the possibility of sustained drug release by utilizing an API intercalated nanoclay dispersed in the polymer matrix is investigated. In this particular system, API has to diffuse out from the nanoclay interlayer space through a more tortuous path length vs. the system where API is solely coated by the enteric polymer. Therefore, slower release of API from the hybrid complex is anticipated.

CHAPTER 2

LITERATURE SURVEY

2.1 API Solubilty/Miscibility Effects

It is recognized that amorphous APIs have improved rates of dissolution in biological fluids as compared to their different crystalline forms (e.g., polymorphs). Several studies reported the solubility advantage for amorphous drug forms. For example, Imaizumi[14] reported 1.6-fold increased amorphous indomethacin (IND) solubility as compared to its crystalline form, 2-fold for cefalexin,[15] 2.5-fold for tetracycline[16] and 10-fold for novobiocin acid.[17] Hancock and Park[18] studied the solubility of indomethacin in deionized water at different temperatures. Amorphous IND showed higher solubility than α or γ type IND. In general, miscible APIs and water soluble polymer systems used in pharmaceutical formulations are desirable since they lead to a fast API dissolution and higher apparent solubility.

By comparing the magnitude of the solubility parameter*s* (δ) of polymers and APIs defined by Equation 2.1:

$$\delta = \sqrt{\frac{E_{coh}}{V}} \qquad \text{(Equation 2.1)}$$

where E_{coh} is cohesive energy and V is molar volume for polymers and APIs, the miscibility of the system can be predicted. The closer the values of the solubility parameters of the polymer and the API, the higher the tendency to be miscible. Greenhalgh et al.[19] showed that molten systems with differences in solubility parameter $\Delta\delta$ ranging from 1.6 to 7.5 $MPa^{1/2}$are considered to be completely miscible; systems with

$\Delta\delta$ from 7.5 to 15.0 $MPa^{1/2}$ show some sign of immiscibility in the liquid state, whereas systems with $\Delta\delta$ above 15.9 $MPa^{1/2}$ exhibit total immiscibility over the entire composition range.

Table 2.1 shows that comparison of the solubility parameters of the polymers (Eudragit® E100 and S100) and APIs (DIK and IND) used in this research indicates three miscible pairs and one immiscible pair. The solubility parameter of a plasticizer (TEC) is also shown. All values were calculated by the Fedor's group contributions method.[20] The group contributions to cohesive energy and molar volume by this method are apparently less accurate than those of other methods such as Small's, Van Krevenlen's and Hoy's. However, Fedor's database contains a larger number of structural groups and could as a result be used for a variety of APIs and polymer systems.

Table 2.1 Solubility Parameters of the Materials used in this Study

Polymer/API	Eudragit® E100	Eudragit® S100	TEC	DIK	IND
Solubility parameter, δ ($MPa^{0.5}$)	19.7[21]	24.6*	26.3*	27.9[22]	24.5[21]

* calculated

In the following sections, literature data on methods that are used to improve drug aqueous solubility and bioavailability, and/or modify drug delivery are reviewed. The systems include:

1) Compounds of polymers with APIs prepared by melt mixing, including hot melt extrusion.[1, 2]

2) Compounds of inorganic particles with APIs (hybrids), including intercalated anionic and cationic clays.[8]

3) Compounds of polymers with API-intercalated clays

2.2. Polymer/API Compounds Prepared by Melt Mixing

2.2.1 Hot Melt Mixing Processing (HMMP)

Hot melt mixing processing (HMMP) is one of the most widely used mixing and forming techniques in the plastic industry. HMMP includes batch mixing, ram extrusion, and screw extrusion. HMMP, and in particular the continuous hot melt extrusion (HME), can offer many advantages to pharmaceutical manufacturing vs. batch mixing methods. For instance, molten polymers during melt mixing can function as thermal binders and act as drug depots and/or drug release retardants upon cooling and solidification. Furthermore, HME can reduce the number of processing steps and eliminate time-consuming drying steps since this technique does not require solvents and water. The intense mixing resulting from the rotating screw(s) causes de-aggregation of suspended particles in the molten polymer resulting in more uniform dispersion. Due to these advantages, the number of patents that have been issued on this topic has steadily increased since the 1980s.[3]

2.2.2 Polymer/API Compounds

Liu et al.[23] studied the effects of IND on the properties of an acrylic terpolymer (Eudragit® EPO) prepared by hot melt twin screw extrusion. The effects of three process parameters such as barrel temperature, screw rotating speed and residence time were systematically investigated. In order to fully dissolve in the polymer matrix and thus convert IND, into an amorphous state, long residence time, high temperature, and high screw rotating speed are preferable. The IND state in the polymer matrix was examined by DSC, XRD, polarized light microscopy and FTIR. Particularly, FTIR showed the

transition in the polymer matrix of the IND state from crystalline to amorphous. All the samples showed increased solubility up to around 90% in simulated gastric fluid. All samples showed reduced solubility after they reached a maximum solubility level. This phenomenon was responsible for the recrystallization of IND in the medium since its concentration in the medium was far beyond its saturation capacity.

Physico-mechanical property changes of biosoluble polymers, such as Eudragit® EPO, polyvinylpyrrolidone-vinyl acetate copolymer (PVP-VA), polyvinylpyrrolidone K30 (PVPK30), and poloxamer 188NF (P188), compounded with IND were studied by Chokshi et al.[21] The formations of solid solutions and solid dispersions which indicate miscible one-phase and immiscible two-phase systems, respectively, were predetermined by calculating solubility parameters. The differences between these systems were analyzed by observing thermal property and viscosity changes. EPO mixed with IND produced a miscible system. The T_g of these blends increased with increasing IND loading (loaded amounts were 30, 50, and 70%) and the authors ascribed these changes to the antiplasticization effect of the system. The zero-shear rate viscosity of the system decreased with increasing IND loading due to the solubilization effect of the API in the polymer. The viscosity of the immiscible API/polymer system (IND and P188) tended to increase with increasing IND loading. However, other researchers showed that the T_g of these blends can be decreased at low amounts of IND loading.[24]

Forster et al.[25] studied water insoluble APIs (indomethacin, lacidpine, and tolbutamide) blended with hydrophilic amorphous polymers (polyvinylpyrrolidone and polyvinylpyrrolidone-co-vinyl acetate) by hot melt extrusion. They assumed that amorphous solid dispersion in the polymer matrices is an effective way of increasing the

dissolution rate of these APIs. The extrudates were compared with physical mixtures of API and polymer. XRD results of both APIs and their physical mixtures indicated crystallinity. However, extrusion compounded API-polymers did not show any peaks, which suggests an amorphous state for the API. Similarly, DSC results of extrusion compounded samples did not show any melting temperatures for the APIs. FTIR data showed some degree of hydrogen bonding between drugs and polymers produced by melt mixing suggesting strong interactions. Physical stability of the samples was related to moisture content and glass transition temperature.

Nollenberger et al.[26] reported that addition of felodipine in the Eudragit® E matrix resulted in the API's improved dissolution in acidic environment. This is because the polymer dissolved rapidly and formed a polymer-rich phase in which the API molecules could dissolve resulting in increased solubility and also increased wettability.

Schilling and co-workers[27] studied the effects of plasticizers on theophylline release from polymers including polymethacrylates and cellulosics. Dissolution profiles were evaluated in simulated gastric acid (pH 1.2) followed by phosphate buffer solution (pH 7.4). All excipients containing 10% theophylline showed an initial weak burst effect because the small quantity of drug particles on the surface of the pellets could not be protected by the enteric polymer (Eudragit® L and S series) and were directly exposed to the aqueous medium. Cellulosic pellets plasticized with triethyl citrate showed a relatively higher burst effect and faster diffusion rate in the simulated gastric acid while methacrylic polymers exhibited a good protection with lower API release rates at low pH. Increasing the amount of the plasticizer, not only reduced the glass transition temperature, but also increased the permeability of the polymeric matrix in both dissolution media.

Differences in API release rates among the plasticized samples were attributed to different volume percentages of the plasticizers and different efficiencies. Plasticized pellets showed a more homogeneous dispersion of the crystalline API throughout the polymer matrix with reduced particle size.

The effects on polymeric excipients upon the addition of plasticizers were also studied by Bruce and co-workers.[28] 5-aminosalicylic acid (5-ASA) was used as the model drug. Triethyl citrate (TEC), and citric acid monohydrate (CAM) were used as plasticizers. Eudragit® S100 and L100 were used as excipients. TEC improved API dispersion in the polymer matrix due to increased processability. The application of high loadings of CAM on Eudragit® S100 containing 5-ASA resulted in slower release as compared to the lower loading of CAM. The authors attributed this result to the lowered micro-environmental pH. The locally lowered pH on the matrix due to the citric acid suppressed ionization of the carboxylic groups in the acrylic polymer when exposed to pH 7.4 phosphate buffer solution, thereby delaying the erosion of the tablet matrix and the release of 5-ASA. For the same reason, higher 5-ASA loadings showed a slower release profile as compared to lower loadings.

Improved dissolution properties of API (Itraconazole) through the formation of solid dispersions in different polymers were studied.[29] Two different polymers, Eudragit® E100, and PVPVA 64 were used for this study, and melt extrusion was used for preparing the samples. The T_g of the API-polymer blend was theoretically calculated by the Gordon-Taylor[30] Equation 2.2 shown below. These values showed a good agreement with the experimental results.

$$T_g = \frac{T_{g1} w_1 + T_{g2} K w_2}{w_1 + K w_2} \qquad \text{(Equation 2.2)}$$

where T_{g1} and T_{g2} are the glass transition temperatures of the API and the polymer, respectively, w_1 and w_2 are the weight fractions of API and the polymer in the dispersions, repectively, and K is a constant calculated from the equation below:

$$K \cong \frac{\rho_1 T_{g1}}{\rho_2 T_{g2}} \qquad \text{(Equation 2.3)}$$

in which ρ is the density of the amorphous solids. Increased bioavailability of API depended, not only on the amorphous state of the API, but also on the type of the polymers. PVPVA 64 increased solubility by approximately 40%, while Eudragit® E100 showed 80% increased solubility. API dissolution rate from Eudragit® E100 was slower than from PVPVA64. The authors explained that this was due to the increased pH at the polymer surface when Eudragit® E100 went into the solution and this retarded the dissolution of the remaining undissolved polymer.

Qi et al.[31] studied the effects of paracetamol in a Eudragit® E matrix after hot melt extrusion. The polymer matrix containing paracetamol showed reduced glass transition temperature as compared to the pure polymer and this plasticization trend was more pronounced with increasing amount of the API.

2.3. Compounds of Inorganic Particles with APIs

Clay minerals are commonly used materials in the pharmaceutical industry both as excipients and active agents. Clays can be directly used for medical applications. For example, a cationic nanoclay, MMT, is a potent detoxifier and it can adsorb dietary toxins, bacterial toxins associated with gastrointestinal disturbance, hydrogen ions in acidosis, and metabolic toxins such as steroidal metabolites associated with pregnancy.[12, 32] Hydrotalcite, an anionic nanoclay is a popular antacid and it is used because magnesium and aluminum metal oxides slowly hydrolyze regulating the pH to an optimum value (pH 3 and 4) without provoking a rebound effect in the stomach.[33]

Although some studies reported a decreased bioavailability of several drugs by co-administration with several types of clays,[34] concomitant benefits of the uses of nanoclays, in modified drug delivery systems have been more often reported. Modified drug delivery systems address issues such as release patterns and drug stability/targeting.[8] New drug delivery systems based on clay minerals are shown in Table 2.2.

Many studies have aimed at improving the understanding of the physicochemical aspects of API/Clay complexes. Currently known action mechanisms of API/Clay complexes are as follows:

1) Cationic or anionic clays which have the counter ion in their interlayer space can be ion exchanged with foreign ions (in this case charged API)

2) The intercalated API/Clay complex is able to ion exchange again at the action site and release API molecules.

3) Released API from the clay interlayer space is absorbed at the action site and, thus, API is functioning.

Table 2.2 Drug Delivery Systems Based on Clay Minerals[8]

Issue	Target parameter	Delivery system	Mechanism	Excipients	Original clay
Release pattern	Dissolution rate	Extended release systems	Clay mineral-drug interaction	Natural clay minerals with high cation capacity values, Synthetic clay minerals, Modified clay minerals, Active pillared layered structures.	Smectites, Fibrous clay minerals, LDH, Hydrotalcites, Bentonite, Kaolinite, Montmorillonite
	Site of release	Improved drug solubility systems, Site specific system	Clay swelling, Adsorption	Swelling clays Montmorillonite	
			Enteric coated	Montmorillonite and LDH (oral release),	
Drug stability and Targeting		Microparticles, Nanoparticles	Bioadhesion	Smectite and halloysite (local release)	
	Hydrophilic ambient (sensible molecules) and distribution profile		Encapsulation, Surface precipitation , others	Halloysite, Porous-hollow nanoparticles	Porous silica from clay minerals, halloysite
			Clay-polymer interaction	Clay polymer nanocomposites	Montmorillonite

The API/Clay complexation and *in vivo* API release mechanism is described in Figure 2.1 by Aguzzi et al[8] .

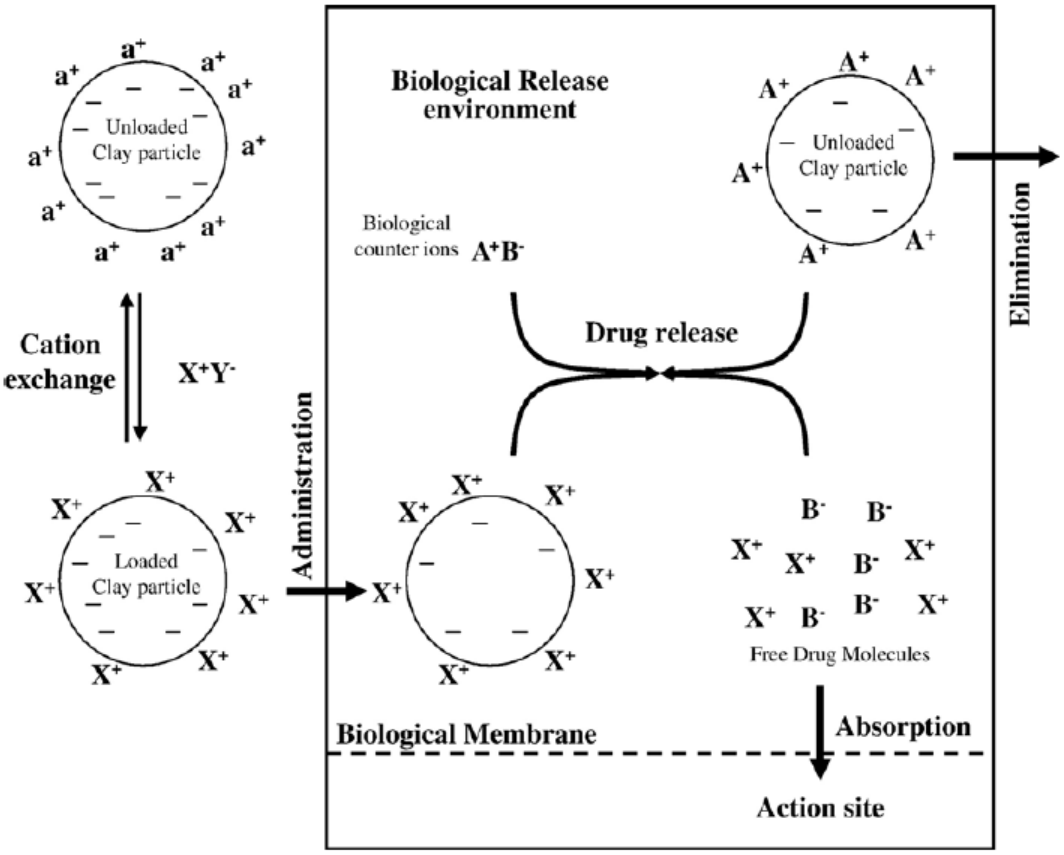

Figure 2.1 Idealization of API/Clay complexation and *in vivo* API release mechanisms (clay mineral surface charge (-); compensating cations (a+); cationic drug (X+); drug associated anions (Y-); *in vivo* counter ions (A+); anions associated with the counter ions (B-)).[8]
Note: In the case of anionic clay, the surface charge is positive and anions are the compensating ions

2.3.1 Cationic and Anionic Clays

As mentioned in the previous section, clay minerals are able to sorb certain anions and cations and retain them in an interchangeable status, in which they can exchange for other anions or cations by treatment with ions in a solution. The exchange reactions are stoichiometric and the exchange capacities are generally measured in terms of milliequivalents per gram or more frequently per 100 grams.[35] The importance of ion

exchange is that the exchangeable ion may influence the physical properties of the material.

Cationic clays have negatively charged metal containing layers, which have cations in the interlayer space to balance the charge.[36] Cationic clays, with a cation exchange capacity, include many aluminum silicates such as montmorillonite, vermiculite, smectites, and swelling micas. These clays are difficult to synthesize and are usually obtained from nature.[37]

Table 2.3 Composition, Crystallography and Symmetry for Some Natural Anionic Clays[38]

Mineral	Chemical composition	Unit cell parameters		Symmetry
		a (nm)	c (nm)	
Hydrotalcite	$Mg_6Al_2(OH)_{16}CO_3{\cdot}4H_2O$	0.3054	0.7603	3R
Manasseite	$Mg_6Al_2(OH)_{16}CO_3{\cdot}4H_2O$	0.310	0.78	2H
Pyroaurite	$Mg_6Fe_2(OH)_{16}CO_3{\cdot}4H_2O$	0.3109	0.7804	3R
Stichtite	$Mg_6Cr_2(OH)_{16}CO_3{\cdot}4H_2O$	0.310	0.78	3R
Barbertonite	$Mg_6Cr_2(OH)_{16}CO_3{\cdot}4H_2O$	0.310	0.78	2H
Takovite	$Ni_6Al_2(OH)_{16}CO_3{\cdot}4H_2O$	0.3025	0.753	3R
Reevesite	$Ni_6Fe_2(OH)_{16}CO_3{\cdot}4H_2O$	0.3081	0.768	3R
Coalingite	$Mg_{10}Fe_2(OH)_{24}CO_3{\cdot}2H_2O$	0.312	1.25	3R

3R and 2H: rhombohedral and hexagonal stacking sequence (three layers polytype and two layers polytype)
a : cation-cation distance within a layer
c : interlayer space

Anionic clays have positively charged metal hydroxide layers with balancing anions and water molecules located interstitially; they occur both as natural minerals and can also be synthesized by reacting dilute aqueous solutions of magnesium and aluminum chlorides with sodium carbonate (in the case of hydrotalcite). Anionic clays obtained by low temperature synthesis have generally the rhombohedral stacking sequence while hexagonal stacking sequences generally form at higher temperature.[38] Several names according to the composition and polytype form of the minerals are shown in Table 2.3.

2.3.2 API /Nanoclay Compounds

Ambrogi et al.[39] investigated the intercalation of diclofenac (DIK) into the interspacing of (HT) followed by its release which was carried out in a simulated intestinal fluid at pH 7.5 to mimic the ionic conditions of the small intestine. To functionalize an anionic clay, (HT-CO_3^{2-}), having carbonate ions at the interspacing, the anions were initially replaced by chloride ions by reaction with dilute HCl solution to produce HT-Cl. HT-Cl was then reacted with 2X the stoichiometric amount of DIK in hydroalcoholic solution (50% vol/vol) at 60 ^oC for 3 days. The intercalation of the anionic clay was confirmed by TGA, XRD, DSC and FTIR. Approximately 55% of DIK was intercalated into the interspace, and as a result the interlayer distance increased from 0.78 nm to 2.36 nm. *In vitro* drug release profiles in simulated intestinal fluid showed a slower drug release from the intercalated HT as compared to DIK physically mixed with HT. DIK release from HT physically mixed with DIK was completed within 15 minutes whereas DIK release from intercalated HT was completed after 9 hours (38%: 15 mins; 60%: 90 mins; 90%: after 9 hrs).

Costantino et al.[40] intercalated several anionic drugs, belonging to the anti-inflammatory class, such as indomethacin, thiaprofenic acid, ibuprofen, diclofenac, ketoprofen, and flurbiprofen into the interlayer of hydrotalcite; they confirmed their intercalation by observing XRD peak shifting to lower angles (2θ). Calculated drug loadings in the HT interspace ranged from 50.0% to 55.0%. When API was released from HT, the solubility of some of these poorly soluble drugs in biological fluids increased as compared to drugs physically mixed with HT. In the case of HT/intercalated indomethacin in simulated gastric fluid (pH 1.2) solubility was 14 mg/ml, while for the same combination physical mixture the solubility was 2 mg/ml. Similar increases were observed from HT functionalized with ketoprofen (1.3 times higher solubility) and thiaprofenic acid (1.6 times higher solubility).

Controlled drug release of donepezil intercalated in smectite clay was investigated by Park et al.[41] Montmorillonite (MMT), laponite (LA), and saponite (LA) were used in order to avoid the adverse effects of donepezil due to the increase in gastric acid secretion caused by enhanced cholinergic activity through the gastrointestine. According to XRD and TGA results, MMT modified with donepezil showed the largest expansion of the basal spacing and the highest weight loss, respectively. Authors explained that these results were due to the higher cationic exchange capacity (CEC) of MMT as compared to other clays. The API in the clay showed slightly increased thermal stability as compared to pure API. From the FTIR results, it was confirmed that donepezil molecules intercalatated in the interlayer spacing were not crystallized but resided in molecular form. The API release from the clays showed sustained releases profiles in accordance

with their CECs. Therefore, MMT showed the slowest drug release followed by SA and LA. Their CECs are 100, 71, and 63 meq/ 100g, respectively.

The fundamentals of the interaction between clay and API were investigated by White and Hem[11] since clay-API interactions affect the drug action and produce either desirable or undesirable effects. Several effects occurring when the API interacted with the clay were discussed. For instance, clindamycin absorbed on montmorillonite was not removed by washing with deionized water at pH 2 but it was readily desorbed by water at pH 11. Therefore, this API/clay complex may be stable in the stomach and could be released in the intestines thereby achieving sustained API release. A negative impact of API-clay interaction was that a neutrally absorbed by hydrogen bonding dioxin on montmorillonite (MMT) was degraded by acid catalyzed hydrolysis. Furthermore, in the case of atrazine, the API showed increased dissociation possibility with MMT. Finally, the authors concluded that careful examination of API-clay interactions is very important in order to avoid undesired reactions.

McGinity and Lach[42] studied sustained drug release by using MMT and amphetamine sulfate as the model API. API-MMT (1:20) complex was compared with pure API and a 1:1 combination API-complex. API release tests were done *in vivo*. API excretion rates were obtained from the measured concentration of amphetamine sulfate in the subject's urine. The API-MMT (1:20) complex showed sustained drug release pattern while the pure drug showed a burst effect in the early stages. The MMT affected the pharmacological response of the API from all formulations. The effect of amphetamine in the complexed form reached its maximum effect several hours after drug administration. Some experimental subjects were suffering from headache after administration of the

pure drug and the 1:1 combination drug complex; however the API - MMT complex (1:20) reduced or caused no headache at all due to the sustained drug release out of the API-MMT mixture.

It has been reported that MMT could increase the solubility and dissolution rate of hydrophobic drugs.[43] Dissolution tests on three different hydrophobic APIs (griseofulvin, indomethacin, and prednisone) and their complexes with MMT were investigated. All three APIs absorbed by MMT showed faster dissolution rates and increased solubility as compared to the unmodified APIs. The authors ascribed the increased dissolution rate and apparent solubility to certain unique properties of MMT. In particular:

1. MMT has an extremely large surface area (750 m^2/g). Therefore, it adsorbs a large amount of API on its surfaces.

2. MMT is hydrophilic and swells in aqueous media. These properties help to facilitate the wetting of hydrophobic drug substances, thereby increasing solubility.

It should be noted that back in the 1970s and 1980s our understanding of the structure of nanoclay products was very minimal. Hence, in articles from this period the reported results are not based on the notion of API intercalation into the clay interspacing but rather on adsorption on the clay surfaces. However, this dissertation is mainly focused on the intercalation of organic modifiers into the clay interlayers.

Suzuki et al[10] studied layered materials for diclofenac sodium (DIK-Na^+) delivery. One promising inorganic material, synthetic mica (sodium difluorotetrasilicate), was used for this drug delivery system. Since high molecular weight ions are hardly able to intercalate into the host inorganic compound, a phospholipid was first intercalated before ion exchange reaction with DIK-Na^+. Diclofenac was then successfully intercalated into the synthetic mica interlayers. Mica/DIK results show slow DIK release,

low solubility and steady dissolution profile while DIK-Na^+ alone showed high solubility and recrystallization of DIK after 10 minutes at pH 5.0. This complex showed an increasing resistance to humidity, absorbing less than 2 wt% in the temperature range between 50 and 100 ^oC whereas the hygroscopic API alone showed 20 wt% absorption.

Choy et al[44] reported that in attempts to develop possible applications of biohybrid materials as gene or drug delivery carriers, biomolecules such as cytidine-5'-monophosphate (CMP), adenosine-5'-monophosphate (AMP), guanosin-5'-mono-phosphate (GMP) and deoxyribonucleic acid (DNA) can be intercalated into the layered double hydroxides by an ion exchange process.

Li et al.[9] studied a fenbufen (FBF) delivery system produced by incorporation with LDH. FBF-LDH complexes were prepared through a co-precipitation method at different pH conditions ranging from 8 to 13. Fenbufen was successfully intercalated into the LDH interlayer and this intercalation was confirmed by XRD analysis. However, XRD patterns were different depending on the pH conditions of the FBF-LDH synthesis suggesting different crystalline structures of the FBF-LDH complexes. Furthermore, the chemical composition of the complexes prepared under different pH was also different. FBF content in LDH was increased with increasing pH during co-precipitation. Release patterns were also different in accordance with different metal elements. LDH composed of Mg/Al showed sustained API release while the one containing Li/Al showed the maximum release within 20 minutes.[9]

A study on dissolution and solubility of fenamates from layered double hydroxides was reported by Del Arco et al.[45] Mefenamic and meclofenamic acid were intercalated into chloride LDH interlayer by ion exchange reaction. Intercalation of APIs

was confirmed by XRD analysis. Solubility of APIs from the LDH hybrids containing mefenamic was tested at three different pH of 1.2, 4.5 and 6.8. Hybrids showed increased solubility at all three conditions. The authors attributed the increased solubility of the API from the LDH-mefenamic hybrid at pH 1.2 to the API released in its molecular form and to dissolution of LDH under the acid condition. Release profiles of LDH-mefenamic and LDH-meclofenamic acids hybrids showed sustained API release as compared to pure APIs and API - LDH physical mixtures releases in the simulated body fluids (pH 7.5 and 9). These slower releases were ascribed to ion exchange reaction between API in the LDH interlayer and anions in the buffer solutions.

Intercalation of indomethacin (IND) into the interlayer space of layered double hydroxides (LDH) was successfully achieved by Del Arco et al.[46] Co-precipitation and calcination methods were used for the modification of the LDH with API. During the clay modification, the pH of the solution was controlled to about 8-9 and the expanded interlayer space of the modified LDH was confirmed by XRD. The LDH modified by the co-precipitation method showed more IND loading (≈ 56 wt%) than the calcination method (≈ 25 wt%) in its interlayer space and this was confirmed by elemental analysis. Pharmacological studies *in vivo* showed that mice that consumed the LDH modified with IND had reduced ulcerating damage as compared to the ones that were treated with IND alone.

2.3.3 Compounds of APIs with Other Types of Inorganic Materials

Studies on API release from different inorganic matrices have also been carried out.[47] Two different types of mesoporous materials, silica (MCM) and alumina (ALO), and a layered double hydroxide (LDH) were used to compare the rate of Naproxen release from those inorganic matrices. LDH and the other two mesoporous materials containing the API were prepared by synthesis followed by an ion exchange reaction with Naproxen. The API loading was confirmed by XRD and FTIR. ALO showed higher Naproxen loading than MCM by measuring N_2 adsorption at -196 ^{o}C. All the samples showed sustained drug release to different degrees in a phosphate buffer solution. MCM showed the slowest drug release while LDH showed the fastest drug release among the samples. The authors attributed these different rates to different particle morphology and size. The release process of the mesoporous materials followed Fick's law while that of the LDH showed a non-Fickian anomalous process. The Korsmeyer-Peppas model inspired from the Higuchi equation was applied to the release mechanism.

Monkhouse and Lach[48] studied the effects of increased dissolution rate of water insoluble model APIs such as indomethacin, and aspirin by incorporation with adsorbents such as fumed silicon dioxide or silicic acid. The rationale of their research was that the low solubility of the APIs was mainly responsible for their aggregation in the medium since their hydrophobicity minimized their surface area. Therefore, they presumed that increasing the surface available for contact with the media might increase the dissolution rate. All the APIs were surface absorbed by adsorbents and dissolution rates were compared between pure APIs and APIs on different adsorbents. APIs incorporated on adsorbents showed increased dissolution profile as compared to pure APIs. Increased

solubility varied from 1 to 10 times depending on the types of adsorbents and their surface area. The results also showed increased dissolution rate with increased agitation of the medium although dissolution rank orders were not changed with increased agitation speed.

Das et al.[49] studied the influence of surface functionality and pore size of mesoporous alumina (Al_2O_3) host on ibuprofen (IBU) loading and release. Surface acidity was varied due to the density of OH groups on the alumina surface. This density difference did not change the mesopore characteristics such as pore size, distribution, surface area although the *in vitro* IBU release kinetics were influenced by the varying surface acidity. Al_2O_3 with higher surface acidity showed the highest IBU loading and the slowest release rate. Diffusion of IBU was also affected by pore size, with smaller pores showing slower release.

2.4 Compounds of Polymers with API-Intercalated Clays

For drug delivery applications, polymer-API intercalated nanoclay composites are anticipated to provide interesting advantages as compared to polymer-API systems. It may be possible to achieve more controllable API release pattern as compared to polymer/API system since the system have one more controllable parameter which is the API release from the clay.

LDH and fenbufen (FBF) complex was prepared by the co-precipitation method and coated with enteric polymers, Eudragit® S100 and L100 by solvent mixing. Dissolution tests were done under pH 1.2 for 2 hours, pH 6.8 for 2 hours and pH 7.4 for 5 hours in order to simulate passage through the human gastrointestinal tract. Eudragit® L and S efficiently protected the API-clay complex at low pH. Enteric polymer coated LDH-FBF showed slower drug release rate as compared to enteric polymer containing the API alone.[50]

Bugatti et al.[51] studied mechanical and barrier properties of LDH and poly ε-caprolactone (PCL) nano-hybrids. LDH was modified with active molecular anions such as benzoate (Bz), 2, 4-diclorobenzoate (BzDC), p-hydroxybenzoate (p-BzOH), and o-hydroxybenzoate (o-BzOH). The modified LDHs were incorporated in PCL by high energy ball milling. According to XRD results, modified LDH showed different forms of dispersion in the PCL matrix depending on the type of modified active molecular anions. Compared to the pure PCL, all the PCL nano-hybrids showed improved elastic modulus that increased in proportion to the modified LDH loading, up to a critical point. PCL nano-hybrids showed improved barrier properties because LDH created more tortuous paths. The release test of Bz directly from PCL in saline solution showed faster rates

compared to the Bz lamellar solid incorporated into the PCL. All the Bz molecular ion from sodium benzoate dispersed into PCL are released within 250 hours, whereas only 40% is released in the same time from the nano-hybrid into PCL

Ambrogi et al.[39] studied an anionic clay composite system for colonic delivery of diclofenac. Eudragit® L-100 and S-100, pH sensitive polymers, were used to coat HT functionalized with DIK. These polymers are insoluble at pH below 5 but soluble at pH above 6 and 7, respectively. Therefore, functionalized HT coated by Eudragit® can pass through the stomach without any premature release of the drug. Coated samples were prepared by using an oil-in-oil solvent evaporation method. The samples were exposed under simulated gastric solution (pH 1.2) and incubated at 37 ^{o}C for 2 hours and then in a simulated enteric fluid (pH 7.5) that was used for the *in vitro* drug release studies. X-ray diffraction analysis and SEM pictures confirmed that the Eudragit® coating protected the HT containing DIK under the acidic gastric environment. The drug release kinetics of this system followed Higuchi and Bhaskar's equation[52]. Higher amounts of Eudragit® S or L coating resulted in slower drug release rates but did not change the release mechanism.

Donepezil intercalated in a smectite clay along with Eudragit® E100 showed increased API release rate. This increased release rate was explained by considering that Eudragit® E100 could replace the intercalated Donepezil molecules by ion exchange reaction and facilitate the swelling of the clay. Furthermore, many hydrophilic chemical groups such as NH_4^+ of Eudragit® E100 could improve the hydration of the drug-clay and polymer hybrid. [41]

In order to examine the effects of nanocomposites on controlled release, Cypes et al.[53] studied poly(ethylene-co-vinyl acetate) (EVAc) solvent mixed with silicates with

different aspect ratios (Cloisite 20A, SOMASIF-MAE100, and SOMASIF-MAF300) containing dexamethasone. TEM images showed that silicate clays having a high cation exchange capacity produced better clay dispersion in the EVAc matrix. Dexamethasone release tests carried out in pH 7.4 phosphate buffer solution followed the Fickian model for diffusion from a disk[54] (all samples were prepared as circular pellets) as shown below:

$$\frac{M_t}{M_\infty} = 4\sqrt{\frac{D_{app}t}{L^2\pi}} \qquad \text{(Equation 2.4)}$$

Where M_t is the mass released in time t, M_∞ is the initial mass loading, D_{app} is the apparent diffusion coefficient, t is time, and L is the disc thickness.

A study on composites of paracetamol loaded poly(ethylene glycol) (PEG) with a naturally derived and partially synthetic layered silicate nanoclay prepared by hot melt extrusion was reported by Campbell et al.[55] The API was efficiently distributed in the PEO matrix. The dissolution rate of paracetamol from the nanocomposites was retarded with increasing amount of nanoclays from 1% to 5%. The retarded API release from the composites was ascribed to a tortuous path created by the nanoclay in the PEO matrix.

Forni et al.[56] studied the effect of montmorillonite (MMT) on API (papaverine hydrochloride) release from polyvinyl alcohol (PVA). Results showed that MMT addition can modify the drug release rate from the PVA based matrix by clay interaction with the API through a cationic exchange process. Therefore, the API /MMT ratio was an important factor for controlling the API release rate.

Nanocomposite hydrogels for mucoadhesive applications were synthesized by Lee and Chen[57]. *In vitro* release studies of differently charged APIs (Vitamin B2, Vitamin B12, etc) from poly(AA-co-PEGMEA)-bentonite nanocomposite gels showed that the release amount was lower when the API and hydrogel were oppositely charged.

The use of nanoclay/API in biodegradable or biosoluble polymers may allow improved efficacy, less toxicity and better patient compliance than conventional drug delivery devices. However, little knowledge on the nature of the intercalated nanoclay/API composites is yet available and practically no data have been published on such ternary systems produced by melt processing. Therefore, continuous and intensive investigations are required in order to fully utilize these systems for pharmaceutical applications.

CHAPTER 3

EXPERIMENTAL

3.1 Materials

3.1.1 Active Pharmaceutical Ingredients

One of the active pharmaceutical ingredients (API) used in this study is the sodium salt of diclofenac (DIK-Na^+) purchased from Spectrum Chemical & Laboratory Products (Gardena, CA). Its structure is shown in Figure 3.1(a). DIK-Na^+ is a non steroidal anti-inflammatory drug exerting a preventive effect against colon cancer.[58] It is a white powder with molecular weight of 296.14 g/mol and melting point (T_m) of 284 ^oC. It is very soluble in methanol, whereas its aqueous solubility depends on the pH (Table 3.1).

Table 3.1 Solubility of Diclofenac Sodium (DIK-Na^+) in Stock Buffer Solution [59]

Medium	Solubility (mg/mL)
Hydrochloric acid 0.1M	0.0012
Hydrochloric acid 0.01M	0.0017
Hydrochloric acid 0.001M	0.28
Purified water	14.18
Phosphate buffer solution pH 5.8	0.14
Phosphate buffer solution pH 6.0	0.15
Phosphate buffer solution pH 6.8	0.67
Phosphate buffer solution pH 7.0	1.36
Phosphate buffer solution pH 7.4	5.15
Phosphate buffer solution pH 8.0	12.14

The reported DIK-Na^+ density varies from 1.501 to 1.546 g/ml.[60] DIK-Na^+ is considered as anionic drug since its carboxylic anions would allow API intercalation between the hydrotalcite layers through anionic exchange reaction. DIK-Na^+ was selected for the immiscible API-polymer system since its solubility parameter differs by more than 7.5 $MPa^{1/2}$ compared to Eudragit® E100 (Table 2.1). However, DIK-Na^+ was expected to be miscible with Eudragit® S100 and its TEC plasticized versions since their solubility parameters differ by less than 7.5 $MPa^{1/2}$.

Another API used for the miscible API-polymer system is indomethacin (IND) purchased from Spectrum Chemical & Laboratory Products (Gardena, CA). IND is a non-steroidal anti-inflammatory drug, which is commonly used to reduce fever, pain, and swelling. IND is a white powder with molecular weight of 357.7 g/mol and melting point (T_m) of 162 ^oC. It has very poor water solubility reported as 3.8 μg/ml in simulated gastric fluid (pH 1.2) and 767.5 μg/ml in simulated intestinal fluid (pH 7.2), but dissolves very well in methanol.[1] IND can also be considered as anionic drug due to the presence of carboxylic groups in its molecular structure (Figure 3.1 (b)). Therefore, IND can also intercalate into the LDH interspacing through anionic exchange reactions. IND was selected for the miscible API- polymer system since it has a solubility parameter differing by less than 7.5 $MPa^{1/2}$ compared with Eudragit® E100 (Table 2.1).

Three dimensional structures of APIs, simulated by the Materials Studio® version 4.4 of Accelrys Inc.[61] are shown in Figure 3.2. DIK has a maximum end-to-end length of 9.35Å while the maximum length for IND is 12.95Å.

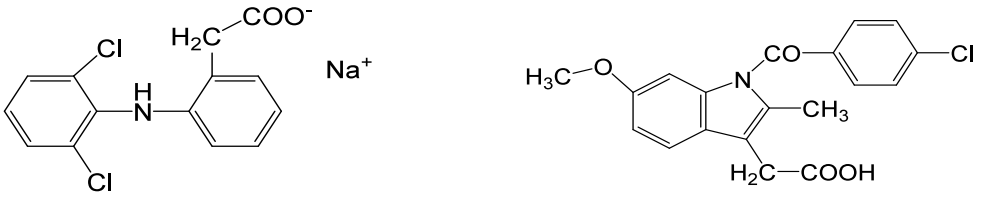

(a) (b)

Figure 3.1 Chemical structures of (a) DIK-Na^+, and (b) IND.

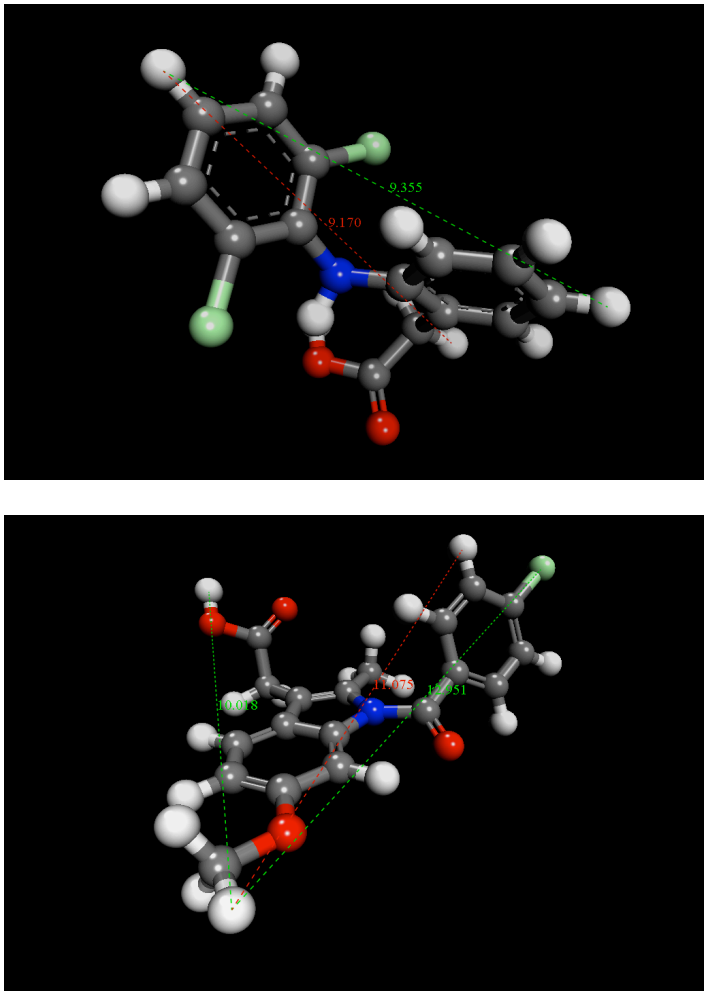

Figure 3.2 Three dimensional structure of (top) DIK and (bottom) IND.

3.1.2 Anionic Nanoclay

The anionic LDH clay used in this work is a synthetic aluminum magnesium hydroxyl carbonate donated by Sasol Germany (CAS # 11097-59-9, trade name: Pural MG 63 HT). It has a double layered metal hydroxide structure consisting of magnesium and aluminum hydroxide octahedrally interconnected via the edge (Figure 3.3); the manufacturer's reported weight ratio of Al_2O_3: MgO is 38:62.

The chemical formula is $Mg_4Al_2(OH)_{12}CO_3nH_2O$, the basal spacing is 0.77 nm and the anionic exchange capacity (AEC) has been reported to be approximately 340 meq/ 100 g. Calcined HT, designated as CHT, was prepared as shown in Section 3.2.1.

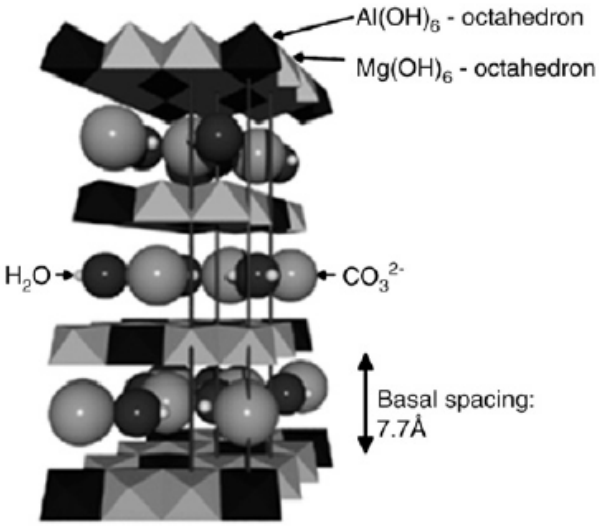

Figure 3.3 Molecular structure of LDH.[62]

3.1.3 Polymer Excipients

An amorphous cationic butyl/ methyl methacrylate-dimethylaminoethyl methacrylate terpolymer (1:1:2), (Eudragit® E 100: granule) donated by Evonik Industries (Piscataway, NJ) (Figure 3.4 (a)), was used as the excipient of the APIs and the API modified clays. Eudragit® E 100 is soluble in the gastric fluid up to the pH 5.0. This polymer has a

reported T_g of 48 ^oC and a maximum processing temperature of 220 ^oC. Real density of Eudragit® E100 was reported as 1.09 g/cm.[3,63]

An amorphous anionic methacrylic acid-methyl methacrylate (1:2) copolymer, (Eudragit® S 100: powder) donated by Evonik Industries (Piscataway, NJ) (Figure 3.4 (b)), was also used as the excipient of the APIs and the API modified clays. Eudragit® S100 is soluble in the colonic fluid at pH above 7.0. This polymer has a reported T_g of 172 ^oC[27] and a maximum processing temperature of 186 ^oC.[64] Therefore, adding plasticizers such as triethyl citrate (TEC), acetyltributyl citrate, or citric acid monohydrate, are necessary in order to lower the melt processing temperature.

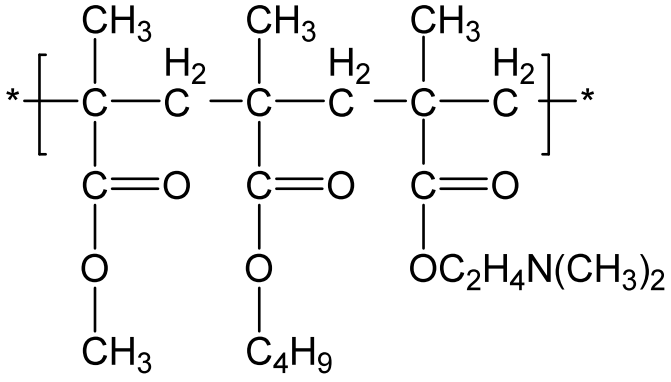

(a)

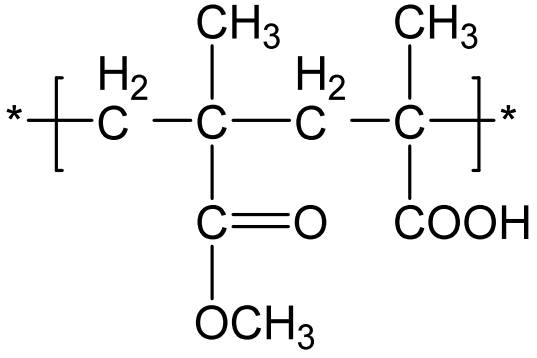

(b)

Figure 3.4 Chemical structures of (a) Eudragit® E100 and (b) Eudragit® S100.

3.1.4 Plasticizer

In order to facilitate melt processing of Eudragit® S100 triethyl citrate (TEC) (Sigma-Aldrich) was used as a plasticizer (Figure. 3.5). TEC is a colorless, odorless liquid with molecular weight 276.2 g/mol and density 1.137 g/mL. Its reported melting point is -55 ^{o}C and its boiling points are 127 ^{o}C at 1 mm Hg and 294 ^{o}C at 760 mm Hg. Reported solubility in water is 62 g/L.[65] A variety of applications for TEC are reported in the food and pharmaceutical industries.

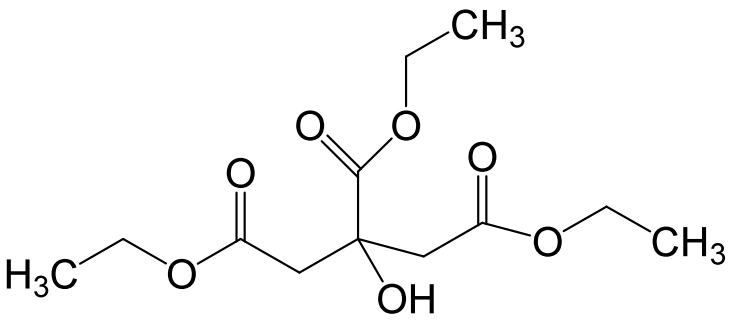

Figure 3.5 Molecular structure of TEC.

3.2 Sample Preparation

3.2.1 Calcined Hydrotalcite (CHT)

Substitution of carbonate ions in the hydrotalcite (HT) interlayer spacing with foreign ions is very difficult due to the high affinity of the carbonate ions to the positively charged HT interlayers. Removal of carbonate anions and water by calcination followed by immersion in a solution containing the modifier ions was the method used in this work. Calcination of hydrotalcite was carried out in a porcelain crucible heated at 490^{o}C for 7-8 hours.

3.2.2 Preparation of DIK Functionalized Clay (DIK/Clay)

Methanol/distilled water (4:1)(250 ml) solution was first prepared and sonicated for 10 minutes at room temperature and then heated at 60 ^{o}C for 5 minutes in order to remove gases, including any residual CO_2.[66] Calcined HT (2g) was then slowly added into the methanol/water (4:1) solution. Since calcined HT increases the pH of the solution, and increased pH may convert any traces of remaining carbon dioxide to carbonate ions,[67] the solution pH was set to 6.0 by adding 0.05 N of HCl. It is to be noted that lowering excessively the pH may prevent intercalation since the solubility of DIK-Na^+ is very limited at the low pH (see Table 3.1). Five grams of DIK-Na^+ (more than its stoichiometric amount based on AEC) was then added into the slurry.[68] The reaction was carried out at 60 ^{o}C for 2 days in a closed reactor in the absence of N_2. An additional run was carried out for 5 days to investigate possible degradation.

A schematic of the CHT and DIK-Na^+ reaction is shown in Figure 3.6. The collapsed HT crystalline structure after calcination is regenerated in the presence of the foreign anions.[69] After the reaction, the modified clays were filtered under vacuum

(Genuine Whatman filter paper, 1.6 μm pore size), washed with a methanol/water mixture (4:1) and then separated from the solution by centrifuging. These washing procedures were repeated over 5 times in order to remove the residual DIK from the clay surface. The modified clays were then dried at room temperature for 24 hours and dried again at 80 ^{o}C for 24 hours.

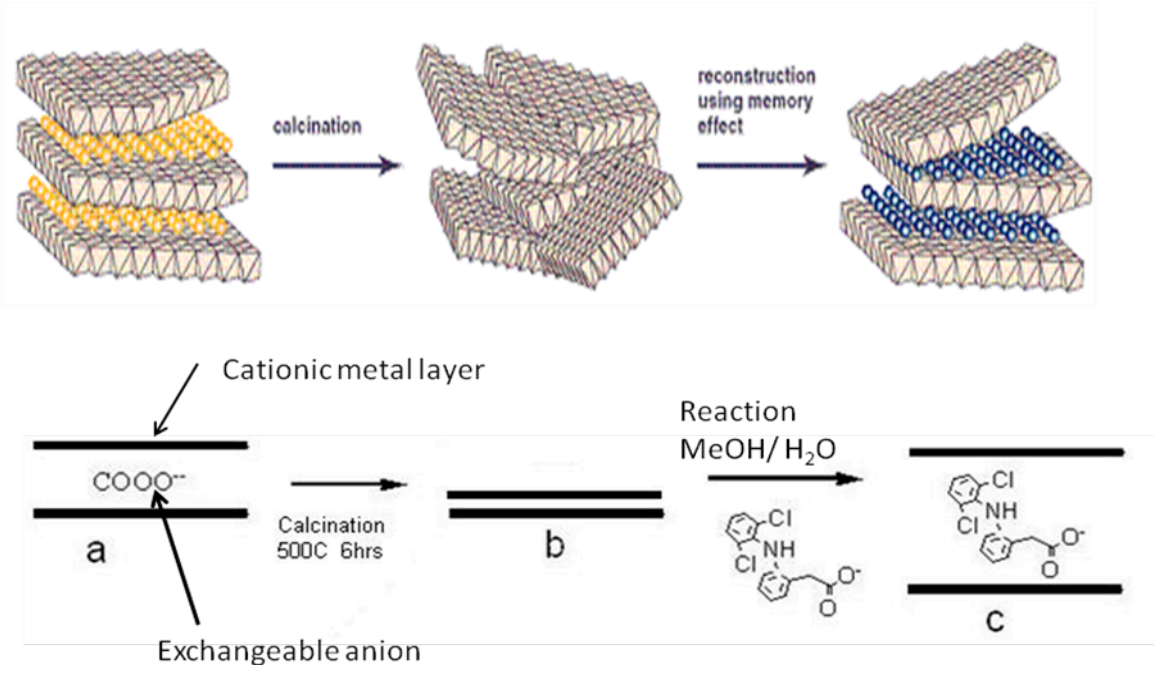

Figure 3.6 (Top) LDH reconstruction process of calcined LDH[69], (bottom) schematic of DIK intercalation into HT interlayer spacing.

3.2.3 Preparation of IND Functionalized Clay (IND/Clay)

The procedure used was similar to the above with the following exceptions:

- 400 ml of a methanol/distilled water (3:1) solution was used
- No pH adjustment were made for this reaction since IND was lowering the pH of the solution
- 1 g of CHT and 3 g of IND were used
- The reaction was carried out from 1 day to 5 days and FTIR and XRD spectra were taken regulary during this period.

The pH changes after adding clays and APIs to the methanol/water solution are shown in Figure 3.7.

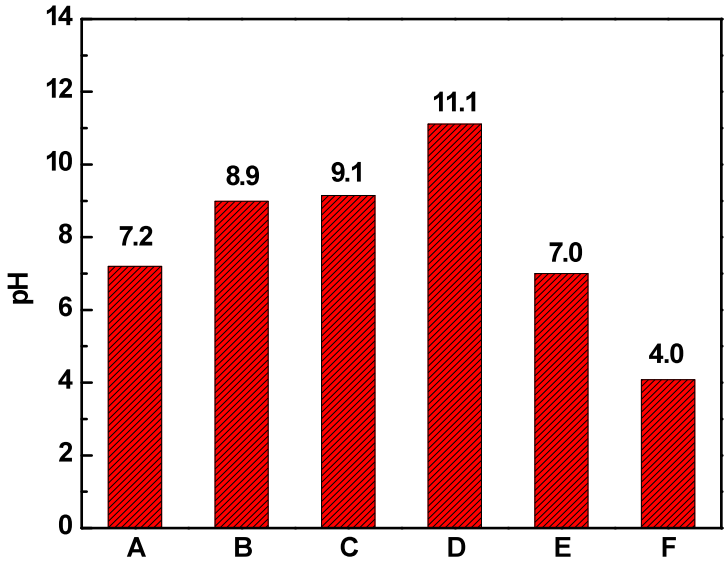

Figure 3.7 pH changes after adding clays and APIs to methanol/water: (A) 200 ml methanol/50 ml water, (B) added 5g DIK-Na^+ into solution (A), (C) added 2g HT into solution (A), (D) added 2g CHT into solution (A), (E) 300 ml methanol/100 ml water, and (F) added 3g IND into solution (E).

3.2.4 Preparation of Eudragit®E100/DIK-Na^+, and Eudragit®E100/DIK/Clay Compounds by Melt Mixing

Eudragit® E100 compounds containing 4 wt% or 15wt% DIK-Na^+ and 10 wt% DIK/Clay (containing 4wt% DIK) were prepared by compounding in a Brabender batch mixer (PL2000, C. W. Brabender) at 50 rpm and 130 ^oC for 5 minutes. After melt mixing, the compounds were pressed for 50 seconds at 130 ^oC into thin disks for further analyses.

3.2.5 Preparation of Eudragit®E100/DIK-Na^+, and Eudragit®E100-DIK/Clay Compounds by Solvent Mixing

Solvent mixing was carried out in order to compare the dispersion of the DIK-Na^+ or API/Clay particles in the polymer matrix with that obtained by melt mixing in the batch mixer. Eudragit® E100 pellets (10g) were dissolved into 100 ml of a 50/50 methanol/acetone solution. DIK-Na^+ (4 wt% or 15 wt%) and DIK/Clay (10 wt%) were added into the mixture and stirred for 5 hours at room temperature. DIK-Na^+ was fully dissolved and DIK/Clay was suspended in the solution. The DIK-Na^+ solution and the DIK/Clay mixture were then transferred to aluminum dishes to remove solvents. The samples were then stored in an oven at 80 ^oC and kept for 1 day under vacuum. The dried samples were collected by removal of aluminum dish and collected samples were hot pressed at 130 ^oC for further analyses.

3.2.6 Preparation of Eudragit® E100/DIK-Na^+, and Eudragit®E100-DIK/Clay Compound by co-Rotating Twin-Screw Extrusion

A co-rotating twin screw extruder, APV MP 2015, was used in order to compare the dispersion of API and API/Clay complex in the polymer matrix with that obtained with the batch mixer and by solvent casting. The diameter of the APV MP 2010 screw is 15 mm, and the ratio of the barrel length to the screw diameter is 15. The screw contains one set of kneading blocks as shown in Figure 3.8 that provide intensive mixing.

Figure 3.8 Screw configuration of APV twin screw extruder.

The barrel temperature was set at 130 ^oC and the screw speed was 50 rpm. A physical mixture of Eudragit® E100/DIK-Na^+ and Eudragit® E100-DIK/Clay was fed into the extruder by a volumetric feeder (SCHENCK AccuRate® 102M). The ratio of Polymer/API and Polymer-API/Clay was the same as for the conditions of batch mixing. Feeding rate was 0.03 kg/hr and calculated residence time was around 5 minutes, similar to that used for the batch mixer.

3.2.7 Preparation of Eudragit®E100/IND and Eudragit®E100-IND/Clay Compounds

Eudragit® E100 was compounded with 4 wt% or 15 wt% IND and 10 wt% IND/Clay as desribed above for the case of DIK. After melt mixing, the compounds were pressed for 50 seconds at 130 ^{o}C into thin disks for further characterization.

3.2.8 Preparation of Eudragit®S100/ DIK-Na^{+} and Eudragit® S100- DIK/Clay Compounds in Batch Mixer

Eudragit® S100 was premixed with 20wt% TEC in a wrist action shaker (Burrell Corporation, Pittsburgh PA) for 3 hours. 4 wt% or 15 wt% DIK-Na^{+} and 10wt% DIK/Clay (containing 4wt% DIK) were melt compounded with the premix in the batch mixer at 170 ^{o}C for 4 minutes. After compounding, samples were pressed into thin disks for further characterization.

3.3 Characterization

3.3.1 Fourier Transform Infrared (FTIR) Spectrophotometry

FTIR spectra of unmodified clays, APIs, API modified clays, polymer excipients with or without APIs or API modified clays were obtained using a Spectrum One FTIR Spectrometer® (Perkin-Elmer Instruments) in the mid infrared range wavelength 400-4000 cm^{-1}. Samples (1 wt%) were mixed with potassium bromide and dried at 80 ^{o}C for 24 hours under vacuum. Transparent KBr pellets (13 mm in diameter) were prepared by torque wrench (Craftsman).

3.3.2 Thermogravimetric Analysis (TGA)

Thermogravimetric analysis (TGA) was carried out with a TGA Q50 thermogravimetric analyzer (TA Instruments). Tests were carried out using a ramp from room temperature to 500 ^{o}C, at a heating rate of 20 ^{o}C/min in a nitrogen atmosphere (flow rate 40 cm^3/min). Initial sample weight was set as 0.9-1.5 mg with thickness of 0.3-0.5 mm.

3.3.3 Differential Scanning Calorimetry (DSC)

Glass transition temperature (T_g), melting temperatures (T_m) and other thermal properties were determined by differential scanning calorimetry (DSC) (DSC Q100, TA instruments). Heating and cooling rates were 20 ^{o}C/min at a predetermined temperature range under 40 cm^3/min nitrogen flow. Weight of all test samples ranged from 4 to 9 mg. All samples were hot pressed and prepared as thin films before the analysis. T_g of samples was calculated out of three DSC runs of each sample.

3.3.4 Wide-Angle X-ray Diffraction (XRD)

Wide-angle X-ray diffraction (XRD) analysis was performed for pure APIs, HT, calcined HT, API modified HT, and the corresponding polymer composites with a Philips PW3040 diffractometer (Cu K_a radiation λ=0.154 nm), operated at 45 kV/ 40 mA. All specimens were scanned in the 2θ range from 2^o-40^o at a rate of 0.003^o/sec. The interlayer spacings of unmodified and organomodified clays were calculated using Bragg's law of diffraction:

$$2d = \frac{n\lambda}{\sin\theta} \qquad \text{(Equation 3.1)}$$

Where, n is an integer, 1 in this case, λ is the wavelength of the incident X-ray beam in Å, and θ is the angle of incidence in degrees.

3.3.5 Scanning Electron Microscopy (SEM)

APIs, API modified clays and the fracture surfaces of polymer compounds were examined by Scanning Electron Microscopy (LEO 1530 VP Emission SEM) at 3-5 keV working voltage.

3.3.6 Energy Dispersive X-Ray Analysis (EDX)

In order to detect the API and the clay particles and their degree of dispersion in the polymer matrix, Energy Dispersive X-ray analysis (EDX) (2400 Perkin-Elmer Elemental mapping), was used. By selecting characteristic elements, corresponding elemental mappings were possible and the detected elements were identified as dots. The working voltage was 5 kV and mapping time was 300 seconds for all species.

3.3.7 Laser Diffraction Method

Particle size distribution of IND and DIK-Na^+ was measured by a Laser diffraction method (Beckman-Coulter LS 230 Particle size analyzer). The Laser diffraction method sizes particles by utilizing the diffraction pattern of scattered light. Size distribution can be obtained in the range from 0.04 μm to 2 mm.

3.3.8 Elemental Analysis

Elemental analysis for carbon, hydrogen, and nitrogen was performed at QTI Laboratories, NJ, USA. The nitrogen content in the API modified HT was determined using a Perkin-Elmer 2400 Elemental Analyzer. The nitrogen content was then used for calculating the API content in the nanoclay, since the latter does not contain nitrogen. This analyzer uses combustion to convert the sample elements to simple gases, such as carbon dioxide, water, and nitrogen. Upon entering the analyzer, the sample is combusted in a pure oxygen environment. The product gases are separated under steady state conditions, and measured as a function of thermal conductivity.

3.3.9 Dissolution Test and UV-Vis Analysis

Drug dissolution (also referred to in the literature as drug release) was studied in a Distek dissolution system 2100A with a Distek temperature control system TCS 0200 according to USP dissolution apparatus II with a paddle rotation speed of 50 rpm at 36.5 ± 0.1 ^oC. The dissolution medium was 1L of a pH 1.2 HCl buffer solution for simulating a gastric acid fluid and a pH 7.4 phosphate buffer solution for simulating a colonic fluid. Generally, in dissolution, apparatus II (paddles) showed a slightly faster API release

profile than apparatus I (baskets). Faster dissolution profiles also occurred as stirring speed increased. The clay related dissolution tests were carried out with 100 ± 10 mg powders. Samples of the test fluid were collected at predetermined time intervals, filtered through a 0.45 μm filter and then analyzed at 276 nm and 318 nm for DIK-Na^+ and IND related experiments, respectively, by an UV-Vis spectrophotometer (Evolution 60, Thermo Scientific). The experiments were repeated three times with good reproducibility. Details on calibration procedure can be found in Appendix I.

Eudragit® E100 and S100 compounds with APIs or API modified clay were compressed into 2 mm disks having the same holder geometry (circular). The weight of each sample was 200 ± 20 mg.

3.3.10 Rheometry

In order to study the rheological behavior of the polymer/API and polymer-API/Clay compounds, a Rheometrics Scientific RMS-800 Rheometer used with a plate diameter of 25 mm and a distance between plates of 0.8 mm. A dynamic frequency sweep was performed at a strain of 10 % within the linear viscoelastic region, predetermined by a dynamic strain sweep. All samples from the batch mixer were hot pressed into specimens with 2.54 cm in diameter and 1 mm in thickness before the RMS test. Samples based on Eudragit® E100 and Eudragit® S00 were tested at 130 ^oC and 160 ^oC, respectively.

CHAPTER 4

CLAY/API SYSTEMS

In this chapter, efforts to intercalate anionic hydrotalcite with selected APIs containing anions of different sizes, MW and chemical structures were investigated in order to produce novel nanohybrids that could be used as API reservoir either alone or after addition in the polymer excipients (see Chapter 6). Hybrids were characterized for thermal properties, dissolution characteristics, and morphology.

4.1 Characterization of Clay Modified with DIK-Na^+

4.1.1 FTIR Results

FTIR spectra of DIK-Na^+, unmodified HT, and DIK/Clay are shown in Figure 4.1. Figure 4.2 is a magnification of the dotted area of Figure 4.1. The spectra ascertain the presence of DIK on the clay but not its exact location. The anionic clay contains carbonate ions in its interlayer spacing corresponding to a band at 1357 cm^{-1} (Figure 4.1 (b)). The spectrum of the clay after calcination (CHT) and modification with DIK-Na^+ (Figure 4.1 (c)) does not show a band at 1357 cm^{-1} indicating the successful removal of the carbonate ion from the interlayer space. On the DIK/Clay particles, the newly created peaks can be attributed to DIK that may be present as either a surface coating and/or as an intercalant. The peaks at 1575, 1508, 1499, and 1456 cm^{-1} indicate ring stretching of 1, 2, 3 tri-substituted benzene. The peak at 1585 cm^{-1} results from the benzene ring carbon-carbon vibration. The peaks at 1470 cm^{-1} and 1400 cm^{-1} correspond to the CH_2 bending of ortho-substituted benzene. The band in the region between 1300 and 1150 cm^{-1} is responsible for C-O bonds. The band for aryl halide between 1080 and 1060 cm^{-1} is not visible, apparently due to the strong interaction of ring vibrations.[70] The broad peak between

3700 and 3000 cm^{-1} results from hydroxyl groups of the layers and the reabsorbed interlayer water.

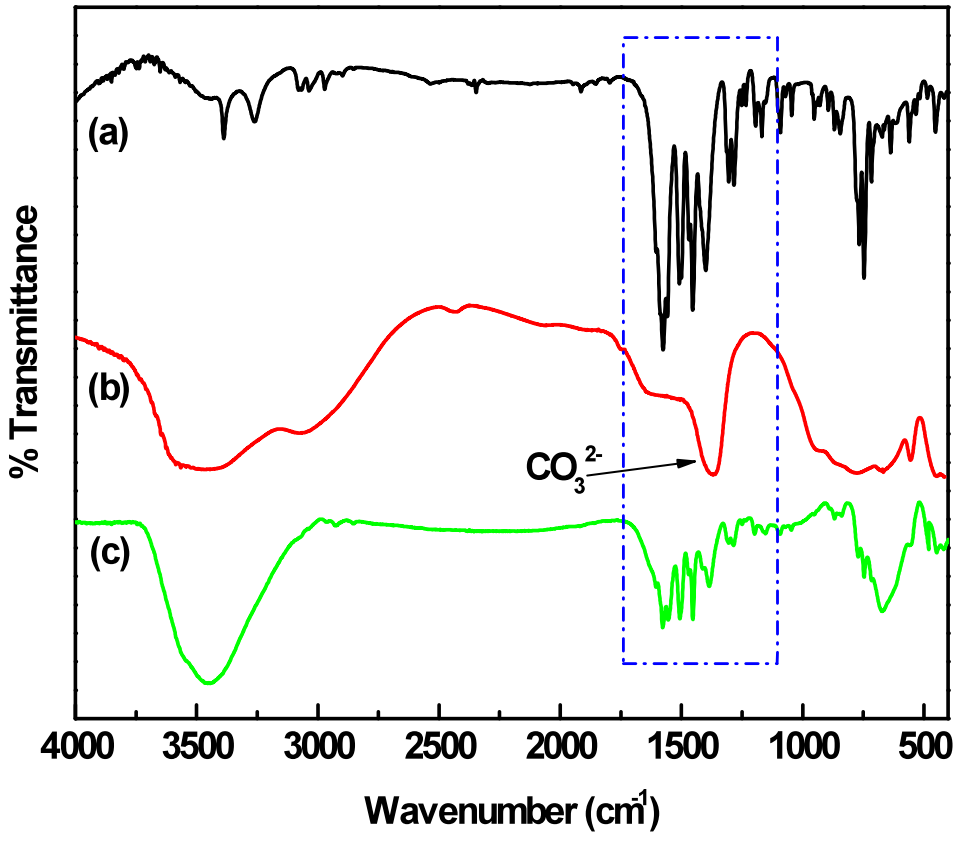

Figure 4.1 FTIR results of (a) DIK-Na^+, (b) pure HT, and (c) CHT modified with DIK-Na^+.

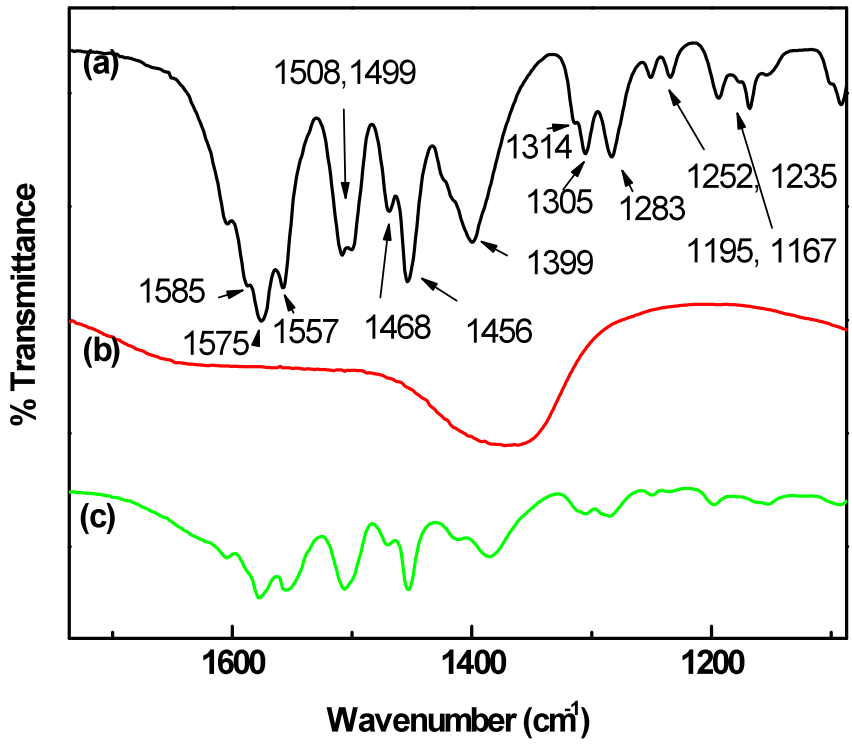

Figure 4.2 Magnified regions of spectra of Figure 4.1.

4.1.2 XRD Results

XRD analysis was used to evaluate the intercalation of DIK into the interlayer space of HT. Figure 4.3 shows the XRD spectra of DIK-Na^+, HT, DIK/Clay and calcined HT. In order to index patterns of HT and HT modified with APIs, Equation 4.1 valid for hexagonal system can be used to designate Miller indices:

$$\sin^2\theta = A(h^2 + hk + k^2) + Cl^2 \qquad \text{(Equation 4.1)}$$

Where *h,k,l* indicate the Miller indices of a plane, which makes fractional intercepts of $1/h$, $1/k$, $1/l$ with the axes, and $A = \lambda^2/3a^2$ and $C = \lambda^2/4c^2$; λ is wavelength, the "a"

parameter of the hexagonal unit cell corresponds to the distance between two metal elements in adjacent octahedral sites while the "c" parameter corresponds to three times the distance between adjacent hydroxyl layers.[71, 72] Due to insufficient information for certain parameters in Equation (4.1), Figure 4.3 contains Miller indices that have been used in references[72-76].

DIK-Na^+ shows sharp peaks indicating highly crystalline structure (Figure 4.3(a)). Pristine HT (Figure 4.3(b)) has a strong peak around 11.5^o (0.77 nm calculated from Bragg's law); it corresponds to its original basal spacing and this value is in good agreement with supplier's specifications. HT also shows a broad, asymmetric reflection marked as star (*) (Figure 4.3 (b)) beyond 30^o, which may be an indication of turbostratic disorder in the layer stacking.[77]

Calcined HT which lost its crystalline structure due to removal of counter anions by heating does not show any peaks throughout the range from 2 to 40^o (Figure 4.3 (d)). Therefore, based also on the FTIR results, it can be concluded that the carbonate ions are fully removed.

Figure 4.3, (spectrum (c)), clearly shows the different X-ray peaks of the DIK/Clay as compared to the parent HT (spectrum (b)). It can be shown that the crystalline structure of HT was reformed by regeneration in the presence of DIK-Na^+ and peaks corresponding to the regenerated HT have shifted to lower angles. The anionic clay modified with DIK-Na^+ shows an angle shifted from 11.5^o to 3.9^o indicating an increased interlayer space from 0.77 nm to 2.39 nm, and an evidence of intercalation. The broadening of the crystalline reflections in the DIK/Clay represents a loss of HT crystallinity.[76] Assuming a thickness of 0.45 nm for the Mg-Al double hydroxide layer,[78]

this result indicates that the interlayer space generated by DIK is 1.94 nm, corresponding to twice the length of the end-to-end distance of DIK (Figure 3.2). Constantino et al.[40] and Ambrogi et al.[39] reported that increased interlayer spacing is responsible for the DIK bilayer presence in the clay interlayer space which is partially interdigitated and perpendicular to the layer plane. It has been reported that the second and the third peaks may correspond to the higher harmonics of the interlayer distance.[79]

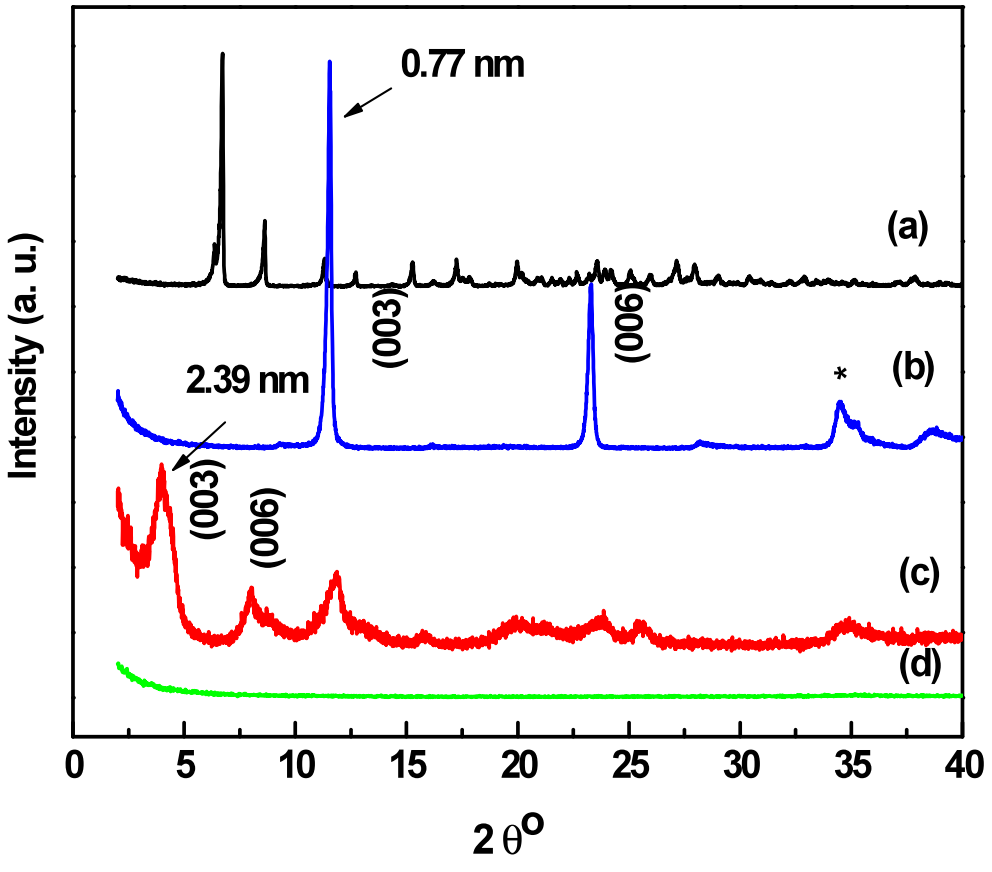

Figure 4.3 XRD results of (a) DIK-Na^+, (b) HT, (c) DIK/Clay, and (d) CHT.

4.1.3 Thermal Analysis

Figure 4.4 shows TGA data of DIK-Na^+, HT, CHT, and DIK/Clay. HT shows typically two different weight loss regions. The first region is related to the dehydration of the HT (100-250 ^oC). The second region (250-527 ^oC) is responsible for the dehydroxylation and decarbonation reactions.[68] DIK-Na^+ is thermally stable and started decomposing around 284 ^oC close to its melting point. Since the anions and water of HT were removed, the TGA results of CHT do not show the typical weight losses of HT. The early weight loss of CHT up to 100 ^oC can be attributed to moisture absorbed during sample preparation. DIK/Clay also does not show a similar pattern of weight loss as compared to the unmodified HT since the original carbonates have been replaced by DIK anions. DIK/Clay shows an early 10 wt% moisture loss and these water molecules may have been absorbed during the DIK-Na^+ / clay reaction or the preparation of the sample for the analysis. Subtracting the moisture content of the DIK/Clay, the approximately 40 % additional weight loss could be attributed to the weight of both intercalated and coated DIK.

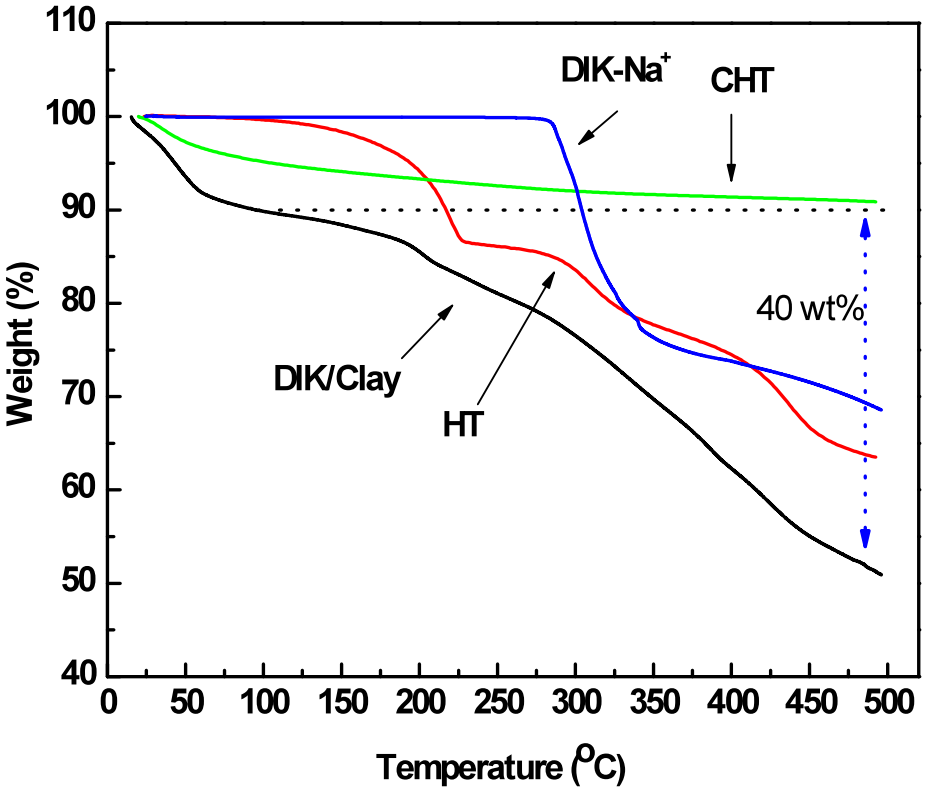

Figure 4.4 TGA results of DIK-Na^+, clays, and CHT modified with DIK-Na^+.

Isothermal TGA was used to estimate the thermal stability of DIK/Clay (when dispersed in a polymer matrix) at melt processing times and temperatures. The results at both 180 ^oC and 200 ^oC for 10 minutes show no differences (Appendix A) in the weight loss between the two temperatures and an overall good thermal stability after an initial moisture loss.

The DSC results of DIK-Na^+ show a strong endothermic peak at 291 ^oC corresponding to its T_m (Figure 4.5). HT shows two broad endothermic peaks attributed to the dehydration, and the dehydroxylation and decarbonation reactions[68] discussed in the TGA analysis. However, unlike the unmodified clay, DIK/Clay that does not contain

carbonate ions and interlayer water shows very weak broad endothermic peaks. Furthermore, DIK/Clay does not show any T_m, which may suggest an amorphous state for DIK.

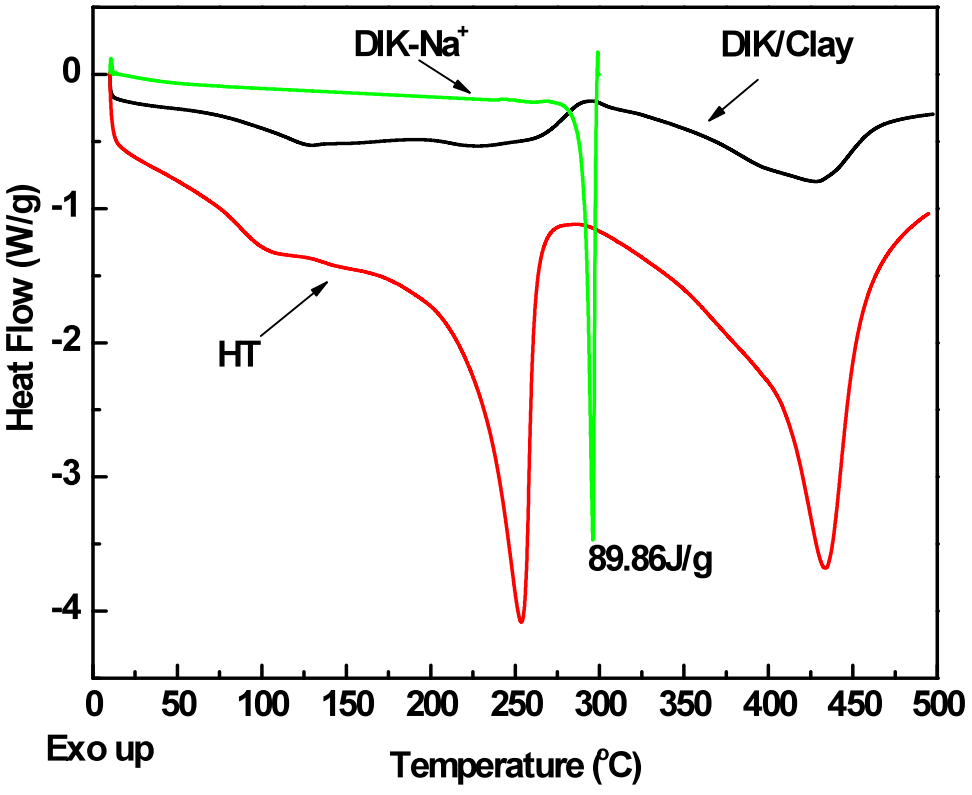

Figure 4.5 DSC heating results of DIK-Na+, DIK/Clay, and HT.

4.1.4 Quantitative Analysis of DIK/Clay

The DIK loading of DIK/Clay was determined by carbon and nitrogen elemental analysis (Table 4.1). Carbon and nitrogen are unique elements present only in the API. Therefore, by using this information and results from the elemental analysis, the content of DIK in the clay can be readily calculated (Appendix B). Calculated DIK loadings on the

modified clays based on carbon and nitrogen are 39.98% and 41.31%, respectively. Therefore, it has been assumed that approximately 40% of the API was loaded on the clay matrix. This is in reasonable agreement with the results of Ambrogi[39] who, by using a different type of hydrotalcite and a different preparation method, reported that roughly 50 % DIK was intercalated.

Table 4.1 Results of DIK/Clay Elemental Analysis

Material	% Carbon	% Nitrogen
HT*	4.0	0.0
CHT*	0.0	0.0
DIK*	56.7	4.7
DIK/Clay**	22.7	1.9

* calculated
** experimental

4.1.5 Particle Size Distribution

Different particle size distributions between pure HT and modified DIK/Clay are shown in Figure 4.6. The SEM individual particle size of HT (Figure 4.7) is much smaller than the one measured by the laser diffraction method. This is because the laser diffraction method takes into account agglomerated clay particles. This also confirms, not only how easily these types of nanomaterials are agglomerated, but also why they require special conditions to achieve nanosized dispersion. The pure HT shows a bimodal distribution, while DIK/Clay shows a unimodal distribution with a peak at 6 μm. It can be concluded that pure HT has more tendency towards agglomeration than DIK/Clay and hence, less uniform size distribution. The tendency of the clays toward agglomeration was also observed by microscopy. HT and DIK/Clay were dispersed in water or water-surfactant

(10 wt%) solution (Figure 4.8). All clay particles are aggregated and their sizes vary from 1 μm to 60 μm, except for DIK/Clay in the water-surfactant solution which shows better separation of the clay aggregates. This suggests that nanoclays can be readily separated by incorporation of a modifying agent with an appropriate structure and by proper selection of the matrix. Obviously, DIK-Na^+ is not the appropriate agent for achieving high degree of clay dispersion.

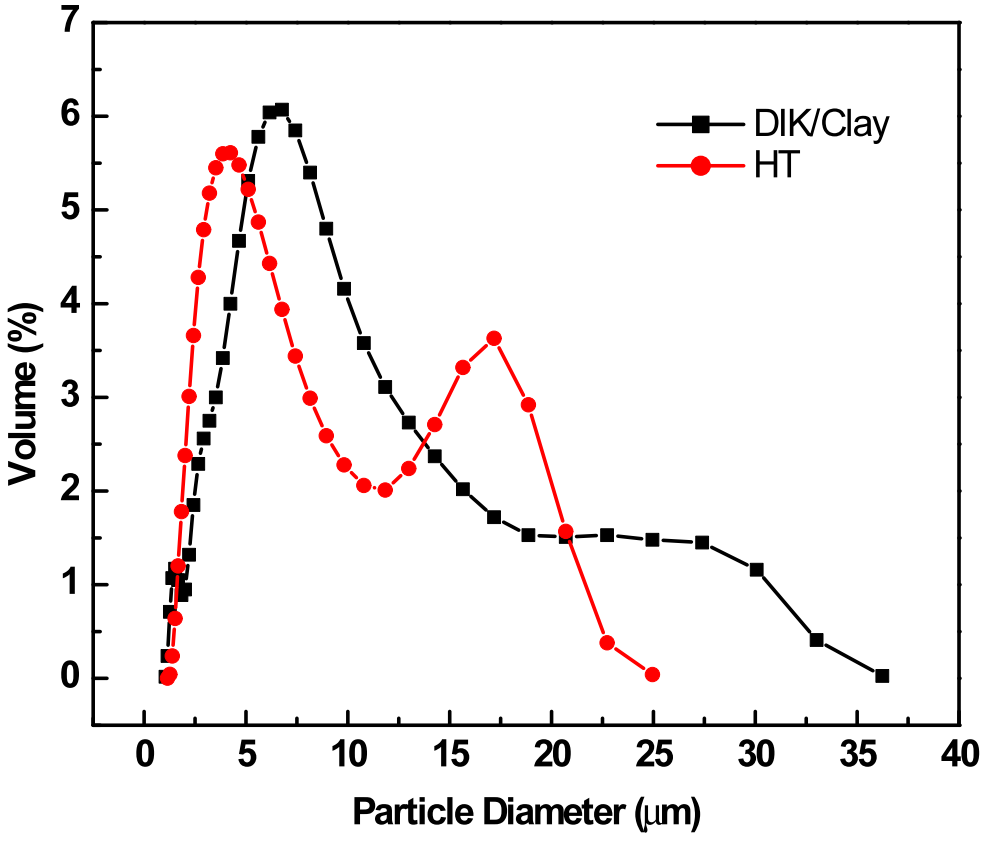

Figure 4.6 Particle size distributions of pure HT and DIK/Clay.

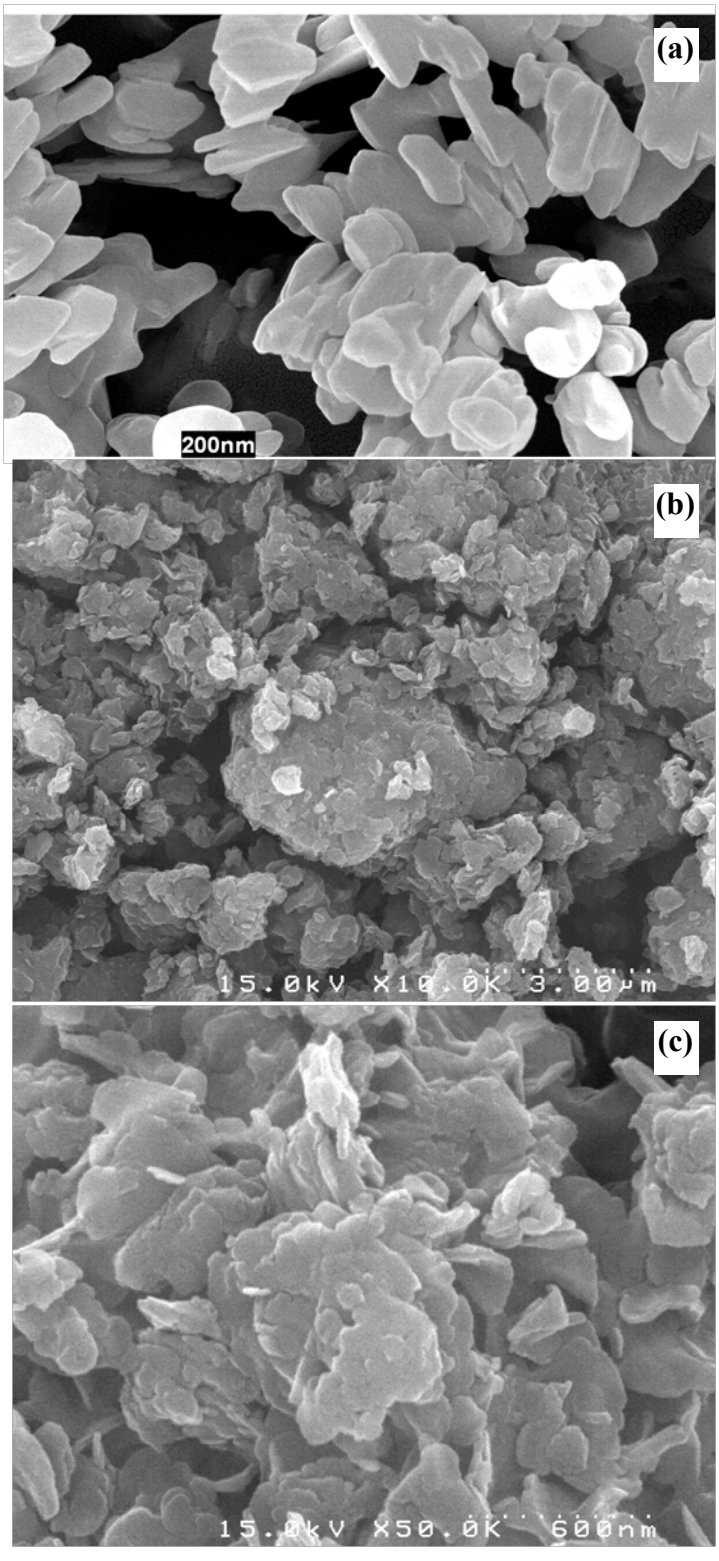

Figure 4.7 SEM images of (a) HT,[80] (b) and (c) DIK/Clay.

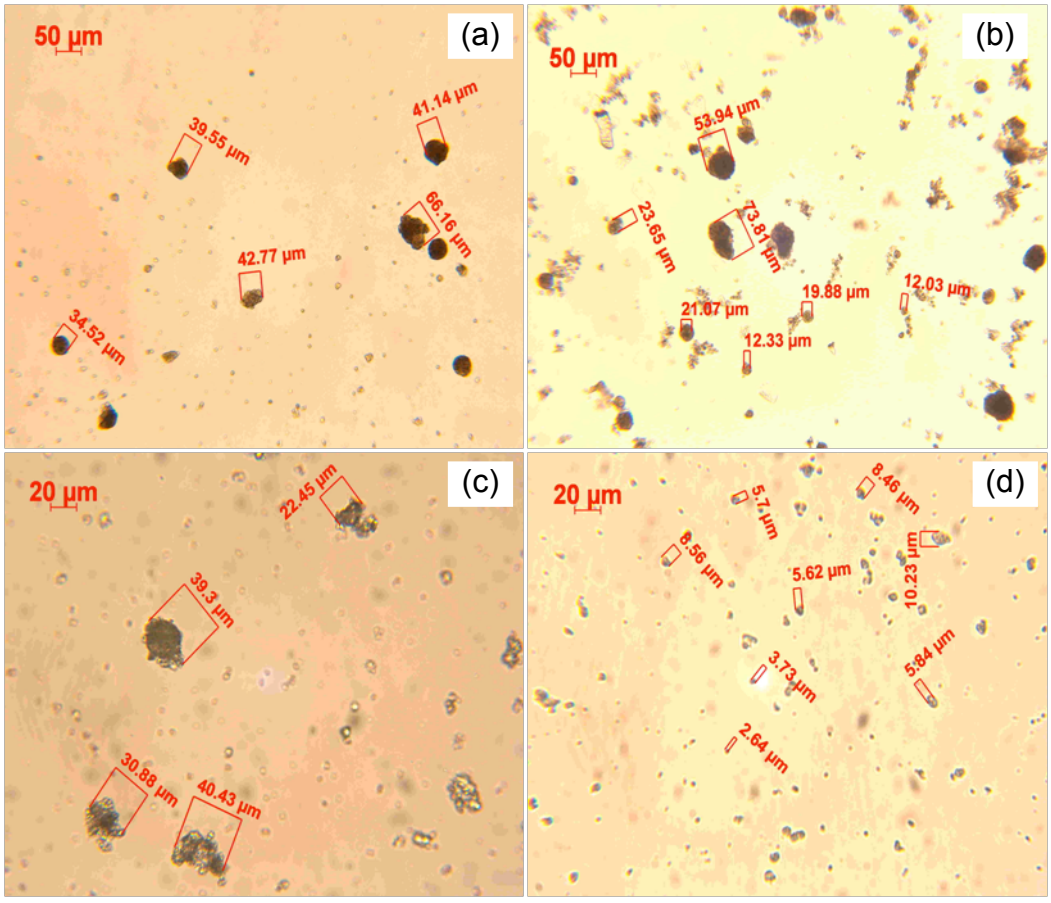

Figure 4.8 Optical microscopy images of (a) HT in water, (b) HT in water-surfactant, (c) DIK/Clay in water (d) DIK/Clay in water-surfactant.

4.1.6 Dissolution Tests at Different pH

Figure 4.9 shows the percentage of the dissolved DIK from DIK-Na^+, DIK-Na^+/ HT physical mixture and DIK/Clay as a function of time in acidic buffer. DIK-Na^+ rapidly dissolves in neutral pH water. However, as mentioned earlier, its solubility is dramatically decreased at lower pH. Figure 4.9 shows that less than 4 % DIK is dissolved from both DIK-Na^+ and from the physical mixture of DIK-Na^+ and HT while less than 10% DIK was dissolved from DIK/Clay in the simulated gastric fluid (SGF) at pH 1.2. Therefore, it is shown that HT does not affect the dissolution behavior of DIK-Na^+. The

increased apparent solubility of DIK from the DIK/Clay can be explained by the following considerations:

1) DIK released in its molecular forms (non-ionized) while HT dissolved rapidly under the acidic conditions. [45]

2) Amorphous- like state of API in the anionic clay interlayer space.

3) Increased wettability of API associated with the anionic nanoclay.[42]

It is to be noted that clays can increase, not only the apparent solubility, but also the API release rate due to their hydrophilic and swelling properties in aqueous solution.[43] Initially, it was expected that DIK/Clay may achieve a sustained API release. However, since HT was dissolved at the low pH medium within 30 minutes (see Appendix C) sustained DIK release was not observed.

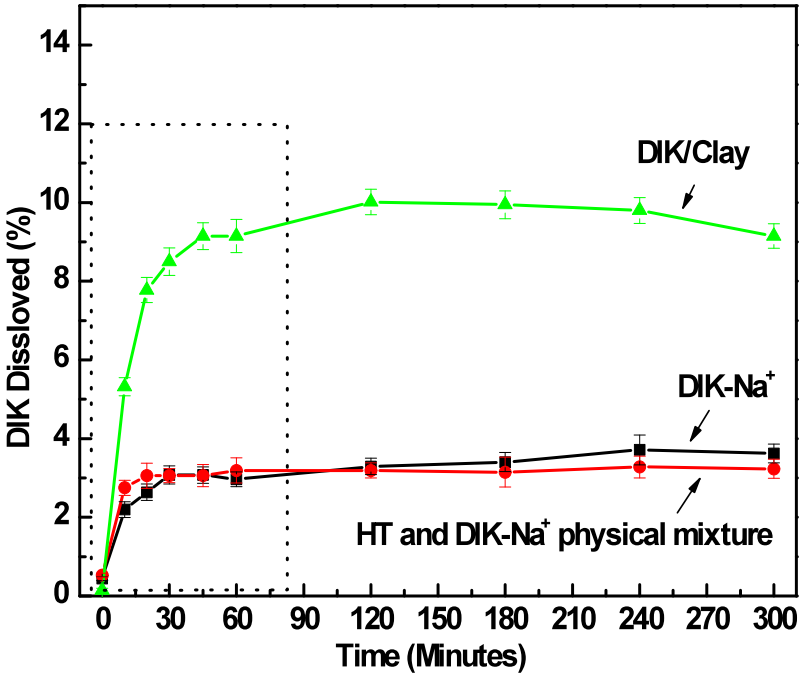

Figure 4.9 Dissolution results in simulated gastric fluid (pH 1.2) of DIK-Na^+, DIK/Clay (containing approximately 40% DIK) and an HT/DIK-Na^+ physical mixture containing 40% DIK-Na^+.

The acidic solution firstly dissolves HT to produce a mixture of $MgCl_2$ and $AlCl_3$ and converts DIK anions into an acid form; the amorphous-like DIK is then exposed to the medium simultaneously. According to the Noyes-Whitney equation[81, 82] the dissolution rate among other parameters is proportional to the total area of the API exposed to the dissolution medium. Therefore, it is not surprising that DIK/Clay shows the highest dissolution rate (Figure 4.10) since, assuming that DIK is in an amorphous state, it is spread over a larger area in the clay interlayer space.

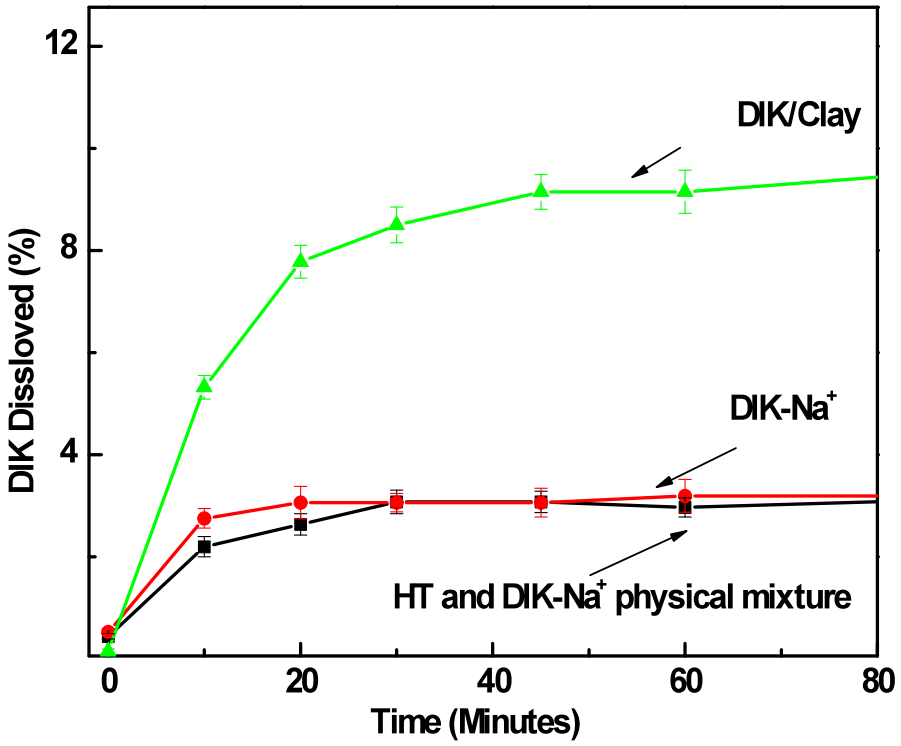

Figure 4.10 Dissolution results of magnified range from Figure 4.9 (pH 1.2).

Figure 4.11 shows the dissolution profile of DIK/Clay in simulated body fluid (SBF) at a 7.4 pH. Since HT does not dissolve in the neutral pH medium, the intercalated DIK anions had to be ion exchanged with the phosphate ions of the medium in order to diffuse out from the clay interlayer.[39] Since this procedure takes time, DIK could be released slowly. However, the DIK release rate at an early stage up to 30 minutes was somewhat faster (dissolution rate: 1.03%/minutes) than the release after 30 minutes. This could provide evidence that DIK is, not only intercalated in the layer space, but is also coating the outside clay surface. Unlike DIK at the interlayer, the DIK at the outside layers will be exposed directly to the medium and will be dissolved immediately.

After 30 minutes and up to 240 minutes, the release rate of DIK slowed down indicating that release from the clay interlayer was dominant (dissolution rate: 0.15%/minutes). Based on Figure 4.11, a rough approximation of the concentration of DIK on the clay surface is 30 wt%. After 240 minutes, the dissolution of DIK/Clay is the slowest. This may be because the precipitated DIK/Clay stacked at the bottom of the vessel even at an agitation speed of 50 rpm, and the inner stacked DIK/Clay was not directly exposed to the medium making diffusion slower. It is shown that DIK/Clay achieved 100% API release after 25 hours. This suggests that the dissolution method can be another method for calculating DIK loading on the clay along with the Elemental Analysis. Note that Figure 4.11 is very similar to Figure 7 in the paper by Ambrogi et al[39] obtained with a different clay and different experimental conditions.

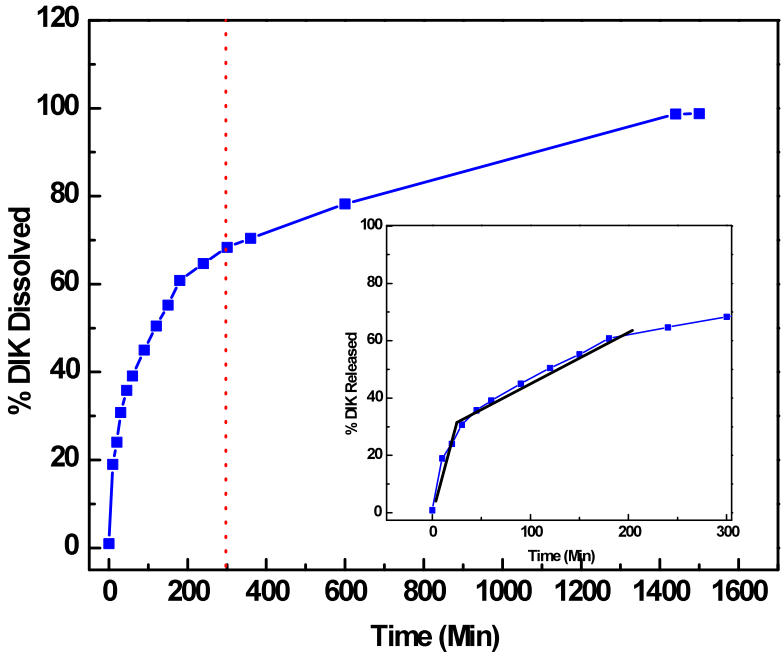

Figure 4.11 Dissolution profiles of DIK/Clay in simulated body fluid (phosphate buffer solution, pH 7.4).

4.1.7 Shelf Stability

For long shelf life pharmaceutical applications, API recrystallization or undesired physicochemical changes need to be minimized. In order to determine an early API release during storage, a 12 month-old DIK functionalized clay was examined by XRD analysis.

As shown in Figure 4.12, peak intensities and peak locations were the same after one day or 12 months following modification. Thus, it appears that the DIK/Clay hybrid can be stored at room temperature without any physical changes.

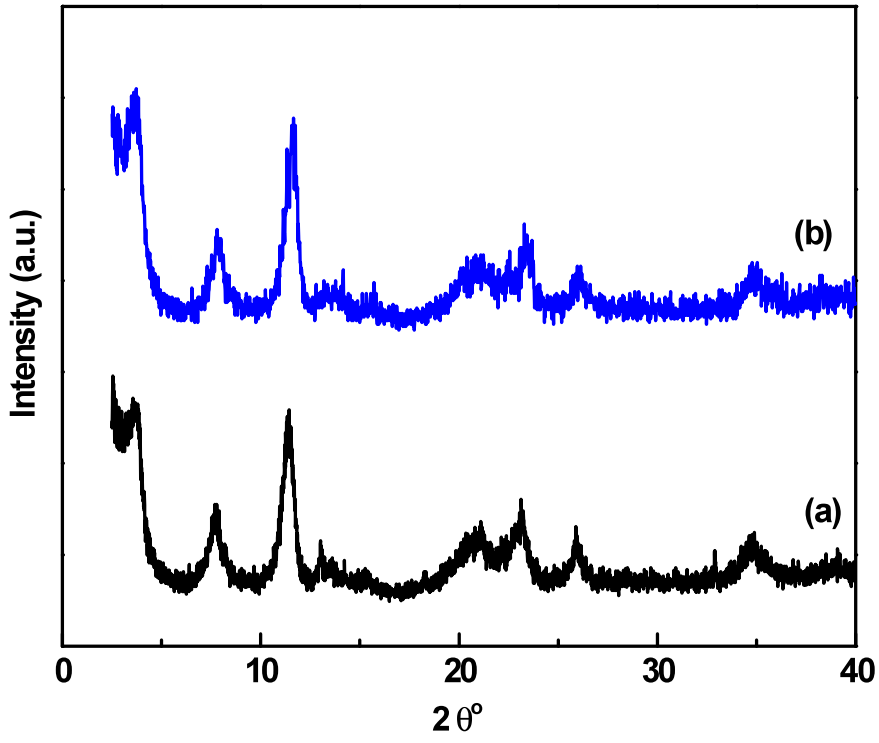

Figure 4.12 XRD results of DIK/Clay (a) 1 day old and (b) 12 months old.

4.1.8 Mechanisms of DIK Release from DIK/Clay at Different pH

API release rates are usually explained by three controlling mechanisms which are diffusion, swelling and erosion.[83, 84] Among other equations, two simple and semi-empirical equations, the Korsmeyer-Peppas model (power law)[54] and the equation developed by Peppas and Sahlin,[85, 86] can be used to describe the API release behavior from a matrix.

The Korsmeyer-Peppas (power law) equation is:

$$\frac{M_t}{M_\infty} = kt^n \qquad \text{(Equation 4.2)}$$

Where M_t and M_∞ are the absolute cumulative amounts of API released at time t and infinite time, respectively, "*k"* is a constant incorporating structural and geometric characteristics of the sample, and "n" is the release kinetics exponent. This "n" value is used in order to differentiate between release mechanisms. The interpretation of "n" value for different diffusion mechanisms is given in Table 4.2.

The heuristic equation developed by Peppas and Sahlin[86] can be used to estimate the effect of API diffusion and polymer erosion on the anomalous transport.

$$\frac{M_t}{M_\infty} = k_1 t^m + k_2 t^{2m} \qquad \text{(Equation 4.3)}$$

Where "k_1", "k_2" and "m" are constants. The first term on the right hand side represents the Fickian diffusional contribution (D), whereas the second term represents the polymer relaxation contribution (R). "m" is geometrical factor (in this case m= 0.5:

disk or film). Equations 4.2 and 4.3 are valid only up to 60 % dissolution ($M_t/M_\infty<0.6$).[87] The ratio of relaxation (R) and diffusion (D) contributions[86, 88] could be calculated as:

$$\frac{R}{D} = \frac{k_2 t^m}{k_1} \qquad \text{(Equation 4.4)}$$

Table 4.2 Interpretation of Diffusional Release Mechanisms from Polymeric Films[87]

Release exponent (n)	Drug transport mechanism	Rate as a function of time
0.5	Fickian diffusion (diffusion dominant)	$t^{-0.5}$
0.5<n<1.0	Anomalous transport (non Fickian diffusion)	t^{n-1}
1.0	Case-II transport* (erosion dominant)	Zero order release
n>1.0	Super Case-II transport**	t^{n-1}

* Case II transport (Case II relaxational release) is the drug transport mechanism associated with stresses and state-transition in hydrophilic glassy polymers which swell or erode in water or biological fluids (non-Fickian).[86, 89]

** Super case - II transport is indicating API release due to the combination of API diffusion and polymer relaxation/dissolution as opposed to simple Fickian diffusion.[90]

Figure 4.13 shows DIK release from DIK/Clay at different pH values of 1.2 and 7.4. Note that the clay is soluble at pH of 1.2 (Appendix C). Table 4.3 shows results calculated from Equations 4.2 and 4.3. The exponent for Equation 4.2 indicates that both systems exhibit anomalous transport. Since the DIK/Clay dissolved very quickly in SGF within 30 minutes, it was anticipated that erosion mechanism would be dominant. From the k_1 and k_2 values of Table 4.3 obtained by regression, the R/ D ratio can be calculated (Equation 4.4) and plotted versus fraction dissolved in Figure 4.14. The results show that for both pH values diffusion dominates over relaxation. However, the R/D ratios in the

pH 7.4 solution are much higher than the ones in the pH 1.2 solution since the clay did not dissolve in the pH 7.4 buffer solution but was able to exchange slowly API anions for buffer anions.

Table 4.3 Dissolution Fitting Results of DIK/Clay at Different pH

System	Power law (Eq. 4.2), $\frac{M_t}{M_\infty} = kt^n$	Peppas and Sahlin (Eq. 4.3), $\frac{M_t}{M_\infty} = k_1 t^{0.5} + k_2 t$	
	n ± 95% CI	k_1 ($min^{-0.5}$) ± 95% CI	k_2 (min^{-1}) ± 95% CI
DIK/Clay at pH 1.2	0.64 ± 0.05	0.11 ± 0.02	0.02 ± 0.01
DIK/Clay at pH 7.4	0.54 ± 0.04	7.78 ± 0.17	0.14 ± 0.01

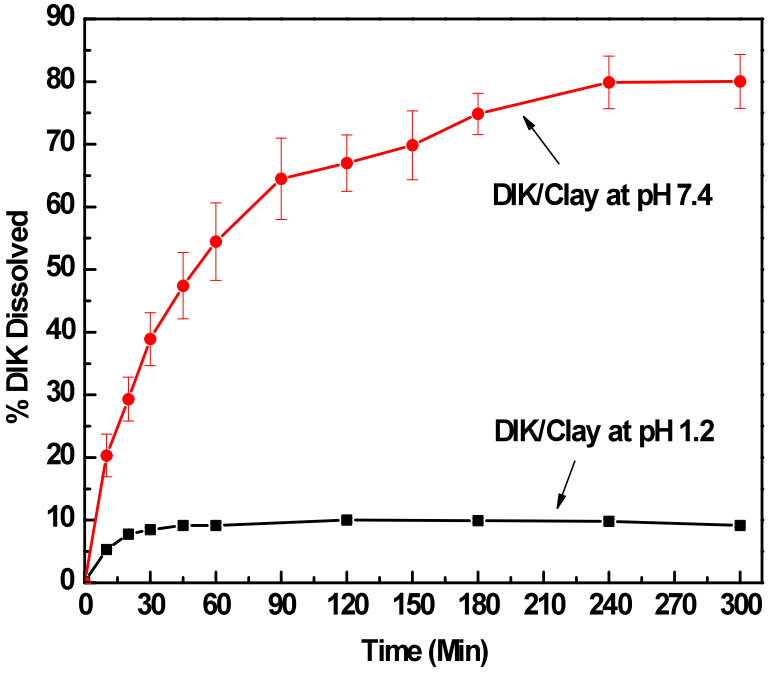

Figure 4.13 DIK dissolution profile from DIK/Clay at pH 1.2 and 7.4.

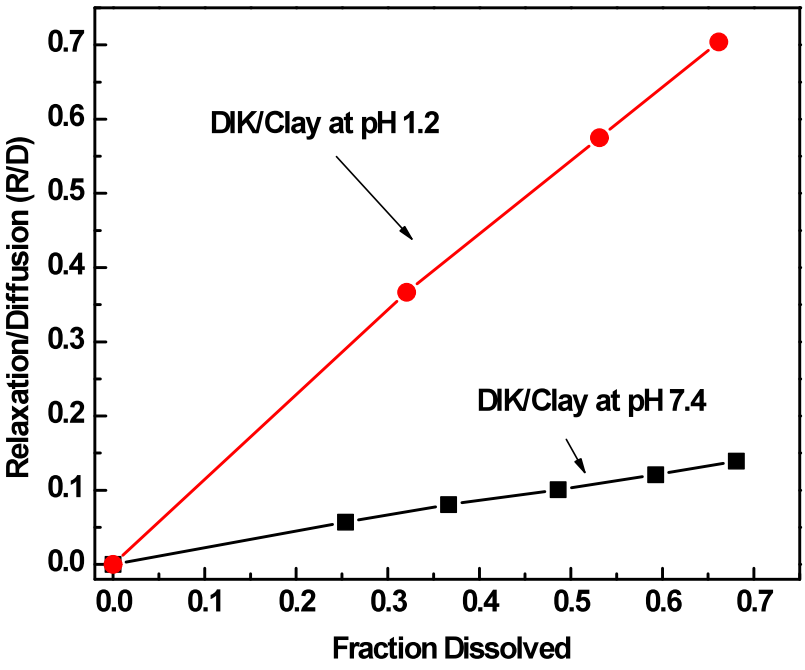

Figure 4.14 R/D ratio values versus fraction dissolved for the DIK/Clay system at different pH of 1.2 and 7.4.

Since both DIK/Clay dissolution profiles from pH 1.2 and 7.4 have a stronger diffusion than relaxation component, dissolution data were fitted to the Fickian model (no erosion) presented earlier which describes API diffusion from a disc.

$$\frac{M_t}{M_\infty} = 4\sqrt{\frac{D_{app}t}{L^2\pi}} \qquad \text{(Equation 2.4)}$$

Since L^2 is initially same for all samples and D_{app} is only dependent on the molecular size of the API and the temperature of release[53], Equation 2.4 can be simplified as Equation 4.5.

$$\frac{M_t}{M_\infty} = Kt^{0.5} \qquad \text{(Equation 4.5)}$$

Figure 4.15 shows dissolution profiles of DIK from DIK/Clay at different pH fitted to Fickian model. DIK release from DIK/Clay at pH 7.4 has larger R^2 value than the one at pH 1.2 since no erosion occurs in this case.

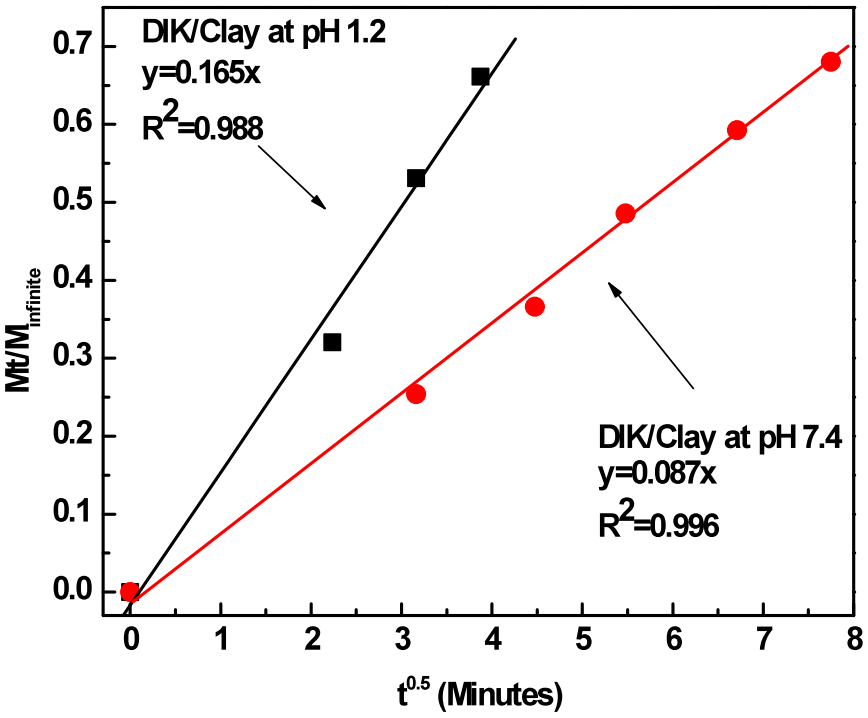

Figure 4.15 DIK release from DIK/Clay as a function of time$^{0.5}$, (■) DIK/Clay at pH 1.2, and (●) DIK/Clay at pH 7.4.

4.2 Characterization of Clay Modified with IND

Before discussing the results on HT modified with IND, it is to be noted that calcined HT appeared to chemically interact with IND as evidenced by FTIR and XRD data obtained up to five days of intercalation reaction. By contrast, such changes were not observed in the CHT modification with DIK. HT interaction with other APIs has also been previously reported.[33, 91, 92] Therefore, the practical pharmaceutical applications of the IND/Clay system would require further studies. In this section, the reported results are based on the IND/Clay, three days after the modification reaction, since after this time significant differences were observed in the FTIR spectra of the IND/Clay as compared to the pure IND.

4.2.1 FTIR Results

FTIR spectra of IND, HT and IND/Clay are shown in Figure 4.16. Generally, the methoxy group attached to the aromatic ring has a sharp isolated band near 2835 cm^{-1}.[93] The aromatic C-H stretching vibrations give rise to multiple bands in the region 3100 - 3000 cm^{-1}.[70] In substituted benzene ring compounds the C-H out of plane bending vibrations give rise to bands in the region 1000-700 cm^{-1}. Indole absorbs near 1460, 1420, and 1350 cm^{-1}.[70] The NH stretch in indole causes absorption at 3400-3100 cm^{-1}.[70]

In Figure 4.17, the sharper peak at 1692 cm^{-1} shifted to 1681 cm^{-1} and became slightly broader, which indicates that the original γ-form was converted to the metastable α-INM. The peaks at 1591 cm^{-1} and 1545 cm^{-1} (Figure 4.17 (c)) may be due to the carbon-carbon interaction within the benzene ring. Five-membered ring compounds generally show three ring stretching bands near 1590, 1490 and 1400 cm^{-1}.[70] FTIR peaks of IND/Clay are shifted slightly to a different wavenumber as compared to IND. This

suggests possible interactions of IND with the clay. Similar FTIR spectra were also obtained by Del Arco et al[46] who ascribed the shifting of the peaks to the presence of ionized IND in the clay interlayer.

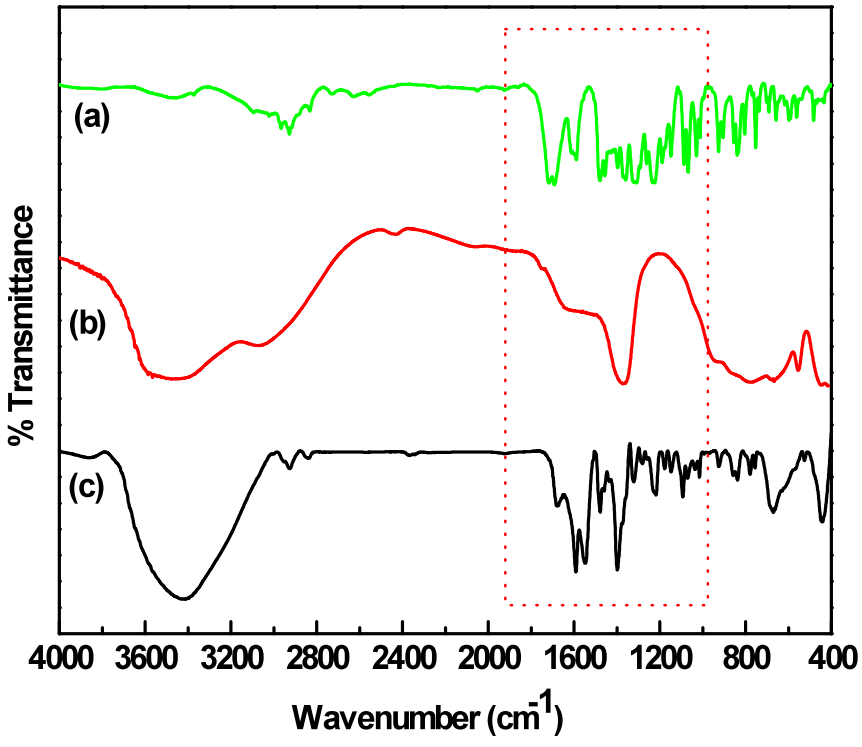

Figure 4.16 FTIR results of (a) IND, (b) HT, and (c) IND/Clay.

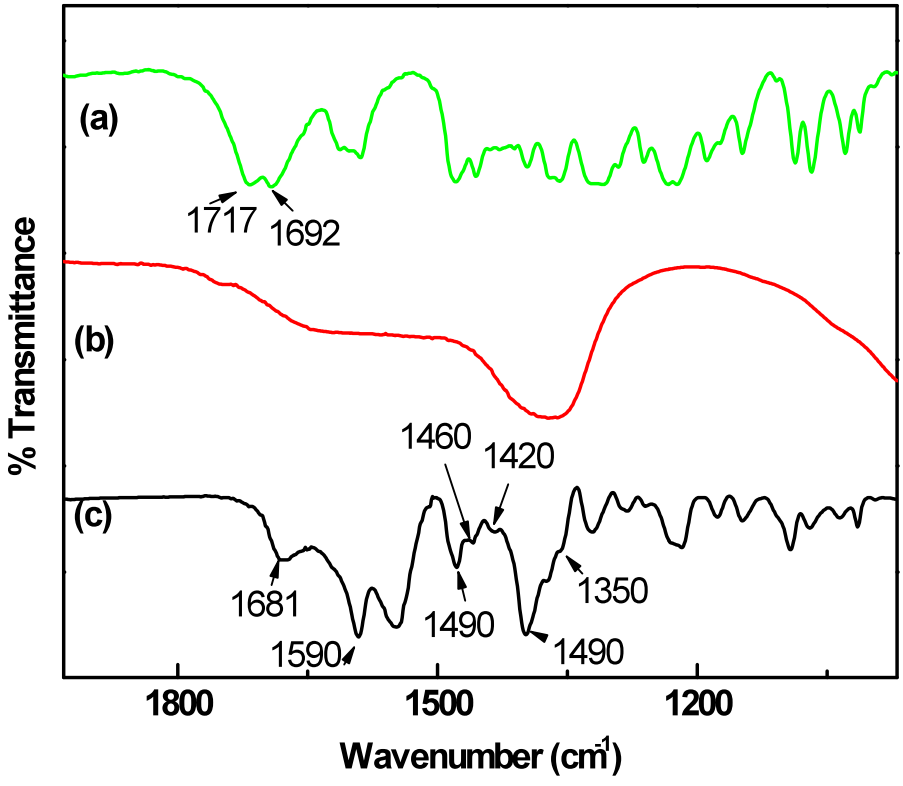

Figure 4.17 Magnified FTIR results from Figure 4.16.

4.2.2 Thermal Analysis

From the TGA analysis (Figure 4.18), the content of IND in the nanoclay can be calculated. Since IND/Clay lost approximately 10 wt% at 150 ^{o}C due to moisture, the 30% weight loss between 230 ^{o}C and 500 ^{o}C can be ascribed to the IND loading in the clay. This rough approximation matches the IND loading calculated from elemental analysis (Table 4.4).

DSC results (Figure 4.19) show a sharp melting temperature (T_m) for IND. However, similarly to the DIK/clay system no transition is shown for the IND/Clay

around the IND T_m. Similar results were observed by Ambrogi et al.[94] who explained that the absence of the IND melting temperature was due to a new compound that was formed by intercalation of IND; however, it may also be due to the amorphous state of IND in the clay interlayer space as was also shown in the case of DIK/Clay.

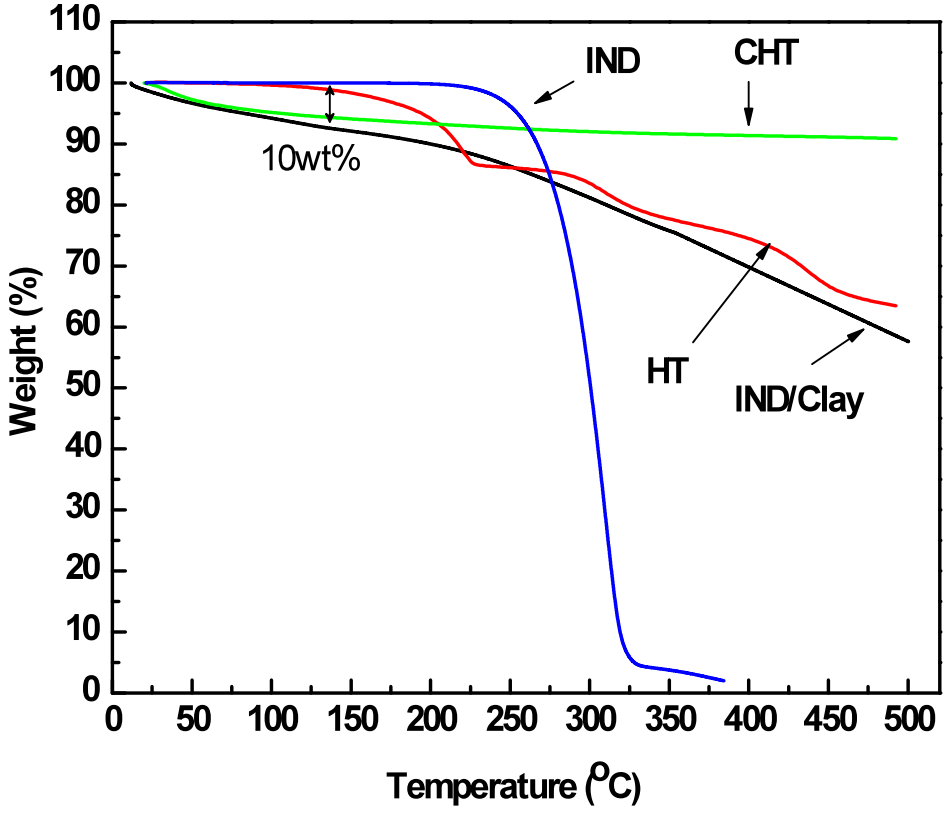

Figure 4.18 TGA results of HT, CHT, IND, and IND/Clay.

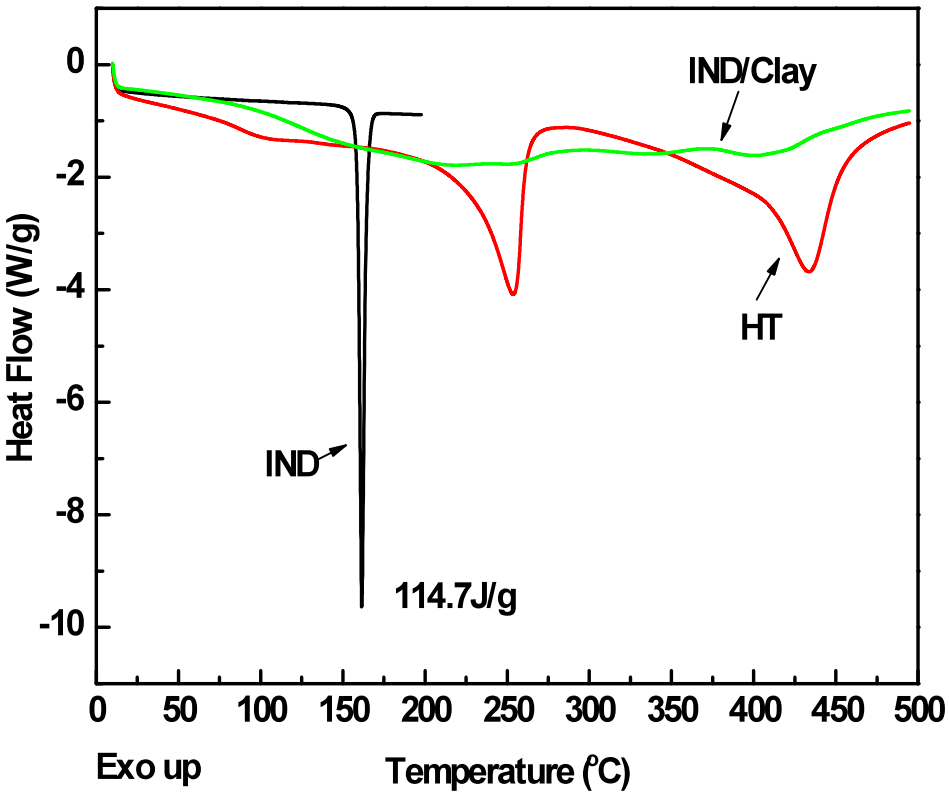

Figure 4.19 DSC heating results of IND, HT, and IND/Clay.

4.2.3 XRD Results

XRD results (Figure 4.20) indicate that IND is intercalated into the clay interlayer. However, the increase in the interlayer spacing is not larger than that of DIK/Clay (calculated spacing is 1.91 nm vs. 2.39 nm). The molecular size of IND end to end based on its MW and its simulated chemical structure (Figure 3.2) is larger than that of DIK. Therefore, it appears that IND may exist in an interdigitated state in the interlayer space.[39] Also, the peaks (*003*) and (*006*) in Figure 4.20 (c) shifted towards lower angles showing that during the regeneration process of HT, IND successfully expanded the clay

interlayer structure. However, it appears that the original crystalline structure has been modified transformed to a different one since the intensity of the (*006*) peak is reduced and became broader. The third peak that is present in the DIK/Clay spectrum (Figure 4.3) is absent since there are no higher harmonic clay layers. Del Arco et al[46] obtained a different XRD spectrum which has more pronounced crystalline peaks (*003*) and (*006*). Their different spectra may be attributed to differences in the pH of the solution during the clay modification.

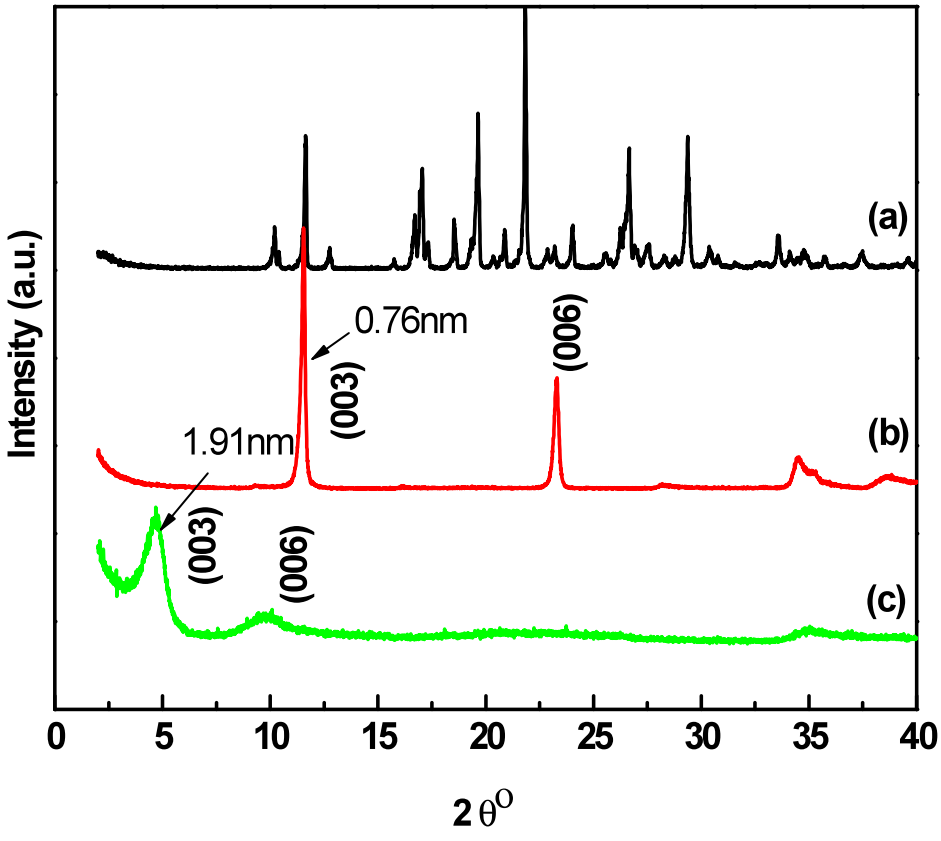

Figure 4.20 XRD results of (a) IND, (b) HT, and (c) IND/Clay.

4.2.4 Quantitative Analysis of IND/Clay

The indomethacin loading of IND/Clay was determined by elemental analysis (Table 4.4) as in the case of DIK/Clay. Calculated IND loading on modified clays based on carbon and nitrogen are 33.6 % and 30.8 %, respectively (See Appendix B). Therefore, it is assumed that roughly 30 % of the API has been loaded in the clay. These loadings are slightly lower than those of the DIK/Clay possibly due to differences in reaction time, molecular structure, and preparation methods.

Table 4.4 Results of IND/Clay Elemental Analysis

Material	% Carbon	% Nitrogen
HT*	4.0	0.0
CHT*	0.0	0.0
IND*	63.7	3.9
IND/Clay**	21.4	1.2

* calculated
** experimental

4.2.5 Dissolution Test

IND dissolution profiles from the HT interlayer spacing and possibly from the HT surface as well are shown in Figure 4.21. IND alone shows almost zero solubility in the simulated gastric acid at a pH of 1.2. However, the dissolution data from the IND/Clay interlayer and possibly from the clay surface suggest higher solubility. As discussed earlier in the DIK/Clay section, increased solubility can be ascribed to increased wettability or the presence of IND in an amorphous state.

IND/Clay has different dissolution profile than DIK/Clay. While DIK/Clay showed a fast DIK dissolution, IND/Clay shows a somewhat slower IND dissolution

pattern. For example, the DIK in the DIK/Clay achieved its maximum solubility in the simulated gastric medium within an hour. On the other hand, IND in the IND/Clay achieved 50% of its maximum solubility within an hour. These different rates of dissolution could be explained by differences in the microenvironmental pH[28] since DIK-Na^+ could increase the pH while IND would tend to decrease it. In order to test this hypothesis, a simple experiment was carried on. 80 mg each DIK/Clay and IND/Clay, each, were added separately into 100 ml of SGF and the pH was measured. As expected, DIK/Clay increased the pH from 1.21 to 1.31 within 5 minutes while IND/Clay changed the pH to only 1.23. Although these pH differences appear not to be significant, they may be important in a microenvironment.

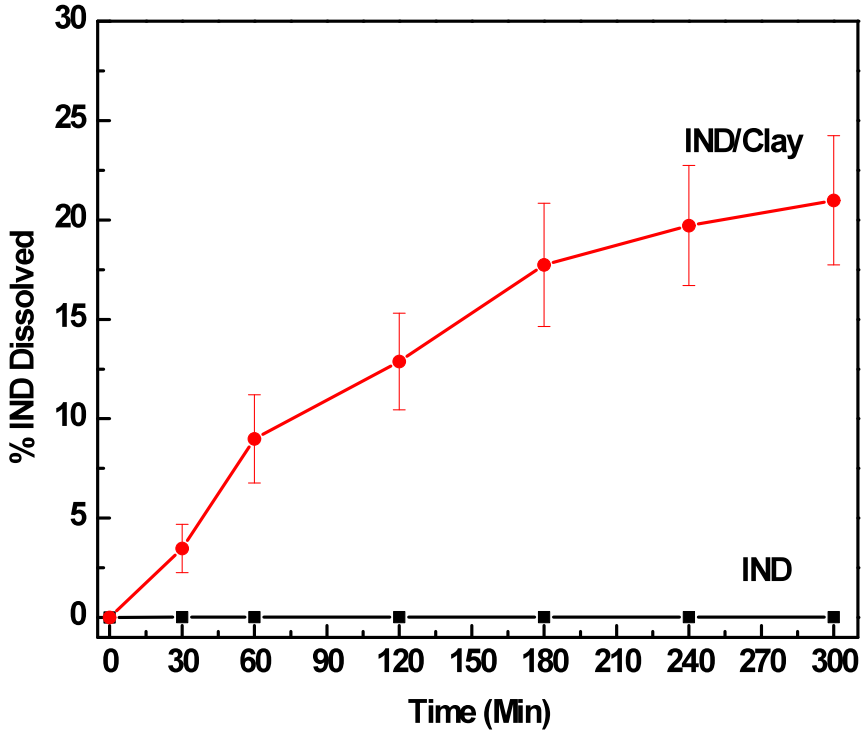

Figure 4.21 Dissolution results of IND/Clay and IND in simulated gastric fluid (pH 1.2).

4.2.6 Stability of IND during Reaction with CHT

In the introductory section 4.2, it was noticed that the stability of IND during its reaction with CHT appeared to be an issue as a result of possible adverse chemical reactions. The IND intercalation into the HT interlayer space, was carried out for 5 days, and FTIR and XRD spectra were obtained every day. Although the reaction after 1 day does not show a carbonate peak, which may have indicated the success of the IND intercalation (Figure 4.22), XRD results (Figure 4.23) do not show any IND intercalation peak. After 2 days there is still no XRD intercalation peak, although the FTIR spectra show some changes (Figure 4.22). Thus, it appears that up to 2 days of reaction, IND was not intercalated into the CHT interlayer space but was rather absorbed on the clay surface. On the other hand, XRD results after 3 days show the IND intercalation peak. After 3 days and up to 5 days FTIR results show significant peak shifting and changes that could be the result of other interactions between CHT and IND. A possible scenario is that IND degrades into 5-methoxy-2-methylindole acetic acid and p-chlorobenzoic acid in the presence of the strongly alkaline CHT as shown in Figure 4.24.[95] The degradation of IND in the presence of hydroxide ions has also been previously reported.[95]

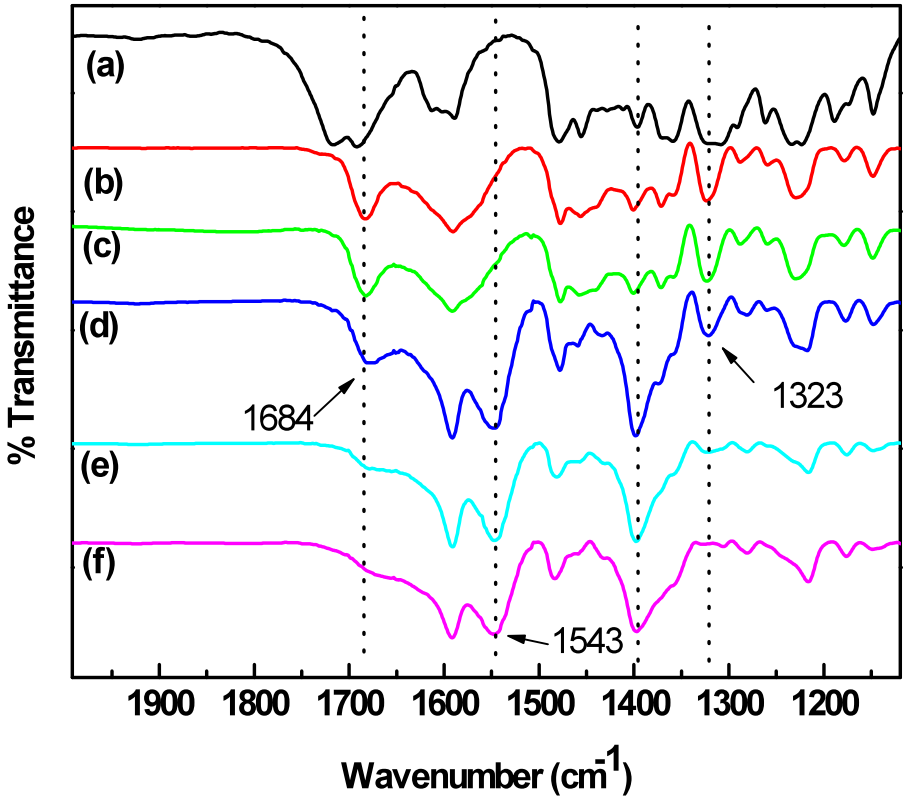

Figure 4.22 FTIR spectra during the IND/CHT reaction: (a) IND, (b) IND/Clay (1 day), (c) IND/Clay (2 days), (d) IND/Clay (3 days), (e) IND/Clay (4 days), (f) IND/Clay (5 days).

Interpretation of the FTIR spectra presents several challenges. Figure 4.22 shows the FTIR peak shifting for the IND reaction with CHT at different reaction times. Shifts occurred around 1684 cm^{-1}, 1543 cm^{-1}, and 1323 cm^{-1}. The peaks at 1717 cm^{-1} and 1692 cm^{-1} indicate the C=O of γ-IND. These peaks were combined together, as reaction proceeded, to one peak at 1684 cm^{-1} corresponding to the C=O peak of amorphous IND. Finally the peak at 1684 cm^{-1} disappeared as the reaction proceeded.

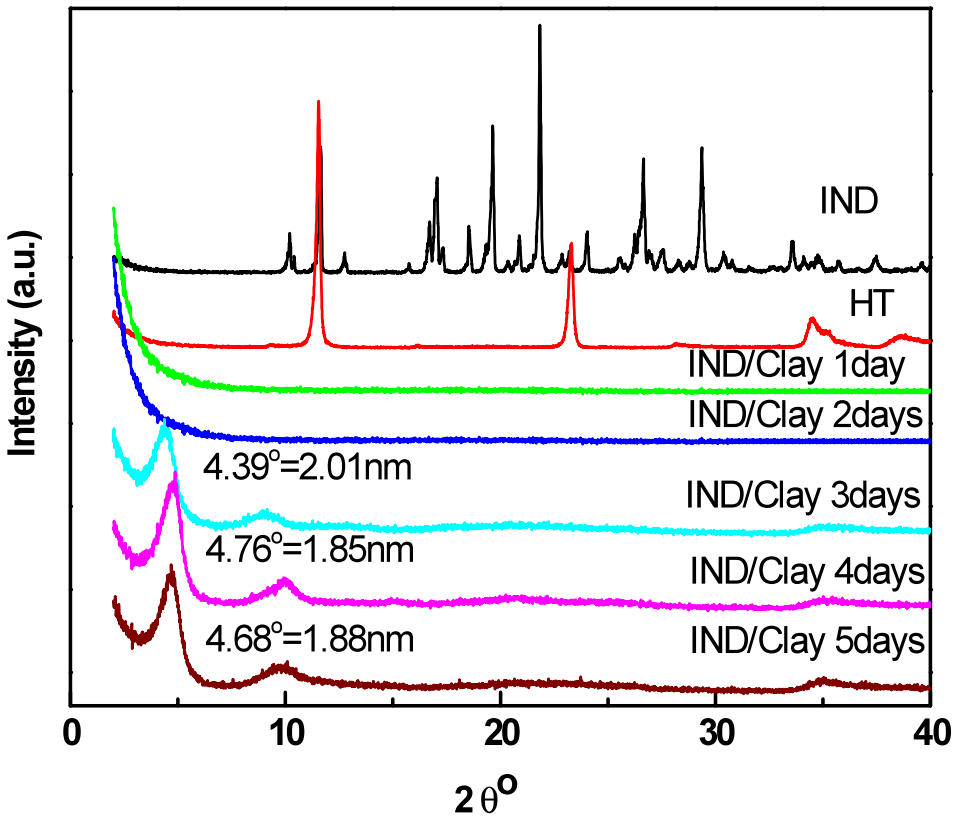

Figure 4.23 XRD results of IND/Clay at different reaction times.

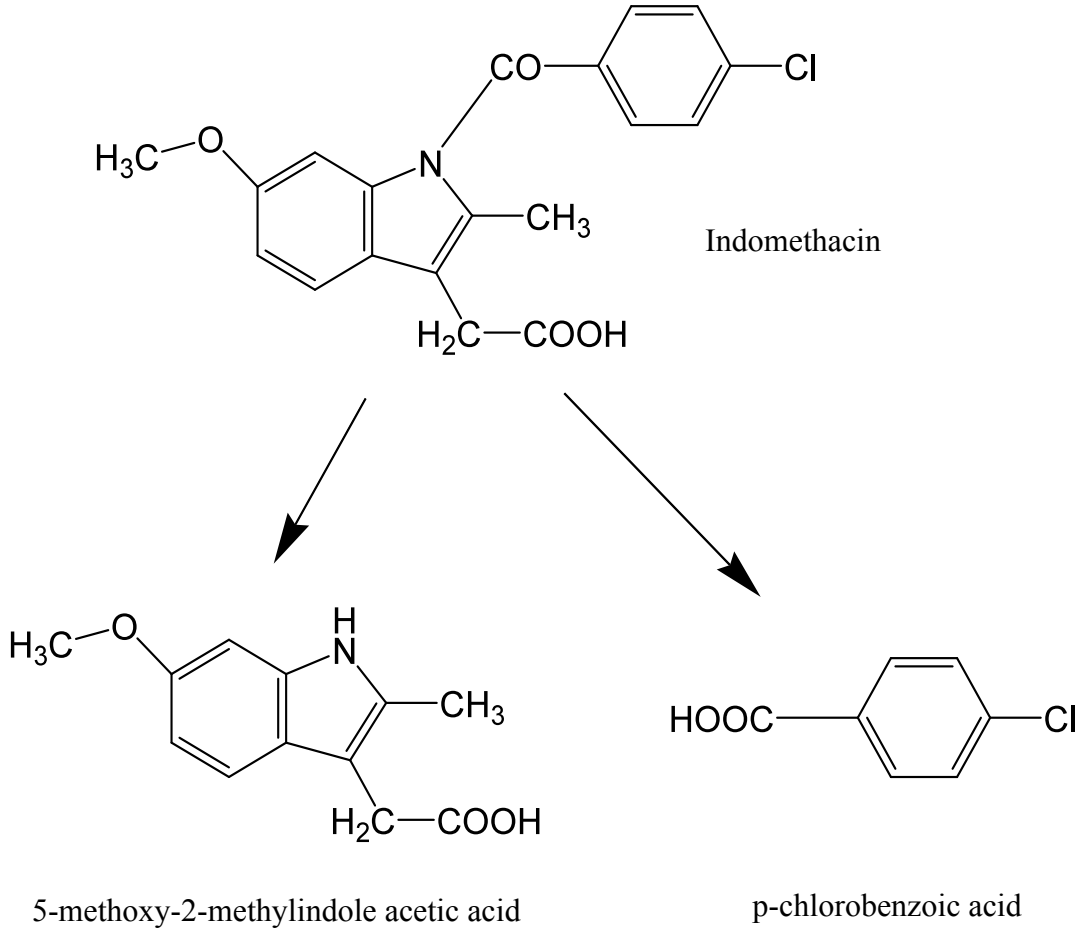

Figure 4.24 Schematic of the possible IND degradation in alkaline pH.[95]

4.3 Conclusions

Anionic nanoclay was successfully intercalated by both APIs. DIK/Clay showed increased interlayer spacing vs. pure HT and relatively well ordered clay crystallinity while IND/Clay showed increased interlayer spacing but reduced crystallinity. Calculated DIK and IND loadings in the clay were roughly 40 wt% and 30wt%, respectively. The different API loadings are due to the different experimental conditions used. DIK/Clay showed less tendency to agglomeration than the unmodified clay. API released from DIK/Clay showed not only increased apparent solubility and dissolution rate than DIK-Na^+ in SGF but also sustained API release in SBF. Increased solubility and dissolution rate in SGF might be due to a) non ionized form of API and rapid dissolution of HT, b) the amorphous state of DIK in the clay interlayer space and c) increased wettabililty. Sustained API release from DIK/Clay in SBF can also be an indication of intercalated API, whereas fast release at the initial stages is due to the presence of DIK coating on the clay. The Korsmeyer-Peppas (Power law) and the Peppas and Sahlin equation predicted the API dissolution mechanism from the nanoclay. DIK dissolution from the modified clay in different pH media showed that diffusion was the dominant mechanism although its magnitude differed among the two different pH buffers used. API dissolution from the clay showed a good fitting with Fickian diffusion. Chemical interactions that might correspond to API degradation during intercalation were not observed in the DIK/Clay but were observed in the IND/Clay systems. The latter system needs further analysis in order to understand the reason for the structural changes of IND.

CHAPTER 5

API/POLYMER SYSTEMS PREPARED BY MELT AND SOLUTION MIXING

In this Chapter, API-polymer miscible and immiscible systems are compared in order to distinguish between the properties of solid solutions and solid dispersions and their effects on API release. The miscibility of the systems was initially determined by comparing the solubility parameters of APIs and polymers. IND and DIK-Na^+ in the water soluble Eudragit® E100 and Eudragit® S100 acrylic copolymers were selected as examples of API-polymer miscible and immiscible systems, and compared for their dissolution profile. API miscibility and morphology in the polymer matrix were determined by XRD and SEM. FTIR spectroscopy, TGA, DSC, and UV-Vis were used for further analysis. The API/ organic polymer systems are compared with the system discussed in chapter 4 where the matrix is an inorganic nanoclay.

5.1 Results on DIK-Na^+ Compounded with Eudragit® E100

Based on solubility parameter calculations, (Chapter 3), DIK-Na^+ would not be miscible with Eudragit® E100 but rather be dispersed in the polymer matrix. A schematic of API dispersion in a polymer is shown in Figure 5.1. The API can form smaller particles by melt mixing as a result of strong shear forces or it can be agglomerated and form larger particles if the compatibility between API and polymer is poor.

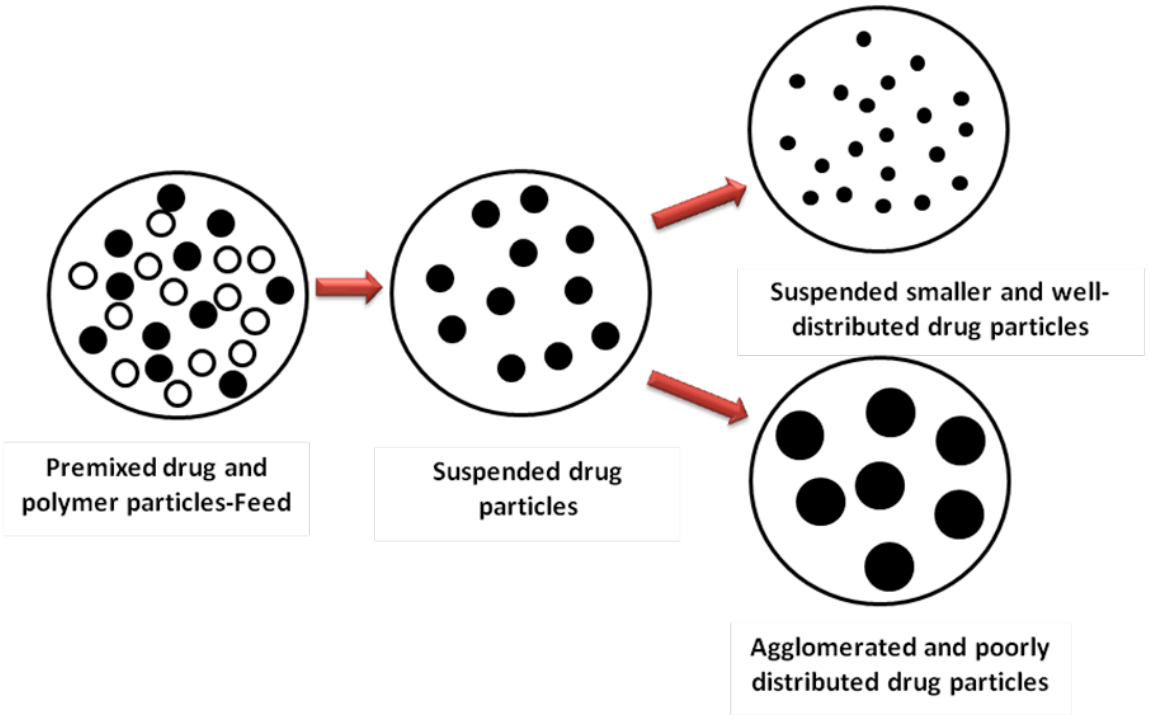

Figure 5.1 Schematic of dispersion of insoluble solid API particles in polymer matrix.[96] (Figure modified from Gogos and Wang, Evonik Workshop 2009)

5.1.1 FTIR Analysis

FTIR spectra of Eudragit® E100/DIK-Na^+ composites and their components are shown in Figure 5.2. Arrows indicate peaks due to the presence of DIK-Na^+. It should be noted that Eudragit® E100 contains similar functional group as DIK-Na^+ such as carboxyl group, methyl, and methylene groups. Therefore, many characteristic peaks are overlapping and difficult to identify. Although it may be possible that there are weak molecular interactions between the API and the polymer, FTIR spectra do not provide any such indications since no peak shiftings are observed.

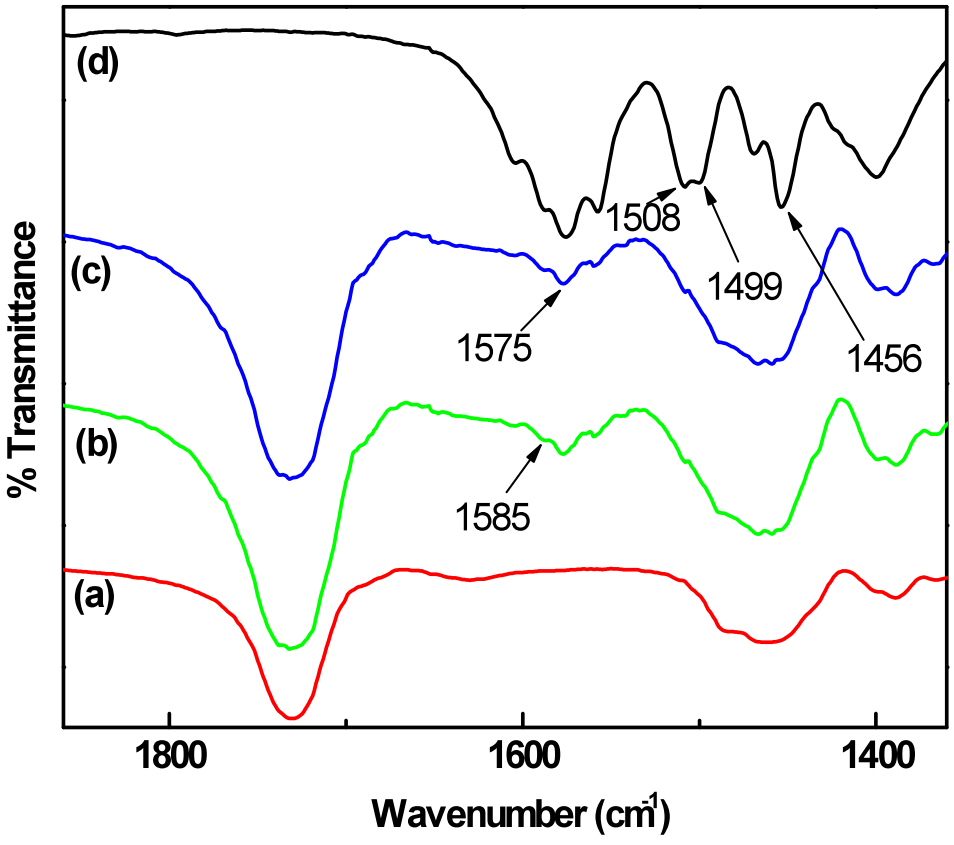

Figure 5.2 FTIR spectra of (a) Eudragit® E100, (b) Eudragit® E100/4wt% DIK-Na^+, (c) Eudragit® E100/15wt% DIK-Na^+, and (d) DIK-Na^+ (samples prepared by batch mixer).

5.1.2 Thermal Analysis

Figure 5.3 shows TGA results for the API, Eudragit® E100 and the polymer containing 4 wt% and 15 wt% of API. DIK-Na^+ starts losing weight at about its melting point (283 ^oC) followed by the unfilled polymer (about 250^oC). In the case of the polymer composites containing API, the onset of degradation temperature is reduced with increasing DIK-Na^+ loading. This decreased thermal stability may be due to catalytic interactions between DIK-Na^+ and the polymer at the higher temperatures. It should be noted that melt mixing

was carried out at 130 ^{o}C, well below the melting point of the API, but above the reported T_g of the polymer (48^{o}C). As a quantitative comparison of thermal degradation, the temperature corresponding to 10 wt% loss is used to rank the materials in terms of thermal stability: DIK-Na^+ > Eudragit® E100 > Eudragit® E100/4wt% DIK-Na^+ >Eudragit® E100/ 15wt% DIK-Na^+.

The thermal decomposition activation energy, E_a, of Eudragit® E100, and Eudragit® E100/ 4 wt% and 15 wt% can be calculated based on TGA data. In general, E_a is associated with the lowest energy needed for degradation and, thus, high E_a indicates high thermal stability. In order to further quantify differences in thermal stability, the Friedman technique was applied into the TGA results.[97] The E_a values calculated by this method represent the thermal decomposition behavior in the temperature range from (onset degradation temperature minus [20 - 40] K) to the onset degradation temperature, in which the linear relation between ln(dα/dt) and 1/T (Equation 5.1) is available.[97]

$$\ln\left(\frac{d\alpha}{dt}\right) = \ln(Z) + n\ln(1-\alpha) - \frac{E_a}{RT} \qquad \text{(Equation 5.1)}$$

Where α is the weight loss of the polymer undergoing degradation at time t, Z is a frequency factor, and T is temperature in K. In plotting the TGA data, the selected temperature range was from about 240 ^{o}C to 280 ^{o}C where the initial degradation occurred for each sample. It is recognized that by comparison to the processing temperature of 130 ^{o}C. This is a very high temperature range and perhaps unrealistic. However, it represents another means to rank the thermal stability of the polymer and

each composite. The calculated E_a values from Figure 5.4 are 2.267×10^3 kJ/mol, 1.984×10^3 kJ/mol, and 1.531×10^3 kJ/mol for Eudragit® E100, Eudragit® E100/ 4 wt% DIK-Na^+ and Eudragit® E100/15 wt% DIK-Na^+, respectively, suggesting that Eudragit® E100 has the highest thermal stability and the thermal stability decreases with increasing loading of DIK-Na^+, in agreement with the 10 wt% loss ranking above.

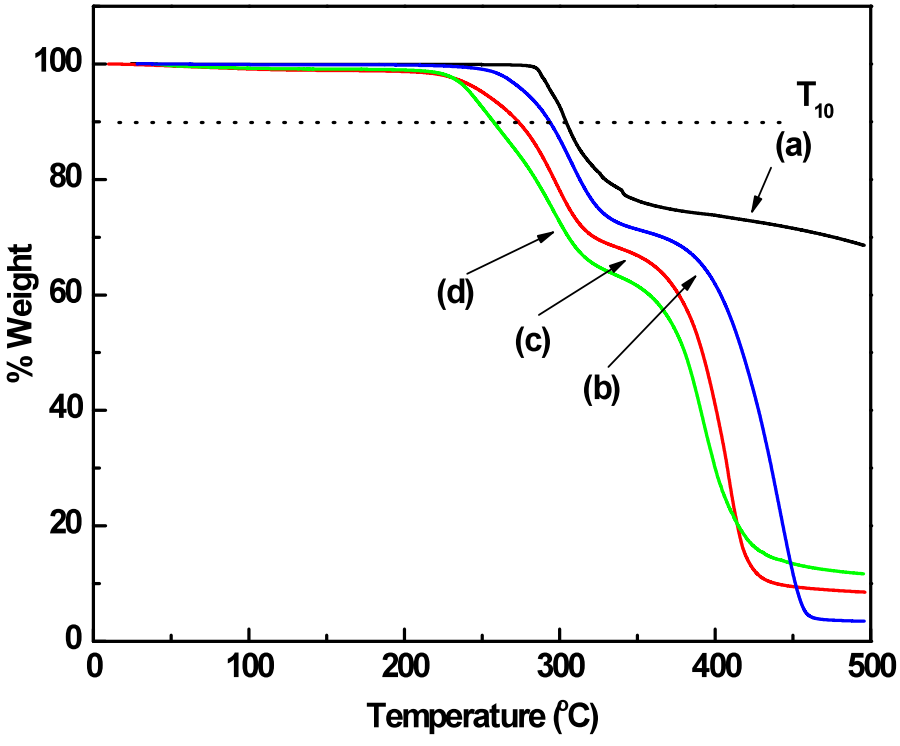

Figure 5.3 TGA results of (a) DIK-Na^+, (b) Eudragit® E100, (c) Eudragit® E100/4wt% DIK-Na^+, and (d) Eudragit® E100/ 15wt% DIK-Na^+ (Samples prepared by batch mixer)

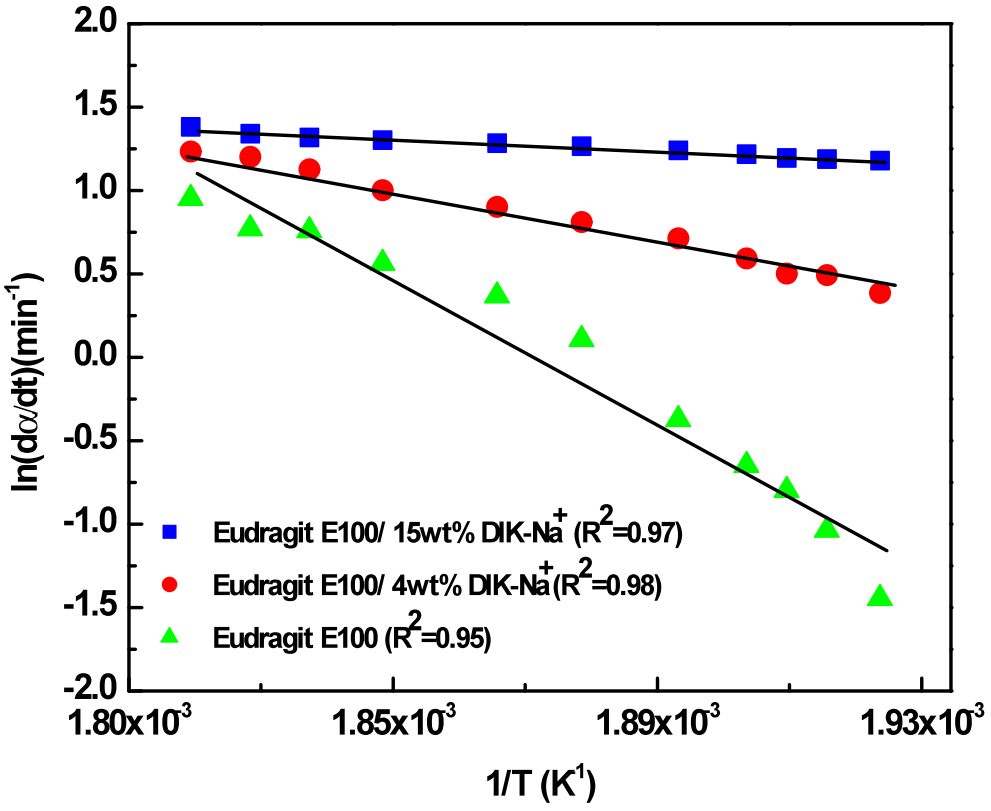

Figure 5.4 Friedman plots of ln(dα/dt) versus 1/T for the direct calculation of E_a of thermal degradation at a heating rate of 20 °C min under N_2 (Eudragit® E100/DIK-Na^+ composites) (Samples prepared by batch mixer).

The glass transition temperatures of Eudragit® E100 and its composites by DSC are shown in Figure 5.5. The T_g values of the composites are slightly higher than that of the unfilled polymer but the difference between the two API loadings is not significant. Glass transition temperatures of these systems vary from 43 °C to 47 °C (Table 5.1). Since as will be shown below this API-polymer combination forms a solid dispersion, the T_g increase would be analogous to that found in composites where the mobility of polymer segments is limited by the presence of the thermally stable at that temperature API.[98]

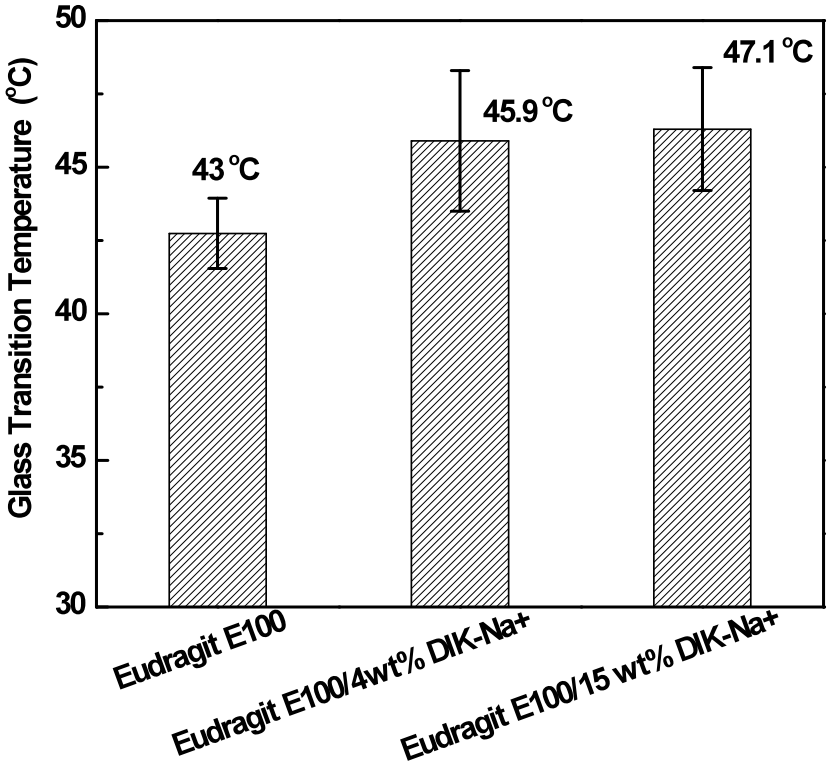

Figure 5.5 Glass transition temperature data of Eudragit® E100 and its DIK-Na^+ composites (Samples prepared by batch mixer).

5.1.3 XRD Analysis.

Figure 5.6 shows XRD results of DIK-Na^+, Eudragit® E100 and its composites containing 4 wt% and 15 wt% DIK-Na^+. DIK-Na^+ shows many sharp peaks through the entire scanned range, an indication of high crystallinity. Strong crystalline peaks located at 6.67^o and 8.65^o, whose intensity increased with increasing DIK-Na^+ loading, appear also in the spectra of the composites. Thus, it is evident that after hot melt mixing DIK-Na^+ remains dispersed in a crystalline form.

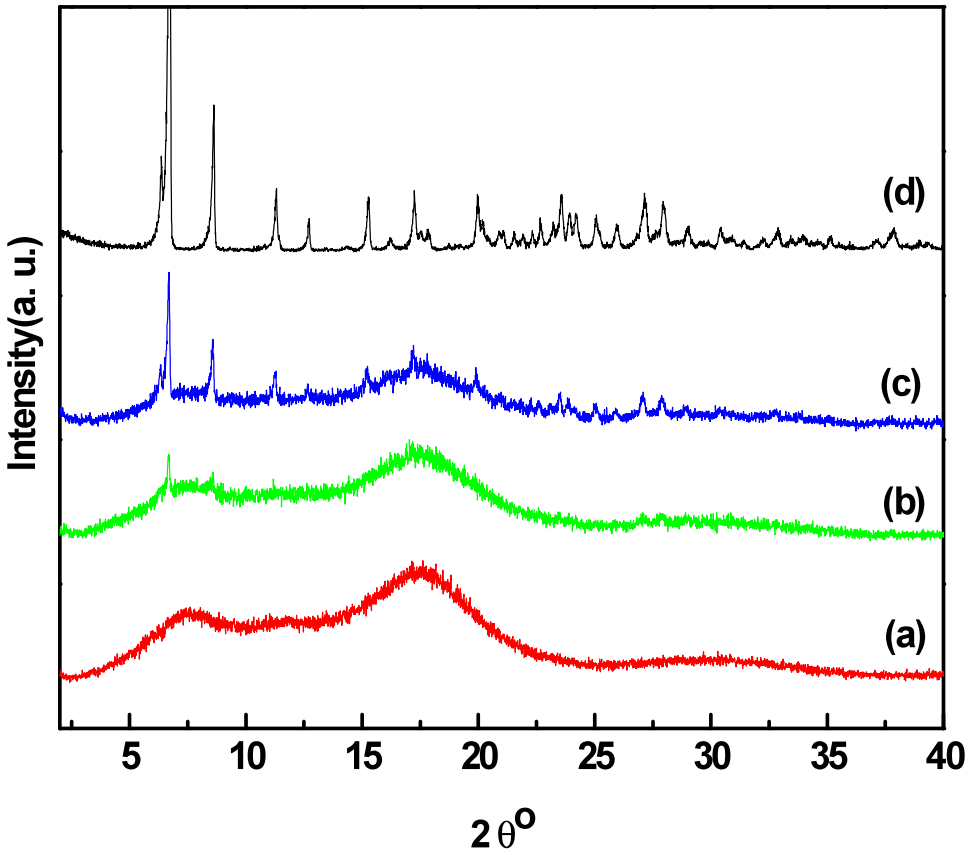

Figure 5.6 XRD results of (a) Eudragit® E100, (b) Eudragit® E100/ 4wt% DIK-Na^+, (c) Eudragit® E100/15wt% DIK-Na^+, and (d) DIK-Na^+ (Samples prepared by batch mixer)

5.1.4 Morphology of DIK-Na^+/ Eudragit® E100 Systems

Analysis of some SEM images of API polymer composites was carried out in order to obtain a general idea of the API dispersion in the matrix. It is recognized that more detailed analysis is required to fully confirm its dispersion state in the matrix. Figure 5.7 (a, c, d) contains selected SEM images showing DIK-Na^+ particles dispersed in the polymer matrix; Figure 5.7 (b) confirms the location of the DIK-Na^+ particles through EDX chlorine mapping images. It is clear that DIK-Na^+ was not dissolved into the

polymeric excipient during melt mixing, but it was rather dispersed in what appears to be agglomerated particles ranging in size from 5 to 50 μm. Previously analyzed by the laser diffraction method, the DIK-Na^+ particle size distribution varied from 1 μm to 40 μm (Figure 5.8). Therefore, it appears that the API became somewhat more agglomerated during the mixing process. This could be due to lack of compatibility between polymer and API and inadequate stabilization of the resulting dispersion toward coalescence.

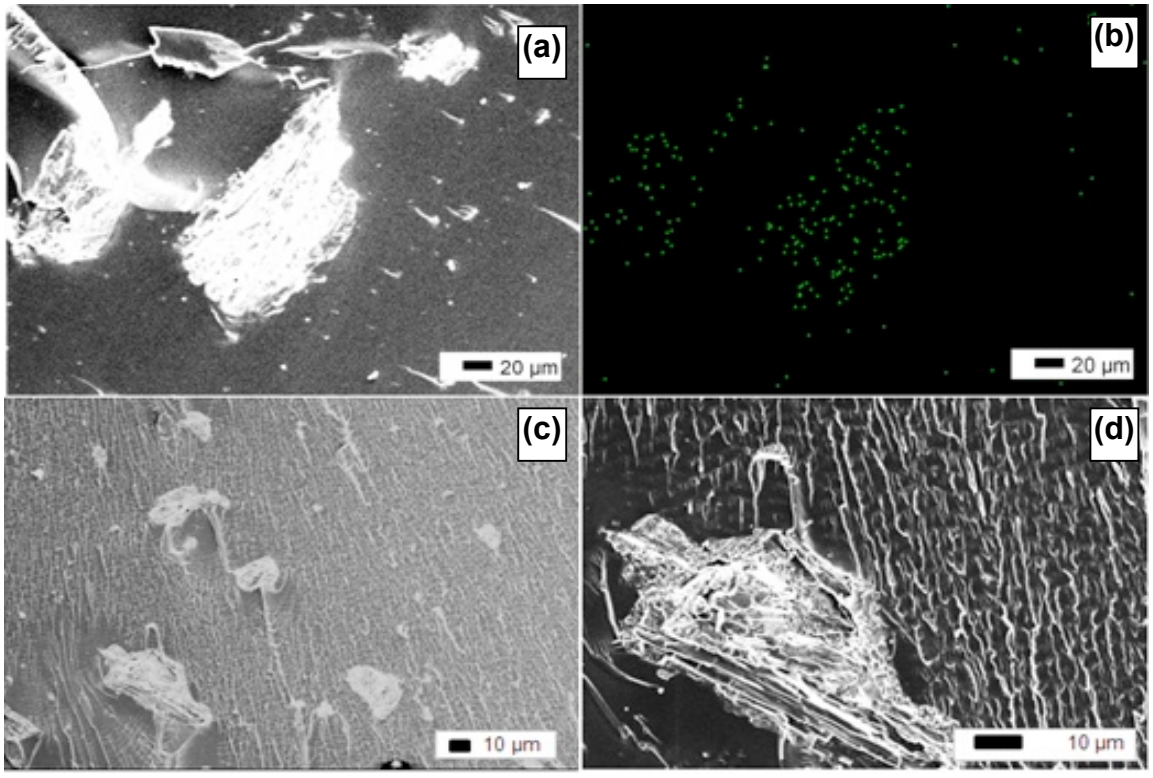

Figure 5.7 SEM images of 4wt% DIK-Na^+ in Eudragit® E100 (a), (c), and (d), and chlorine EDX mapping (b) at the same location as in Figure (a) (Samples prepared by batch mixer).

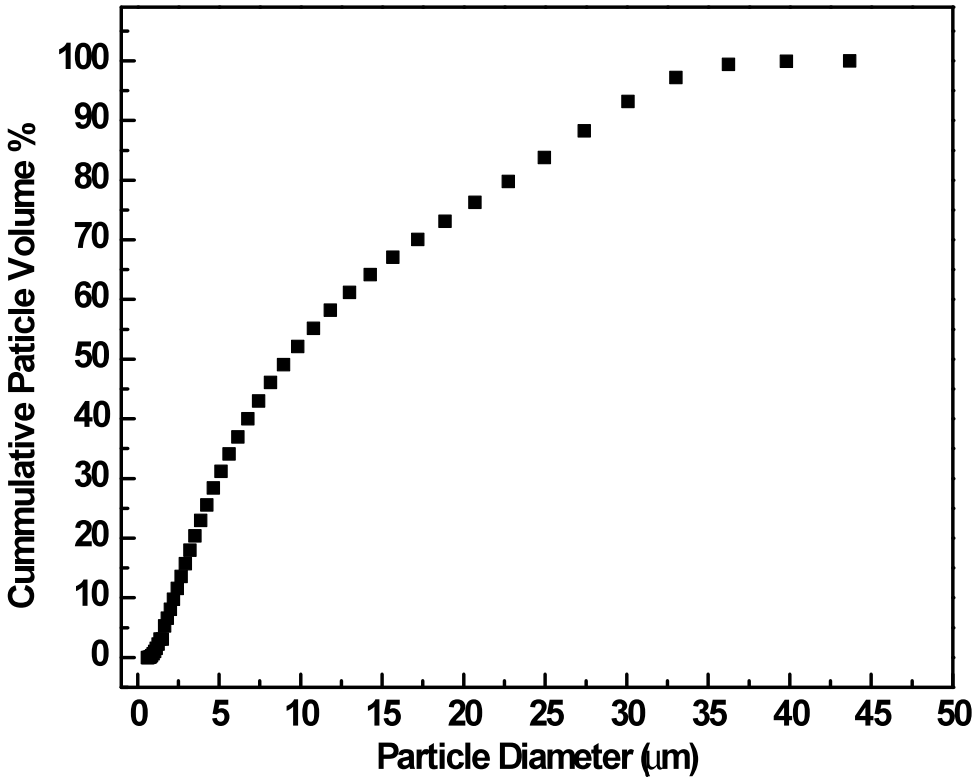

Figure 5.8 Particle size distribution of DIK-Na^+.

Under the polarized light microscopy, the crystalline particles are much brighter than the amorphous matrix. As a result, the dispersed API crystalline particles can be easily distinguished (Figure 5.9), a further confirmation of the formation of a solid dispersion.

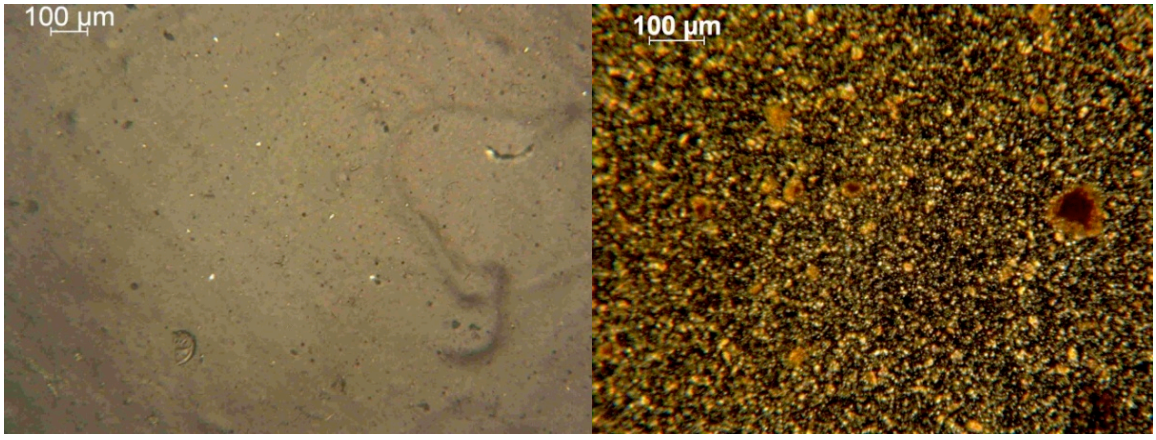

Figure 5.9 Images from polarized light microscopy: (left) unfilled Eudragit® E100, (right) Eudragit® E100/ 4wt% DIK-Na^+.

5.1.5 Rheological Study

Since DIK-Na^+ does not dissolve in Eudragit® E100 during melt processing it was expected that it would act as a filler in the polymer matrix thereby increasing its viscosity. Figure 5.10 and Table 5.1 show RMS results of Eudragit® E100/DIK-Na^+ composites at 130^{o}C. As expected, viscosity as well as G′ and G″ increased with increasing DIK-Na^+ loading. All specimens show shear thinning as the shear rate increased. The effect of increasing DIK-Na^+ concentration on shear viscosity is more pronounced at low shear rates. This is because the yield effect due to the formation of structured networks is frequently encountered at low shear rates and at high loadings of sub-micron particles.[80] On the other hand, the increases in viscosity relative to the unfilled matrix become less pronounced at higher shear rates since high shear rates tend to orient fillers to different degrees depending on their size, rigidity, concentration, and interactions with the matrix.[80] The viscosity of the composites at different shear rates could be expressed with Cross model shown below.

$$\eta = \frac{\eta_o}{1+(\lambda\dot{\gamma})^{1-m}} \qquad \text{(Equation 5.2)}$$

Where η_o is the zero shear viscosity, $\dot{\gamma}$ is shear rate and λ, and m are fitted parameters. In the equation, the value of zero for "1-m" indicates Newtonian behavior with "m" tending to unity for increasing shear thinning behavior. Calculated zero shear viscosity of Eudragit® E100, Eudragit® E100/4wt% DIK-Na+, and Eudragit® E100/15wt% are 1.842×10^4, 2.319×10^4, and 2.923×10^4 Pa-s, respectively.

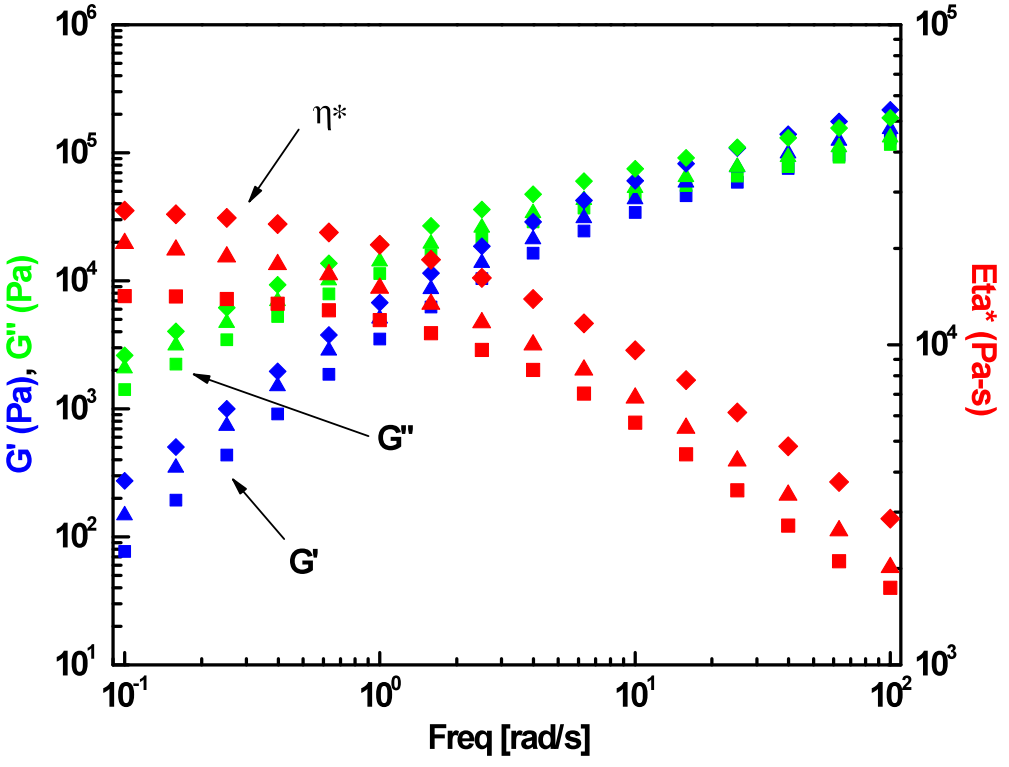

Figure 5.10 RMS results of (■) Eudragit® E100, (▲) Eudragit® E100/4wt% DIK-Na^+, and (♦) Eudragit® E100/ 15wt% DIK-Na^+ (Samples prepared by batch mixer).

Several equations have been proposed in order to predict the ratio of viscosity of particulate composites to the viscosity of the unfilled matrix, (η_c/η_m).[99, 100] These equations include dependence of viscosity on volume fraction, shape factors, aspect ratio, packing characteristics, interaction parameters, and so on. Examples are as follows:

1) The Mooney equation

$$\ln\left(\frac{\eta_c}{\eta_m}\right)=\frac{k_E V_f}{1-\left(\frac{V_f}{\phi_{\max}}\right)} \qquad \text{(Equation 5.3)}$$

2) The Equation proposed by Dougherty and Krieger

$$\frac{\eta_c}{\eta_m}=\left[1-\frac{V_f}{\phi_{\max}}\right]^{-k_E\phi_{\max}} \qquad \text{(Equation 5.4)}$$

Where k_E is a geometric parameter (aspect ratio, degree of agglomeration, and so on) known as the Einstein coefficient (2.5 for dispersed spheres), ϕ_{max} is the maximum packing factor, defined as true volume of filler/ apparent volume occupied by filler (0.637 for spheres random close packing), and V_f is volume fraction of the filler.

3) The Nielsen equation

$$\frac{\eta_c}{\eta_m}=\frac{(1+ABV_f)}{(1-B\psi V_f)} \qquad \text{(Equation 5.5)}$$

Where A, B, and ψ are functions of component properties, packing characteristics, and aspect ratio, respectively. Assuming spherical particles, the viscosity ratios (η_c/η_m) from the experimental results and calculations from the above three equations are compared in Figure 5.11. To have a better comparison, 25 wt% and 40 wt% DIK-Na^+ in the Eudragit® E100 matrix were additionally examined. Details are shown in Appendix D

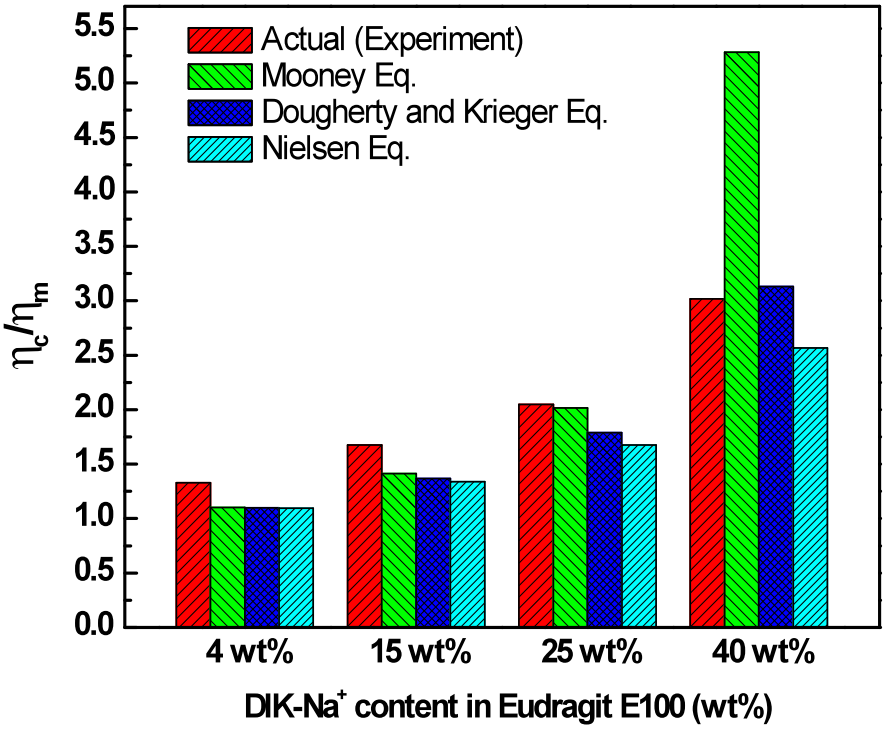

Figure 5.11 Comparison of experimental and calculated viscosity ratio (η_c/η_m) for Eudragit E100® DIK-Na^+ composites (Samples prepared by batch mixer),

Experimental viscosity values showed a reasonable agreement with those from theoretical equations, except for the Mooney equation at higher DIK-Na^+ loading. The Mooney equation is generally not accurate beyond a volume fraction of 0.25.[99] All three equations need the use of either Einstein coefficients (k_E) or maximum packing fraction

(ϕ_{max}). However, these parameters are not easily available because of irregular agglomeration and size variation of the API in the polymer matrix. These limitations add to the differences between experimental and theoretical results.

5.1.6 Dissolution Profiles

Dissolution profiles of Eudragit® E100/DIK-Na^+ composites in a 1.2 pH buffer solution are shown in Figure 5.12. The reported solubility of DIK-Na^+ under these conditions is approximately 1.2 μg/ml. The apparent solubility of the API in the composite increased significantly due to increased wettability of the API by the surfactant effect of the dissolved polymer.[26] Increased apparent solubility may also be the result of increased microenvironmental pH. Eudragit® E100 could increase the pH when it is dissolved in the SGF. In order to observe the pH changes, 100 mg Eudragit® E100 powder was added into 100 ml of SGF and the pH of the prepared solution was measured. The pH of SGF immediately changed from 1.2 to 1.5. This pH change may be significant in a microenvironment and result in increased apparent solubility. Dissolution rate and solubility of both composites (4 wt% and 15 wt%) were similar up to one hour. However, the composite containing 15 wt% DIK-Na^+ shows a decreasing apparent solubility after one hour. This is because the API in the composite recrystallized at this API loading which is presumablely higher than the API solubility limit. Therefore, it should be noted that higher API loadings may accelerate its recrystallization in the medium, and finding an optimum API loading is necessary to achieve its stable release. This type of recrystallization effect has also been observed by other researchers.[23]

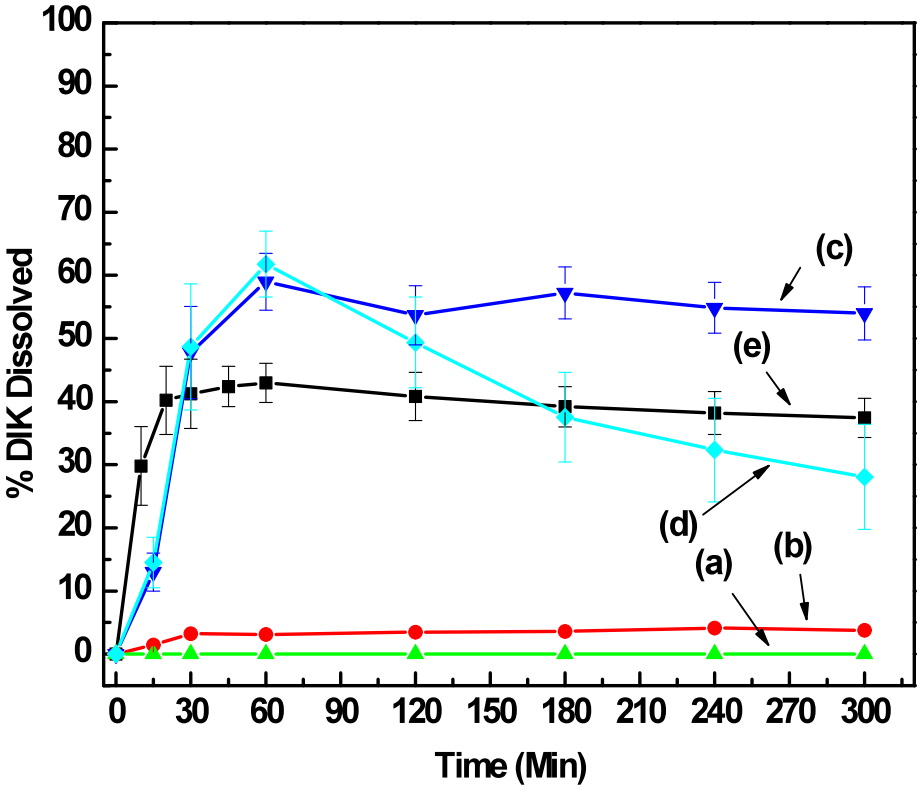

Figure 5.12 Dissolution profile of (a) Eudragit® E100, (b) DIK-Na^+, (c) Eudragit® E100/ 4wt% DIK-Na^+, (d) Eudragit® E100/ 15wt% DIK-Na^+, and (e) physical mixture of Eudragit® E100/ 4wt% DIK-Na^+ (in pH 1.2 solution) (Samples prepared by batch mixer).

5.1.7 Summary

A summary of the characterization results for the melt mixed Eudragit® E100/DIK-Na^+ composites is shown in Table 5.1.

Table 5.1 Characterization results of Eudragit E100/DIK-Na^+ System

	Eudragit® E100	Eudragit® E100 / 4 wt% DIK	Eudragit® E100/ 15 wt% DIK
Miscibility prediction from solubilty parameters	-	Immiscible	Immiscible
FTIR	As expected	As expected - No peak shifts	As expected - No peak shifts
Thermal Stability			
Temp. @ 10% weight loss, ^oC	293.5	273.2	257.3
Activation Energy, kJ/mole	2.27×10^3	1.98×10^3	1.53×10^3
T_g	42.7 ± 1.2	45.9 ± 2.4	46.3 ± 2.1
XRD	Amorphous	API few crystalline peaks	API more crystalline peaks
Morphology	Amorphous	Dispersed API-agglomerates	Dispersed API-agglomerates
Rheology			
Complex viscosity ratio, $10^{-1}/10^2$ rad/s	8.14	9.16	10.28
API dissolution (pH 1.20)	-	60% dissolved in one hour	60% dissolved in one hour – recrystallization after

5.2 Mixing Comparison of Solvent Casting and Twin Screw Extruder

In this section, an attempt is made to evaluate the efficiency of different mixing methods. From an engineering point of view, hot melt extrusion is obviously able to offer a lot of benefits by reducing time consuming steps and increasing output of pharmaceutical products. However, in the case of APIs that are immiscible with the polymers and cannot be well dispersed in individual particles by melt extrusion but are rather agglomerated in the polymer matrix, the efficiency of the system will be inferior. With this motivation, DIK-Na^+ and Eudragit® E100 combination (an immiscible system based on solubility parameters and confirmed by batch melt mixing) was prepared by solvent casting and a comparison is made between its morphology and dissolution results with the ones made by melt mixing including twin screw extrusion and batch mixing.

5.2.1 Morphology of Samples

DIK-Na^+ is not miscible with Eudragit® E100 and this was confirmed in the previous section. However, DIK-Na^+ can be dissolved and mixed with Eudragit® E100 in a common methanol/ acetone solvent. After solvent casting, the dried sample containing the polymer and 4 wt% API was still transparent (slightly yellowish due to the polymer) while the Eudragit® E100/15wt% DIK-Na^+ combination showed a few crystalline particles. These systems containing different API concentrations were hot pressed to 1 mm thickness at 130 ^oC for further analyses. After hot pressing, although the Eudragit® E100/ 4wt% DIK-Na^+ was still transparent, the Eudragit® E100/15 wt% DIK-Na^+ system became opaque after removal of the residual solvent and API recrystallization (Figure 5.13). On the other hand, the transparency of Eudragit® E100/ 4 wt% DIK-Na^+ was

maintained even after hot pressing at 130 ^{o}C a possible evidence of the presence of a small amount of residual solvent. This residual solvent could be dissolving the API since a low concentration of DIK-Na^{+} was used. However, this residual solvent may not be adequate to dissolve the higher API loading (15 wt%). It is known that complete removal of solvent by heating and vacuum techniques from polymeric films is very difficult; spray drying could have been a viable alternative.

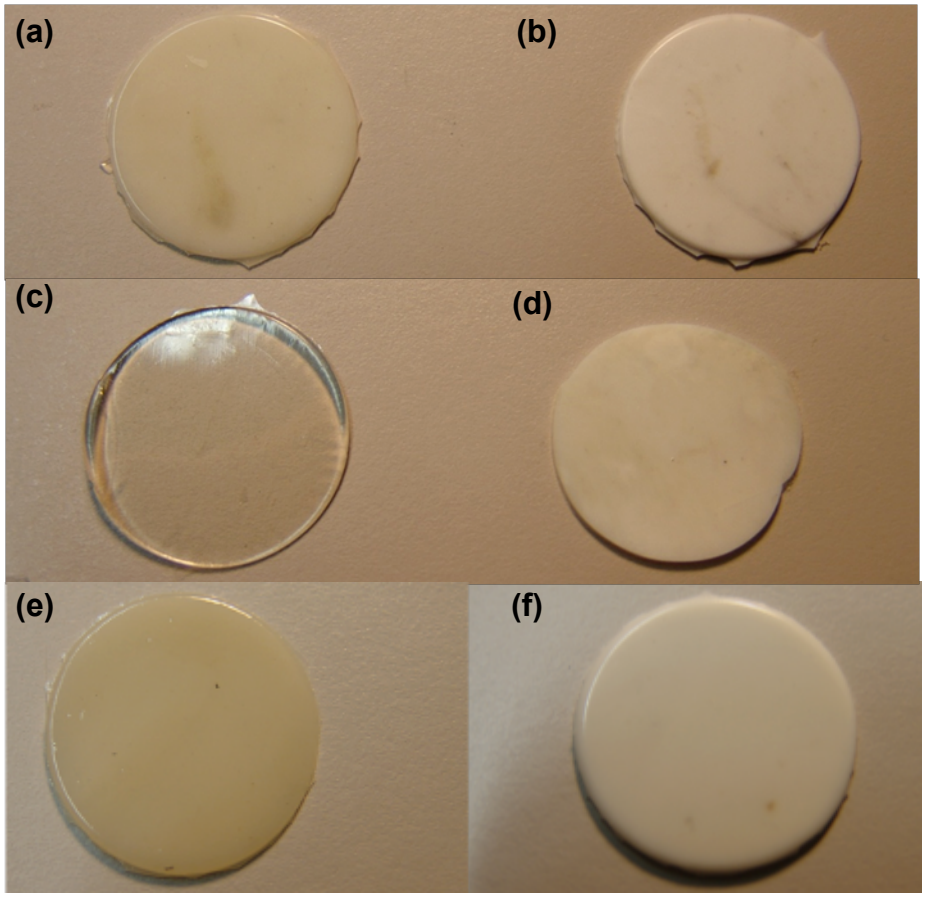

Figure 5.13 Eudragit® E100/ DIK-Na^{+} composites prepared by batch mixing (a) 4 wt% of DIK-Na^{+} loading, (b) 15 wt% DIK-Na^{+} loading; by solvent casting (c) 4 wt% of DIK-Na^{+} loading, (d) 15 wt% DIK-Na^{+} loading; by twin screw extruder mixing (e) 4 wt% of DIK-Na^{+} loading, (f) 15 wt% of DIK-Na^{+} loading.

Figure 5.14 shows the T_g of Eudragit® E100 containing 4 wt% and 15 wt% DIK-Na^{+}, both prepared by batch mixing, twin screw extruder, and solvent casting. The 4 wt% and 15 wt% DIK-Na^{+} systems prepared by solvent casting show lower T_g values than

specimens prepared by melt mixing. This can be a further evidence of the presence of residual solvents in the samples that would lead to plasticization. It could also be possible that the concentration of API was reduced from 4 wt% during sample preparation. However, all samples (Eudragit® E100/ 4wt% DIK-Na^+) prepared by different methods show by TGA analysis similar amounts of residuals at 500 ^oC. This suggests that the API content is similar in all samples (Appendix E).

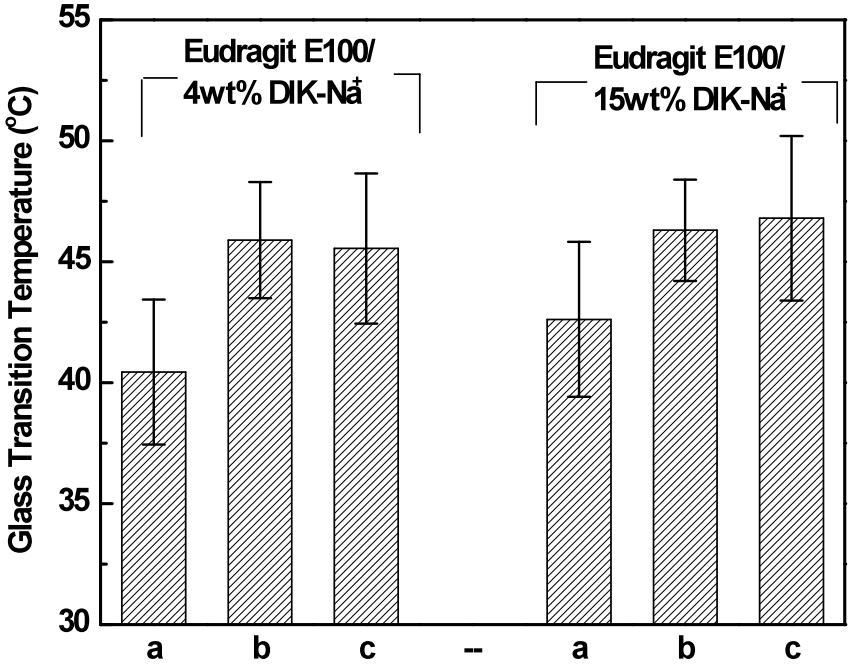

Figure 5.14 T_g of Eudragit® E100/ 4wt% and 15wt% DIK-Na^+ prepared by different methods (a) solvent casting, (b) batch mixing, and (c) twin screw extruder.

The recrystallization of API in the Eudragit® E100/15 wt% DIK-Na^+ sample was confirmed by polarized light microscopy (Figure 5.15). The Eudragit® E100/4wt% DIK-

Na^+ combination produced by solvent mixing did not show any bright particles; this is an indication that the API is in an amorphous state in the presence of the residual solvents.

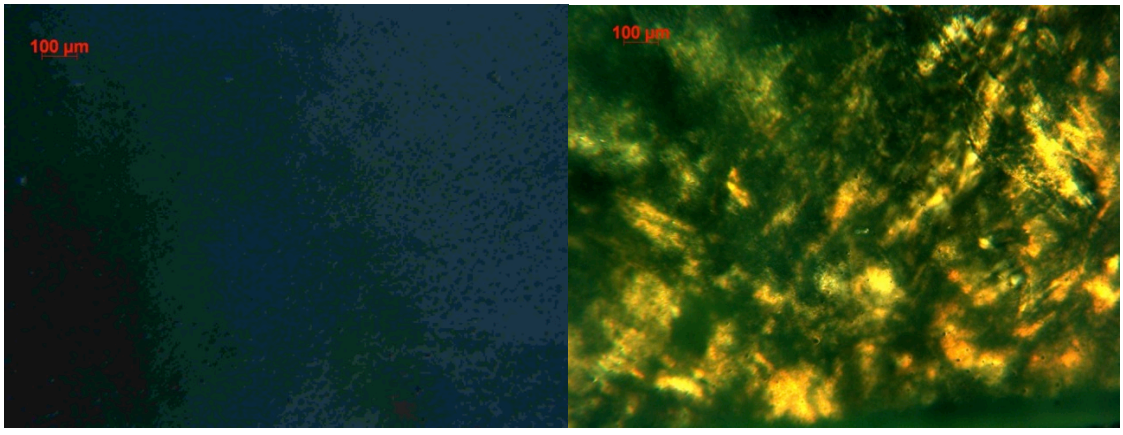

Figure 5.15 Images from polarized light microscopy (left) Eudragit® E100/4wt% DIK-Na^+, and (right) Eudragit® E100/15wt% DIK-Na^+ made by solvent casting.

Eudragit® E100/ DIK-Na^+ composites prepared by twin screw extruder contained finer DIK-Na^+ particles than the ones from the batch mixer as shown in Figure 5.16 (compare with Figure 5.7). Twin screw extruders generally offer better mixing and filler dispersion in polymer matrices due to the high shear forces in the mixing zone. Mixing mechanisms can be categorized as dispersive polymer mixing and distributive mixing.[101, 102] Distributive mixing is described as the random spatial distribution of a minor constituent in a matrix of the major constituent. Dispersive polymer mixing can be described as the act of reducing the average particle size through the application of a shear stress (τ) (Equation 5.6) where $\eta, \dot{\gamma}$,m and n are viscosity, shear rate, power law model parameter and power law exponent, respectively.[101]

$$\tau = \eta(\dot{\gamma})\dot{\gamma} \qquad \text{(Equation 5.6)}$$

$$\eta(\dot{\gamma}) = m\dot{\gamma}^{n-1} \qquad \text{(Equation 5.7)}$$

Shear stress can be increased by an increase in shear rate which can be described as fluid velocity divided by gap between screw and barrel. Hence, as the gap narrows the shear rate increases, and this results in a higher level of shear stress being imparted to the compound. The mixing zone of the APV extruder has a narrower gap between the kneading elements and the barrel than the batch mixer. Therefore, this reduced size of the API particles in the polymer would originate from better dispersive mixing in the extruder. It should be noted that neither the APV nor the batch mixer achieved a nanodispersion of the API. In addition, appearance of the final products was exactly the same as the one produced from the batch mixer (see Figure 5.13 (a) vs. (e) and (b) vs. (f)).

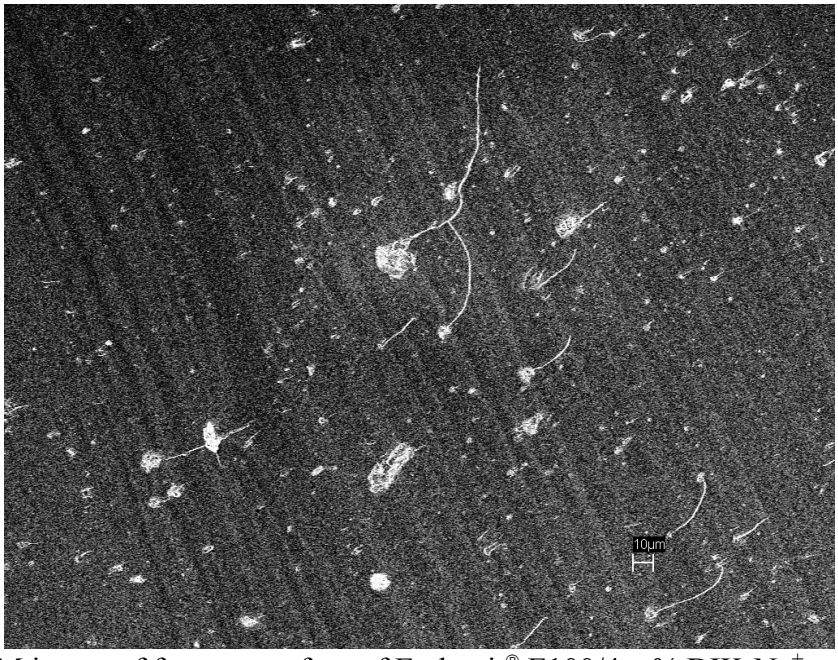

Figure 5.16 SEM image of fracture surface of Eudragit® E100/4wt% DIK-Na^+ produced from APV extruder.

5.2.2 XRD Analysis

XRD results composites containing higher loadings (15 wt%) DIK-Na^+ prepared by solvent casting show some crystalline peaks while lower loadings (4 wt%) show no

crystalline peaks indicating that DIK-Na^+ is in its amorphous state (Figure 5.17). Note in Figure 5.6 the presence of some crystalline peaks in 4wt% DIK-Na^+ prepared by batch mixing. Crystalline peaks in Eudragit® E100/15wt% DIK-Na^+ composites are due to the DIK-Na^+ which recrystallized during drying and hot pressing. Eudragit® E100/ DIK-Na^+ (4wt% and 15wt%) samples produced from the twin screw extruder also showed crystalline peaks, similarly to the samples prepared by batch mixer (Figure 5.6).

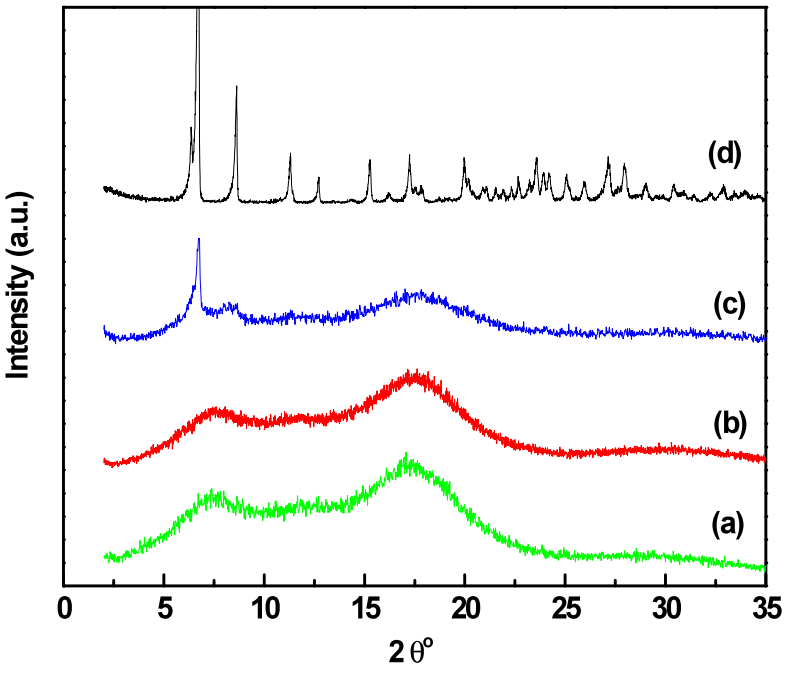

Figure 5.17 XRD results of (a) Eudragit® E100, (b) Eudragit® E100/4wt% DIK-Na^+, (c) Eudragit® E100/15wt% DIK-Na^+, and (d) DIK-Na^+ (all samples were prepared by solvent casting except DIK-Na^+).

5.2.3 Dissolution Profiles

Since the amorphous state of API is a more favorable state for dissolution,[103] it was anticipated that Eudragit® E100 containing 4wt% DIK-Na^+ prepared by solvent casting may have a higher apparent solubility. Figure 5.18 comparing the dissolution profiles of

Eudragit® E100 and DIK-Na^+ mixtures with different API concentrations, and different preparation methods confirms the highest maximum DIK-Na^+ solubility of almost 90% when dissolved from the Eudragit® E100/4 wt% DIK-Na^+ formulation. By contrast, API dissolved from the Eudragit® E100/DIK-Na^+ composites prepared by batch mixing and extrusion mixing were only 60 % and 62 %, respectively. Although Eudragit® E100/ 15wt% DIK-Na^+ prepared by solvent casting shows recrystallization due to the high API loading, the composite showed similar initial increased API solubility to the ones prepared by batch mixing and twin screw extruder. In summary, as expected, the crystalline or amorphous state of the API in the polymer matrix could be the controlling factor of dissolution rather than the method of sample preparation.

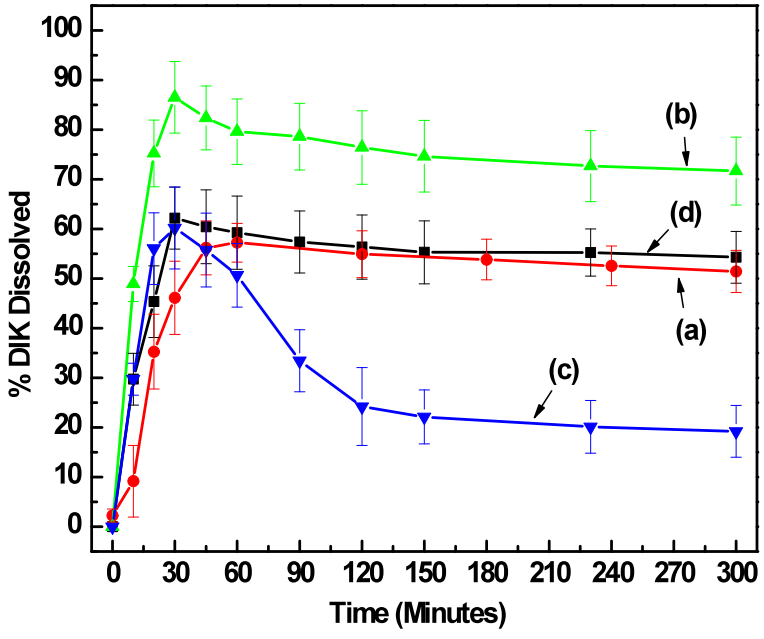

Figure 5.18 Dissolution profile in pH 1.2 solution of: (a) Eudagit® E100/4wt% DIK-Na^+ (batch mixing), (b) Eudragit® E100/4wt% DIK-Na^+ (solvent casting), (c) Eudragit® E100/15 wt% DIK-Na^+ (solvent mixing) and (d) Eudragit® E100/4wt% DIK-Na^+ (APV extruder).

5.3 Results on IND Compounded with Eudragit® E100

From solubility parameter calculations, it was anticipated that IND and Eudragit® E100 would form a miscible system. A possible mixing process of a soluble solid API in a polymer system (Figure 5.19), particularly when the processing temperature is lower than the melting point of API was described by Liu et al.[23]

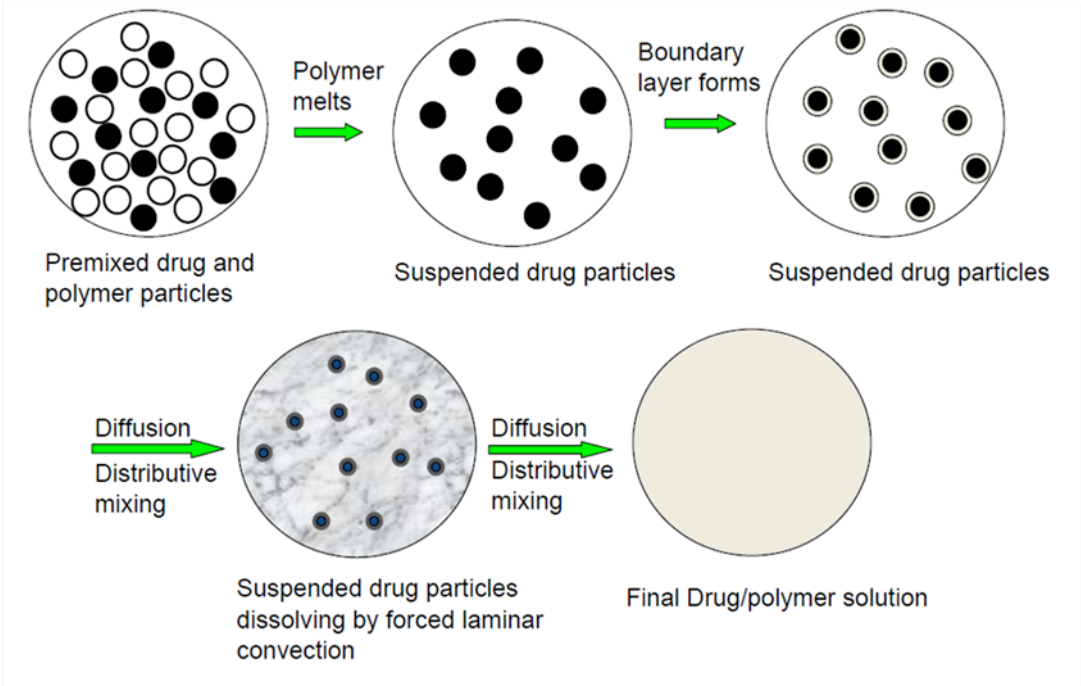

Figure 5.19 Schematic of soluble solid drug particle in the polymer matrix.[23]

5.3.1 FTIR Analysis

The FTIR spectra of IND, Eudragit® 100, and the Eudragit® E100/IND blends are shown in Figures 5.20 and 5.21. It has been reported that IND has different physical states such as a stable γ form, a metastable α form, and an amorphous state.[104] Taylor and Zografi[105] reported how to determine the physical state of the IND by characterizing the FTIR peaks, particularly by analyzing the carbonyl peak. (Table 5.2).

Table 5.2 Infrared Peak Positions and Assignments for the Carbonyl Stretching Region of Indomethacin[105]

Physical state	Infrared (cm^{-1})	Assignment
γ-IND	1717	Asymmetric acid νC=O of a cyclic dimer
	1692	Benzoyl νC=O
α-IND	1735	Non-hydrogen bonded acid νC=O
	1688	Benzoyl νC=O
	1681	Hydrogen bonded acid νC=O
	1649	Hydrogen bonded acid νC=O
Amorphous IND	1735	Non-hydrogen bonded acid νC=O
	1710	Asymmetric acid νC=O of a cyclic dimer
	1684	Benzoyl νC=O

As shown in Figures 5.20 and 5.21 the original crystalline IND particles are in γ-form. However, changes are observed for the samples prepared in the batch mixer at 130 ^{o}C and 50 rpm. The peak at 1692 cm^{-1} shifted to 1684 cm^{-1}, and the sharper peak at 1692 cm^{-1} became slightly broader at 1684 cm^{-1}, which indicates that the original γ-form was converted to amorphous IND. The peak at 1684 cm^{-1} is much broader at a concentration of 4 wt% IND in the polymer excipient indicating a more amorphous state. Thus, it is shown that a lower concentration of API promotes better dissolution in the polymer matrix. The peak at 1718 cm^{-1} shifted to 1734 cm^{-1} indicates the non-hydrogen bonded C=O stretch for amorphous IND and Eudragit® E100.[105, 106] These results are in good agreement with literature results from different IND melt mixing conditions.[23]

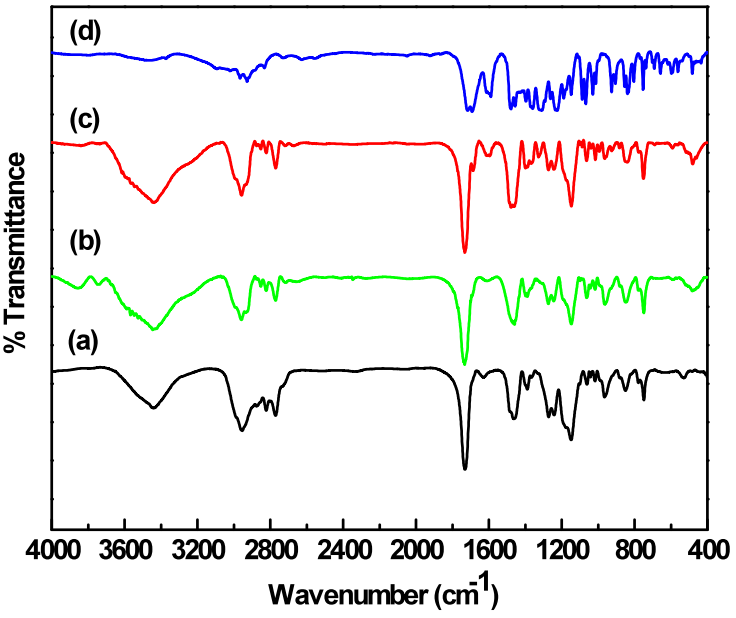

Figure 5.20 FTIR spectra of (a) Eudragit® E100, (b) Eudragit® E100/ 4 wt% IND, (c) Eudragit® 15 wt% IND, (d) IND (Samples prepared by batch mixer).

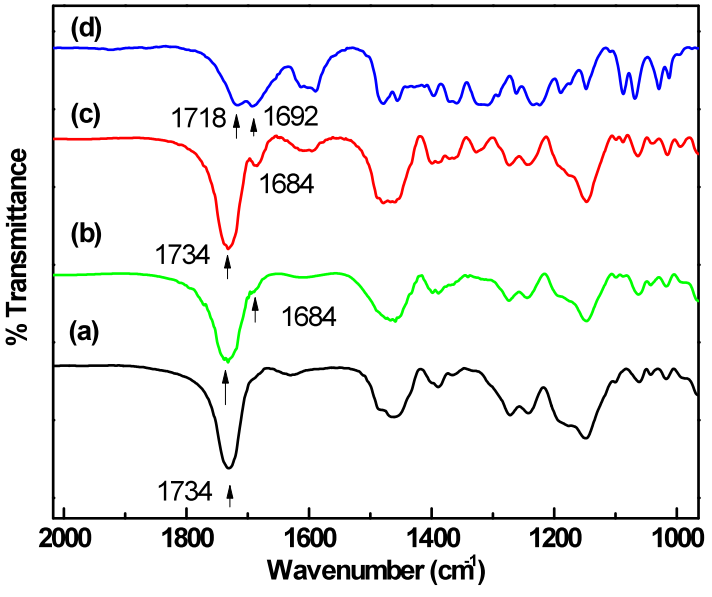

Figure 5.21 FTIR spectra in the range between 2000 and 1000 cm^{-1} of (a) Eudragit® E100, (b) Eudragit® E100/ 4 wt% IND, (c) Eudragit® 15 wt% IND, (d) IND (Samples prepared by batch mixer)

5.3.2 Thermal Analysis

IND started losing weight at about 220 ^{o}C (Figure 5.22), a temperature higher than its melting point (162 ^{o}C) and lower than the onset degradation temperature of Eudragit® E100 (about 250 ^{o}C). Eudragit® E100 containing 4 wt% and 15 wt% of IND showed lower thermal stability than the unmodified polymer (Figure 5.22). Since IND was fully dissolved in the polymer due to favorable interactions,[23] the reduced thermal stability of Eudragit® E100/IND blends is mainly due to the presence of the less thermally stable IND. It should be noted that melt mixing was carried out at 130 ^{o}C, below the melting point of the API, but above the reported T_g of the polymer (43 ^{o}C). As a quantitative comparison of thermal degradation, the temperature corresponding to 10 wt% weight loss is used to rank the materials in terms of thermal stability: Eudragit® E100 > Eudragit® E100/ 4wt% IND> Eudragit® E100/ 15wt% IND.

The thermal stability of Eudragit® E100/IND composites was also quantified by the Friedman equation (Figure 5.23). The calculated E_a values (temperature range between 220 and 280 ^{o}C) from Figure 5.23 are 2.267×10^3 kJ/mol, 1.351×10^3 kJ/mol, and 0.747×10^3 kJ/mol for Eudragit® E100, Eudragit® E100/ 4 wt% IND and Eudragit® E100/ 15wt% IND, respectively; this confirms that Eudragit® E100 has the highest thermal stability, decreasing as the concentration of IND increases.

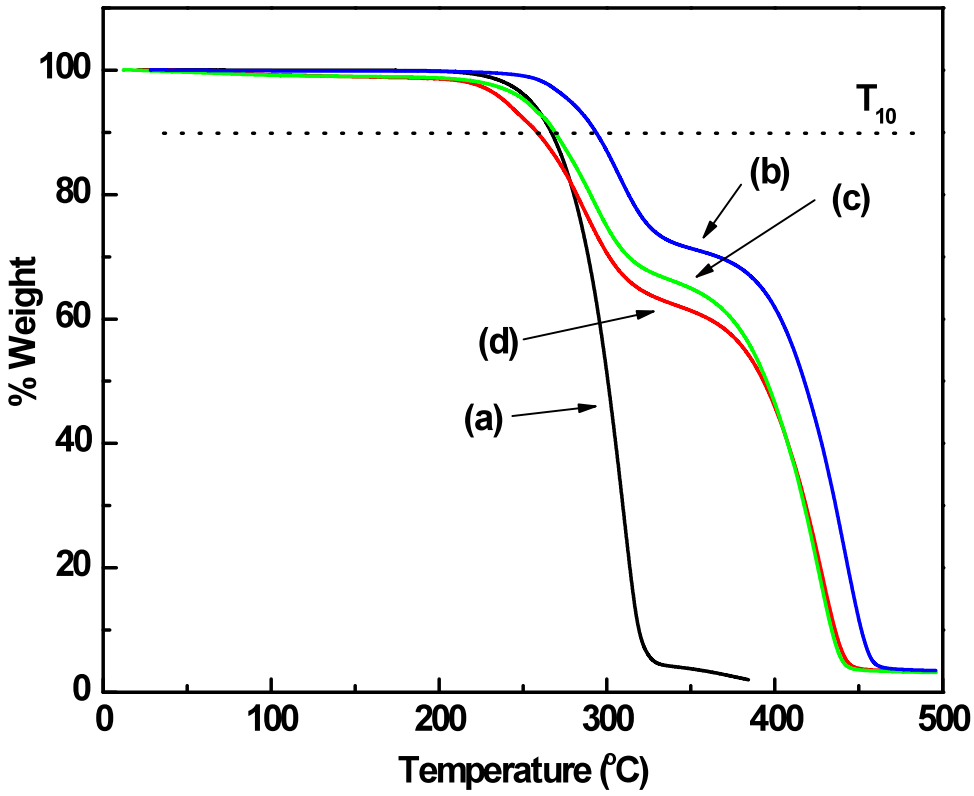

Figure 5.22 TGA results of (a) IND, (b) Eudragit® E100, (c) Eudragit® E100/4 wt% IND and (d) Eudragit® E100/15 wt% IND (Samples prepared by batch mixer).

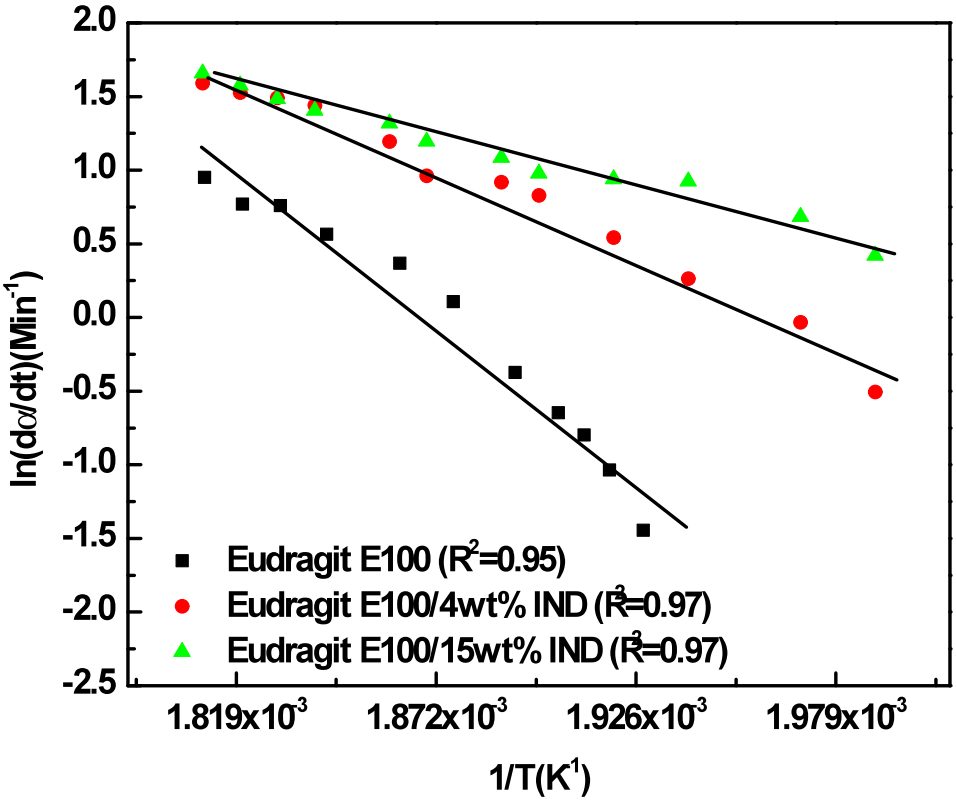

Figure 5.23 Friedman plots of ln(dα/dt) versus 1/T for the direct calculation of E_a of thermal degradation at a heating rate of 20 °C min under N_2 (Eudragit® E100/IND blends) (Samples prepared by batch mixer).

Generally, in miscible systems, the small API molecules would allow the polymer chain segments to have greater mobility freedom - the plasticization effect.[21, 24, 107] As shown in Figure 5.24, the T_g of the IND blends decreased with increasing IND loadings. Similar plasticizing effects with miscible API- polymer systems have been reported in the literature.[2, 108-110] Generally, the reduced glass transition temperature can be calculated by the Gordon-Taylor Equation 2.2 for miscible polymer blends.[29, 111] However, in Figure 5.24, the theoretically calculated T_g values do not correspond to the experimental values since the experimentally determined T_g (46 °C) of IND was higher than that of the

polymer (43 ^{o}C). Note that the T_g of Eudragit® E100/ IND system has been shown to increase at much higher IND loadings (> 20 wt%) in the polymer matrix due to antiplasticization effect.[21, 24]

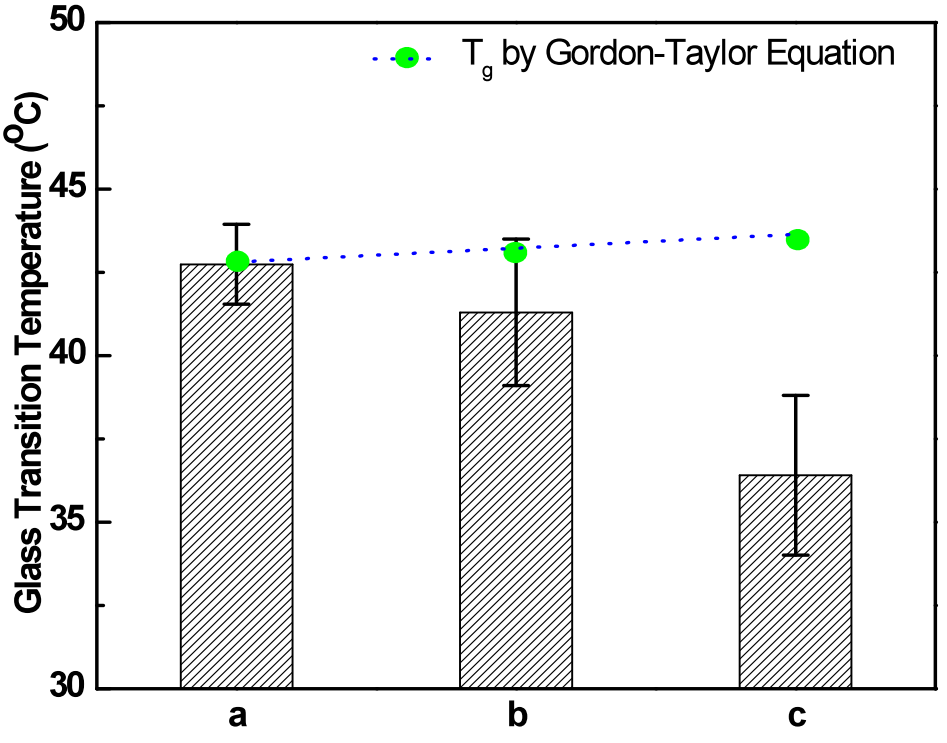

Figure 5.24 DSC glass transition temperatures of (a) Eudragit® E100 (b) Eudragit® E100/ 4wt% IND, and Eudragit® E100/ 15wt% IND (Samples prepared by batch mixer).

5.3.3 XRD Analysis

Figure 5.25 shows XRD results of IND and Eudragit® E100/IND composites. The IND spectrum contains many sharp peaks indicating a high degree of crystallinity. The XRD peaks have the same pattern as those of γ type IND shown in previous research.[104] However, Eudragit® E100/ IND blends do not show any peaks, a confirmation that IND has been dissolved in the polymer matrix and is in an amorphous state. Liu et al[23] studied

the degree of dissolved IND in the polymer under different melt processing parameters and showed that miscibility increased as temperature and mixing rpm increased. Mixing conditions in the present study were in the range where Liu et al[23] produced miscible systems. Figure 5.26 shows XRD patterns of different IND types reported in the literature.[104]

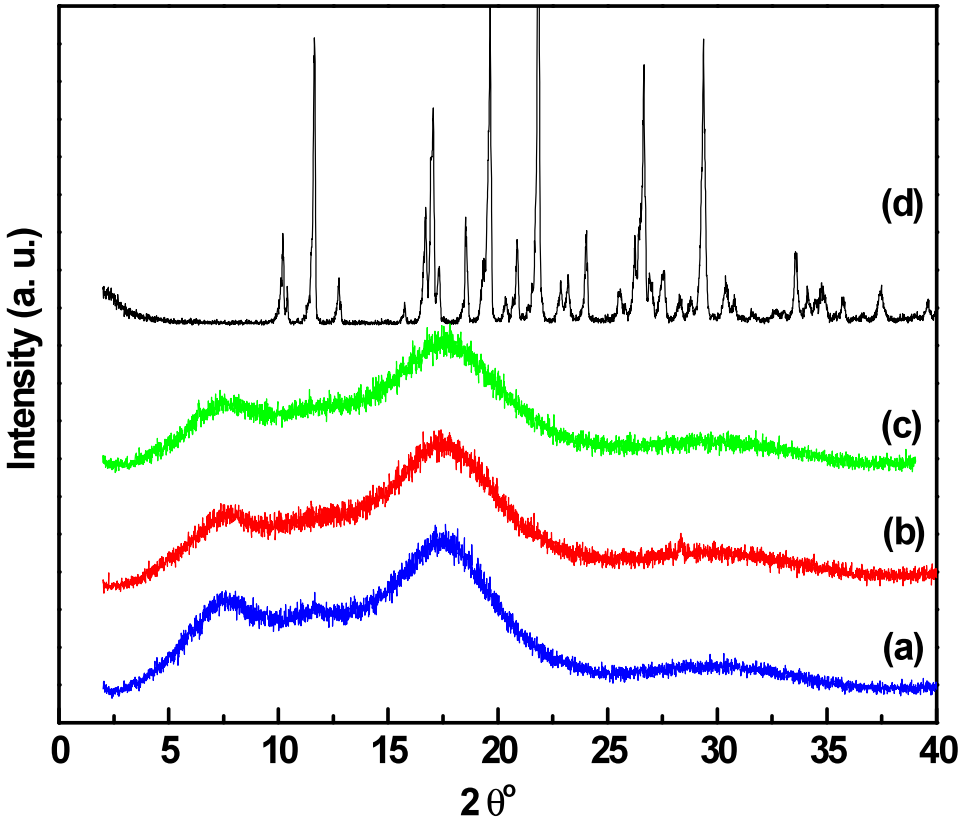

Figure 5.25 XRD results of (a) Eudragit® E100, (b) 4wt% IND /Eudragit® E100, (c) 15 wt% IND/ Eudragit® E100, and (d) IND (Samples prepared by batch mixer)

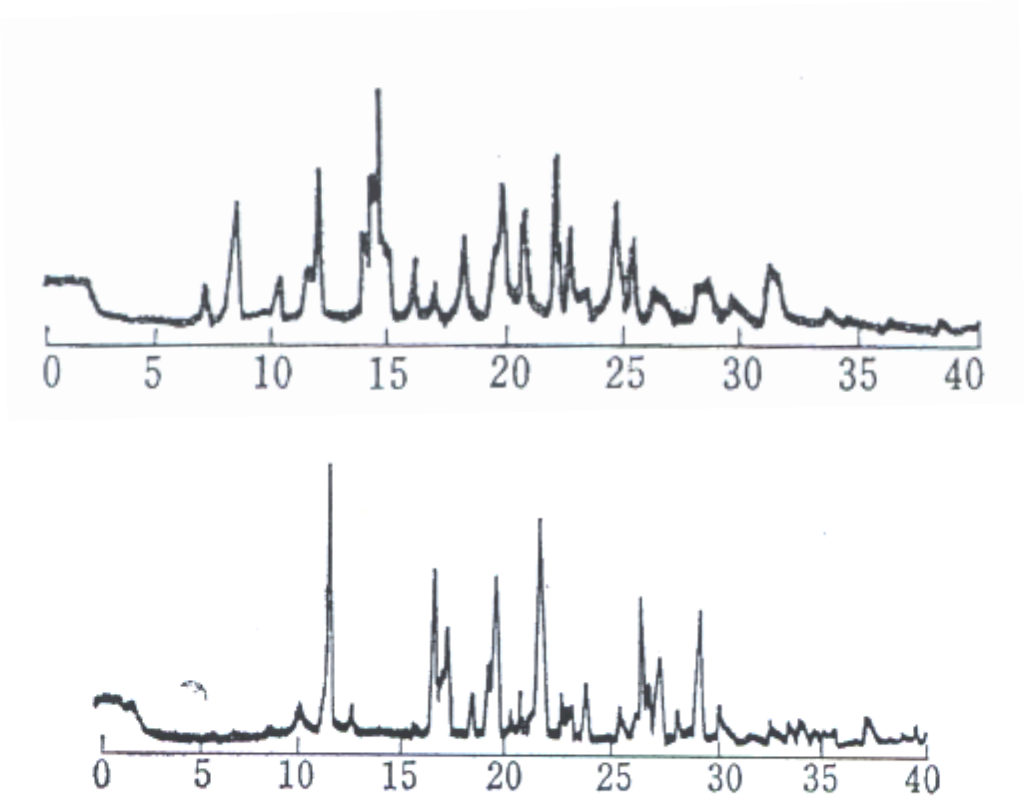

Figure 5.26 XRD pattern of (top) α-type IND, and (bottom) γ- type IND.[104]

5.3.4 Morphology of Eudragit® E100/ IND Blend

Figure 5.27 shows an SEM image of a fractured surface of Eudragit® E100/ 15 wt% IND blend. Unlike the Eudragit® E100/ DIK-Na^+ composite, the entire surface is quite clear and smooth, and no API particles are visible. EDX chlorine mapping in Figure 5.27 (right) indicates a uniform distribution of IND over the entire polymer area and confirms that IND was fully dissolved in the matrix.

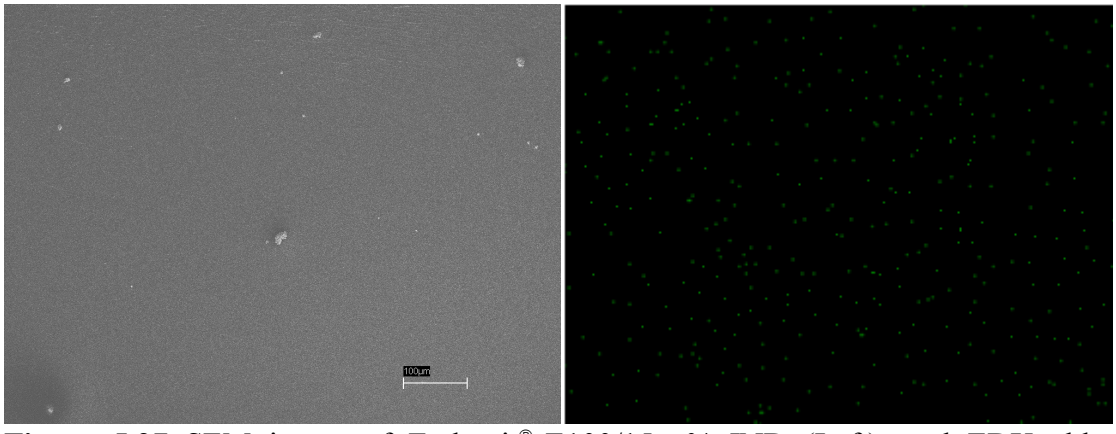

Figure 5.27 SEM image of Eudragit® E100/15wt% IND (Left), and EDX chlorine mapping image of the same region (Right).

It was expected that Eudragit® E100/IND blends would not show any dispersed crystalline particles. However, several particles are observed by PLM (Figure 5.28) that did not disappear on the hot stage above the IND melting point. As in a previous study,[24] it was concluded that these crystalline particles are impurities from the API.

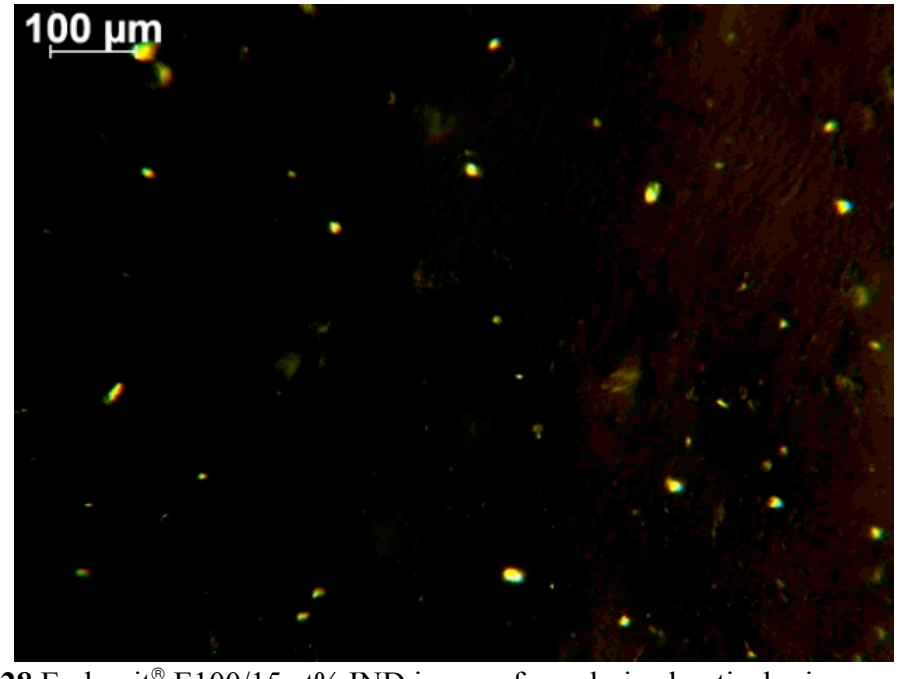

Figure 5.28 Eudragit® E100/15wt% IND images for polarized optical microscopy.

5.3.5 Rheological Study

Figure 5.29 shows RMS results of Eudragit® E100/INDs blends tested at 130 °C. Unlike the Eudragit® E100/DIK-Na^+ composites, the IND blends show decreasing viscosity, G′ and G″ with increasing IND loading. These effects that occur with plasticizers are in good agreement with the DSC results that also showed the plasticizing effect of IND. The zero shear viscosities of Eudragit® E100, Eudragit® E100/ 4wt% IND and Eudragit® E100/ 15wt% are 1.842×10^4, 1.420×10^4, and 8.099×10^3 Pa-s, respectively, in agreement with the plasticization trend.

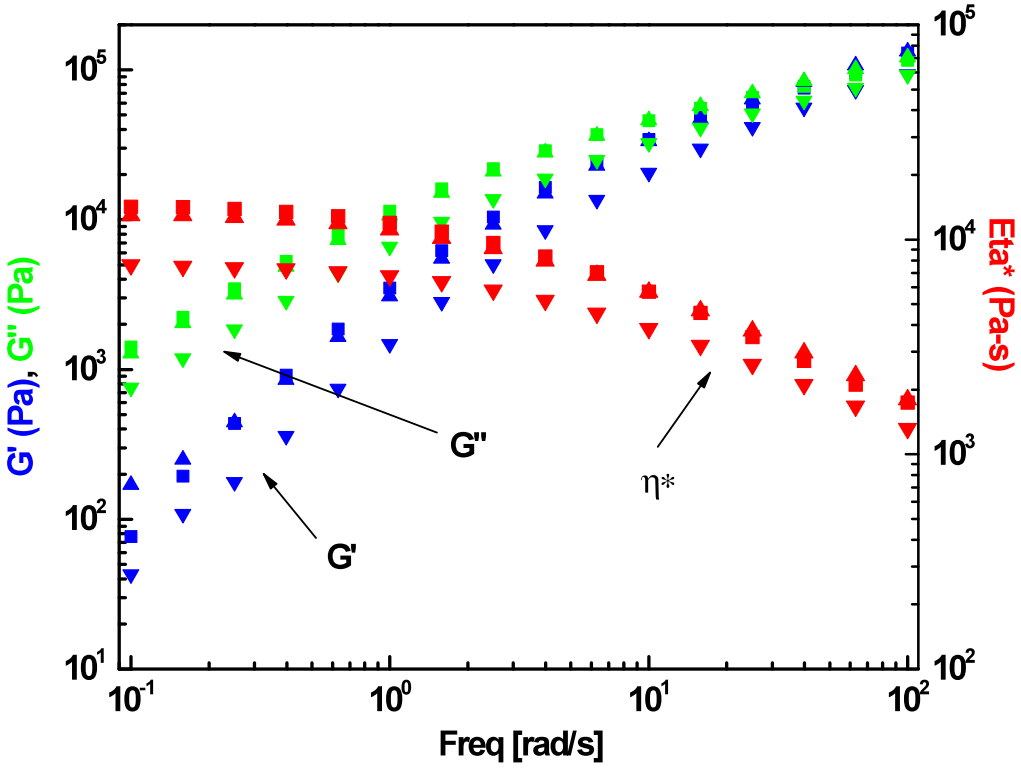

Figure 5.29 RMS results of (■) Eudragit® E100, (▲) Eudragit® E100/ 5wt% IND and (▼) Eudragit® E100/ 15wt% IND (Samples prepared by batch mixer)

5.3.6 Dissolution Profiles

The dissolution profiles of IND and Eudragit® E100/IND composites are shown in Figure 5.30. As expected, IND shows very poor solubility in the simulated gastric acid at pH 1.2. There are several differences of this system as compared to Eudragit® E100/ DIK-Na^+ (Figure 5.12). Eudragit® E100/IND blends achieved almost 100% dissolved IND while Eudragit® E100/ DIK-Na^+ composites achieved up to 60%. Since both APIs have almost equally low solubility in the low pH medium, the increased apparent solubility of IND from the Eudragit® E100/IND blend would be due to the amorphous state of the API in the polymer matrix. Although Eudragit® E100/15 wt% IND blends did not show the recrystallization behavior of the API observed with Eudragit® E100/ 15wt % DIK-Na^+, this difference may be due to the enhanced solubility of the amorphous IND in the polymer matrix. However, it should be noted that if higher IND loadings are used for the dissolution test, the recrystallization effect may reappear.[23] Another interesting observation is related to the Eudragit® E100/IND physical mixture. The DIK-Na^+ in the physical mixture of Eudragit® E100/ DIK-Na^+ showed improved solubility roughly about 40 % from 3 % of its apparent solubility (Figure 5.12). By contrast, IND from the Eudragit® E100/IND physical mixture does not show any enhanced solubility (Figure 5.30). Since the solubility of DIK-Na^+ is improved significantly with increasing pH while IND has a low solubility up to a neutral pH, it appears that the increased microenvironmental pH due to the dissolved Eudragit® E100 was only effective for the DIK-Na^+. Therefore, the state of the API in the polymer matrix is more important in the Eudragit® E100/IND blends than in Eudragit® E100/DIK-Na^+ composites.

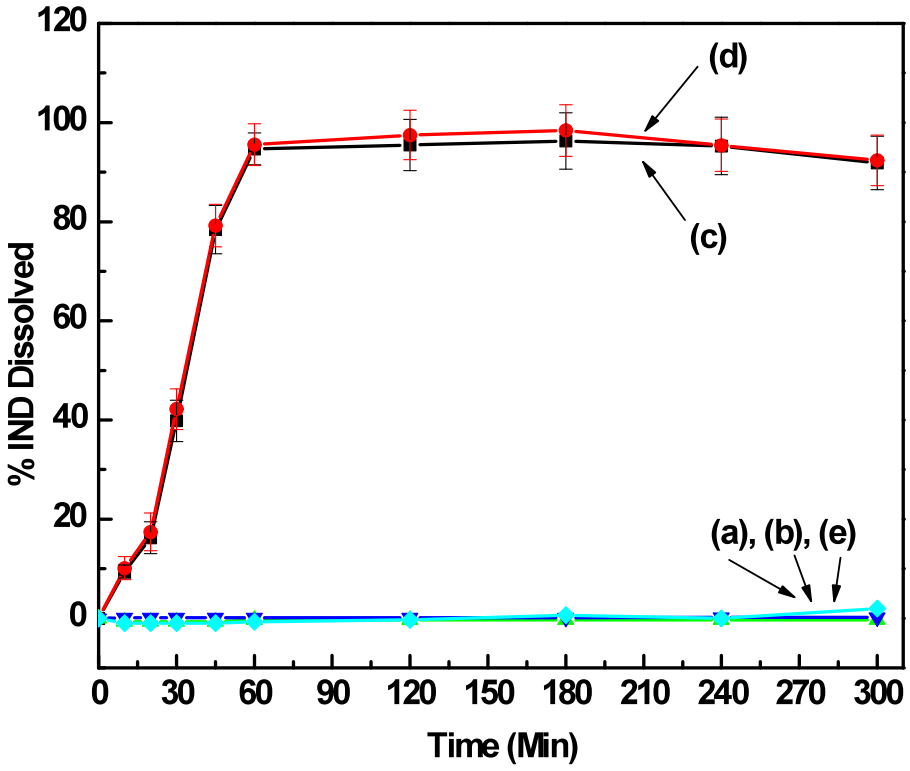

Figure 5.30 Dissolution results of (a) Eudragit® E100, (b) IND, (c) Eudragit® E100/4wt% IND, (d) Eudragit® E100/15wt% IND (e) Eudragit® E100/4wt% IND physical mixture (in pH 1.2 solution) (Samples prepared by batch mixer).

5.3.7 Summary

The characterization results for the melt mixed Eudragit® E100/IND miscible blends are summarized in Table 5.3

Table 5.3 Summary of Eudragit® E100/IND Miscible System

	Eudragit® E100	Eudragit® E100/ 4 wt% IND	Eudragit® E100/ 15 wt% IND
Miscibility prediction from solubilty parameters	-	Miscible	Miscible
FTIR	As expected	Shifts-Amorphous IND	Shifts- Amorphous IND
Thermal Stability			
Temp. @ 10% weight loss, ^{o}C	293.5	269.1	257.4
Activation Energy, kJ/mole	2.27×10^3	1.35×10^3	0.75×10^3
T_g	42.7 ± 1.2	41.3 ± 2.2	36.4 ± 2.4
XRD	Amorphous	API amorphous- no peaks	API amorphous- no peaks
Morphology	Amorphous	Complete miscibility	Complete miscibility
Rheology			
Complex viscosity ratio, $10^{-1}/10^2$ rad/s	8.14	7.17	5.78
API dissolution (pH 1.20)	-	100% dissolved in one hour	100% dissolved in one hour

5.4 APIs Dissolution Mechanisms from Eudragit® E100

Figure 5.31 shows dissolved APIs (IND and DIK-Na^+) from the same polymer matrix Eudragit® E100. The dissolution rates at the early stages in both cases appear to be the same but the apparent solubility of the API from Eudragit® E100/ 4wt% IND is higher than that from Eudragit® E100/ 4wt% DIK-Na^+.

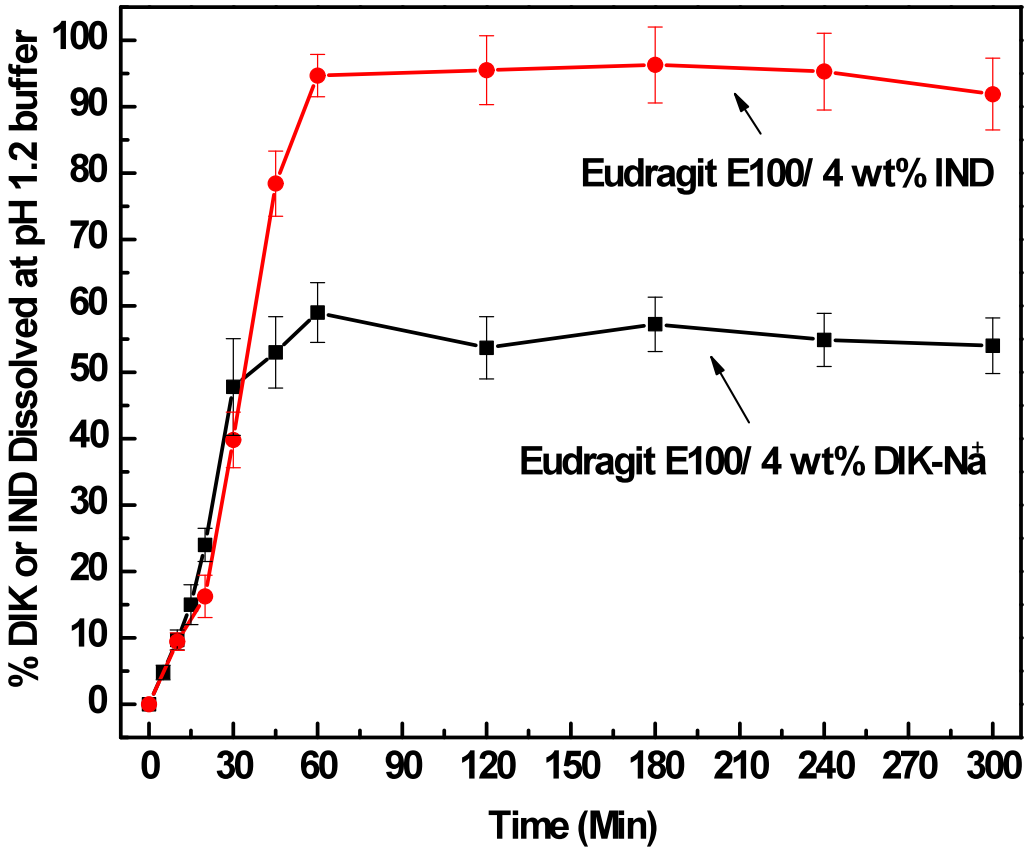

Figure 5.31 APIs release from the same polymer matrix. (Samples prepared by batch mixer)

According to calculation of dissolution profiles by Equations 4.2 and 4.3 (Table 5.4), APIs dissolutions from the Eudragit® E100 matrix at pH 1.2 are erosion dominant. Exponent "n" falls in the range of super case II transport (combination of API diffusion and polymer relaxation/dissolution)[90] (Table 4.2) and the ratios of relaxation to diffusion contributions (R/D) in Equation 4.4 are large (Figure 5.32).

Table 5.4 Dissolution Fitting Results of Polymer/API Binary System at pH 1.2

System	Power law (Equation 4.2) $\frac{M_t}{M_\infty} = kt^n$	Peppas and Sahlin (Equation 4.3) $\frac{M_t}{M_\infty} = k_1 t^{0.5} + k_2 t$	
	n ± 95% CI	k_1 ($min^{-0.5}$) ± 95% CI	k_2 (min^{-1}) ± 95% CI
Eudragit® E100/ 4 wt% DIK-Na^+	1.58 ± 0.04	0.06 ± 0.01	0.37 ± 0.02
Eudragit® E100/ 4 wt% IND	1.73 ± 0.06	0.04 ± 0.01	0.21 ± 0.01

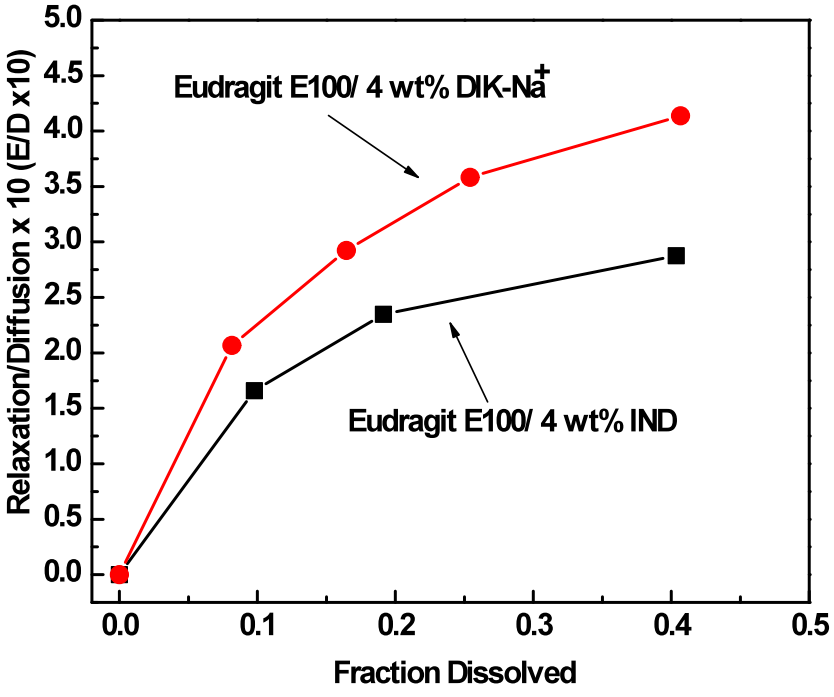

Figure 5.32 R/D ratio values versus fraction dissolved for Eudragit® E100 containing 4wt% DIK-Na^+ or IND.

Since a Fickian model would not fit these dissolution profiles, a model developed by Hopfenberg on the release of APIs from surface-eroding devices[87] is used. Hopfenberg's model (Equation 5.8) describes API release from slabs, spheres and infinite cylinders displaying heterogeneous erosion.

$$\frac{M_t}{M_\infty} = 1 - \left[1 - \frac{k_0 t}{C_0 a_0}\right]^n \qquad \text{(Equation 5.8)}$$

Where M_t is the amount of drug dissolved in time t, M_∞ is the total amount of API dissolved when the pharmaceutical dosage form is exhausted, M_t/M_∞ is the fraction of

drug dissolved, k_0 is the erosion rate constant, C_0 is the initial concentration of API in the matrix and a_0 is the initial radius for a sphere or cylinder or the half-thickness for a slab. The value of n is 1, 2 and 3 for a slab, cylinder and sphere, respectively. Since initial concentration of APIs (4 wt%) in the matrix and radius of the sample (1.27 cm) are the same for both cases and n=1. Equation 5.8 can be simplified as Equation 5.9.

$$\frac{M_t}{M_\infty} = ht \qquad \text{(Equation 5.9)}$$

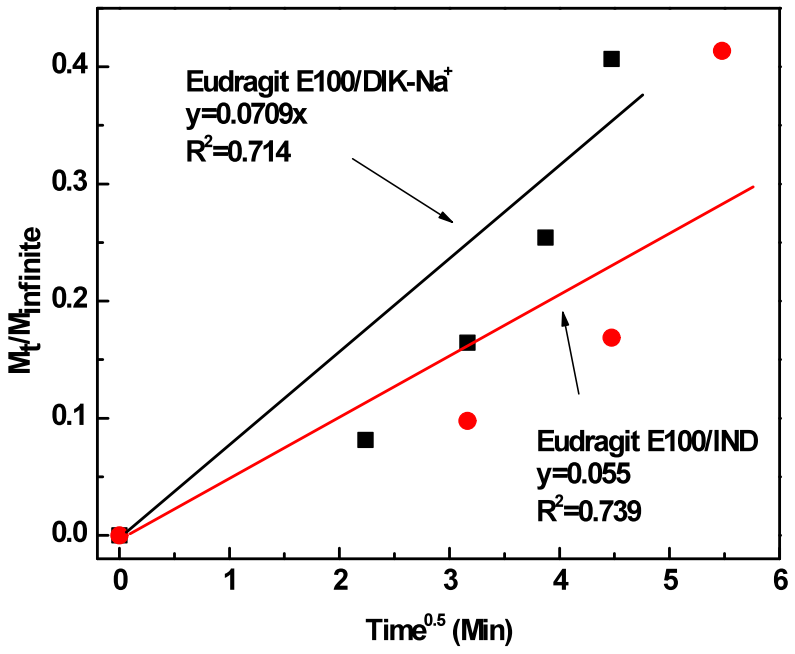

Figure 5.33 APIs dissolution profile (■: DIK-Na^+, ●: IND) from the Eudragit® E100 fitted with Fickian model.

Dissolution profiles of APIs from the samples were fitted to the Fickian model (Equation 4.5) and Hopfenberg model (Equation 5.9) shown in Figures 5.33 and 5.34. As

anticipated, dissolution profiles show a good fitting only with the Hopfenberg surface erosion model (Figure 5.34).

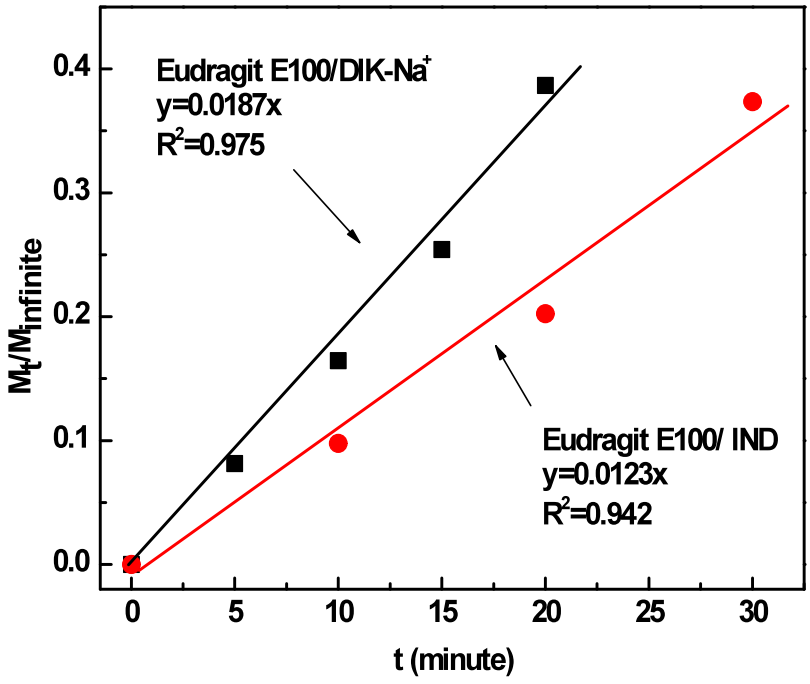

Figure 5.34 APIs dissolution profile (■: DIK-Na^+, ●: IND) from Eudragit® E100 fitted to Hopfenberg model.

5.5 Results on DIK-Na^+ Compounded with Eudragit® S100

Eudragit® S 100 is a copolymer designed for delivering an API to the intestinal tracts. This polymer is not soluble in a low pH medium but dissolves slowly at pH above 7.0. Due to its high T_g (nominal 172°C), which is very close to its thermal degradation temperature of 186 °C,[64] Eudragit® S100 is difficult to melt mix with API. Therefore, a miscible plasticizer needs to be used in order to reduce the T_g and improve processability.

5.5.1 Thermal Analysis

Figure 5.35 shows the DSC results of Eudragit® S100 and Eudragit® S100 containing 20 wt% TEC. The addition of TEC having a solubility parameter of 26.2$MPa^{1/2}$ to Eudragit® S100 (δ = 24.6 $MPa^{1/2}$) effectively reduced the polymer T_g to 97.9 °C as also reported in other studies.[28] Based on calculated solubility parameters (Table 2.1), DIK-Na^+ would be soluble in Eudragit® S100 as well as its mixture with TEC introducing an additional plasticizing effect. Similarly to IND that reduced the T_g of Eudragit® E100, DIK-Na^+ also reduced somewhat the T_g of Eudragit® S100/TEC proportionally to its loading.

Figure 5.36 shows TGA results of the plasticizer and blends containing the plasticizer and API. The plasticizer, TEC, started losing weight at 130 °C due to volatilization and possible decomposition. Eudragit® S100 without plasticizer shows an initial weight loss at 180 °C and a significant decomposition starting at 370 °C. The polymer containing the plasticizer started losing 20 wt% at 150 °C. Note that due to processing difficulties at low temperatures that would also correspond to minimum evaporation of the plasticizer, the temperature of 170 °C was selected for compounding.

At this temperature, the expected evaporation loss could reduce the concentration of TEC in the polymer from the nominal 20 wt% to a lower value.

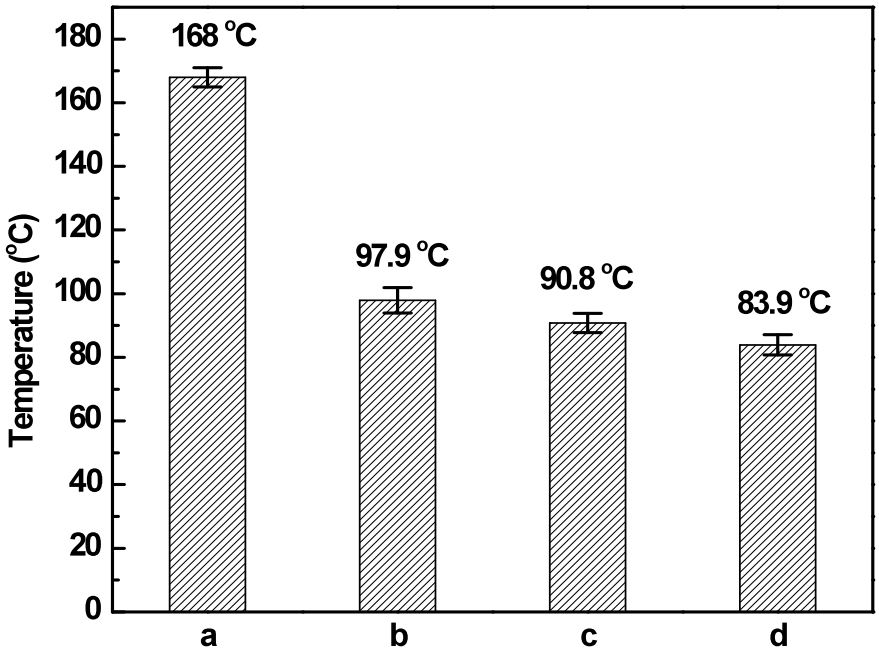

Figure 5.35 T_g of Eudragit® S100 and its blends: (a) Eudragit® S100, (b) Eudragit® S100/ 20wt% TEC, (c) Eudragit® S100/ 20wt% TEC-4wt% DIK-Na^+, (d) Eudragit® S100/ 20wt% TEC-15wt% DIK-Na^+ (Samples prepared by batch mixer).

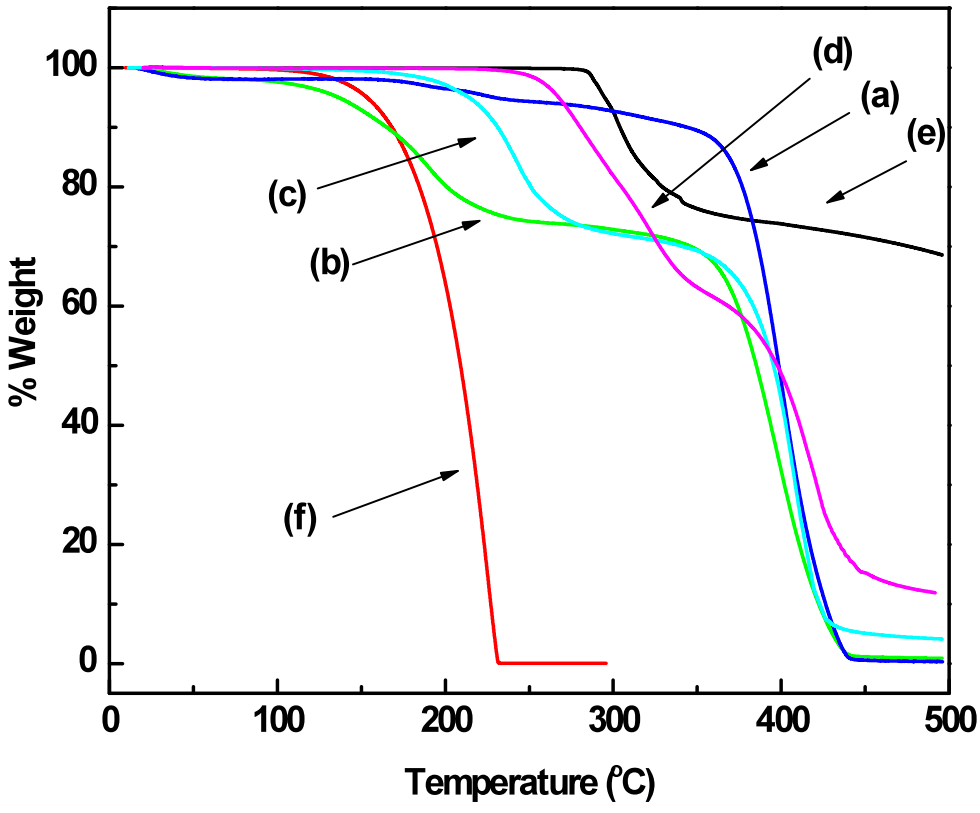

Figure 5.36 TGA results of (a) Eudragit® S100, (b) Eudragit® S100/ 20wt% TEC, (c) Eudragit® S100/ 20wt% TEC-4wt% DIK-Na^+, (d) Eudragit® S100/ 20wt% TEC-15wt% DIK-Na^+, (e) DIK-Na^+ and (f) TEC (Samples prepared by batch mixer).

5.5.2 XRD Analysis

As also expected from solubility parameter calculations, XRD results of Eudragit® S100/ 20 wt% TEC blends did not show any crystalline peaks, an indication of the presence of an amorphous API miscible with the polymer matrix (Figure 5.37).

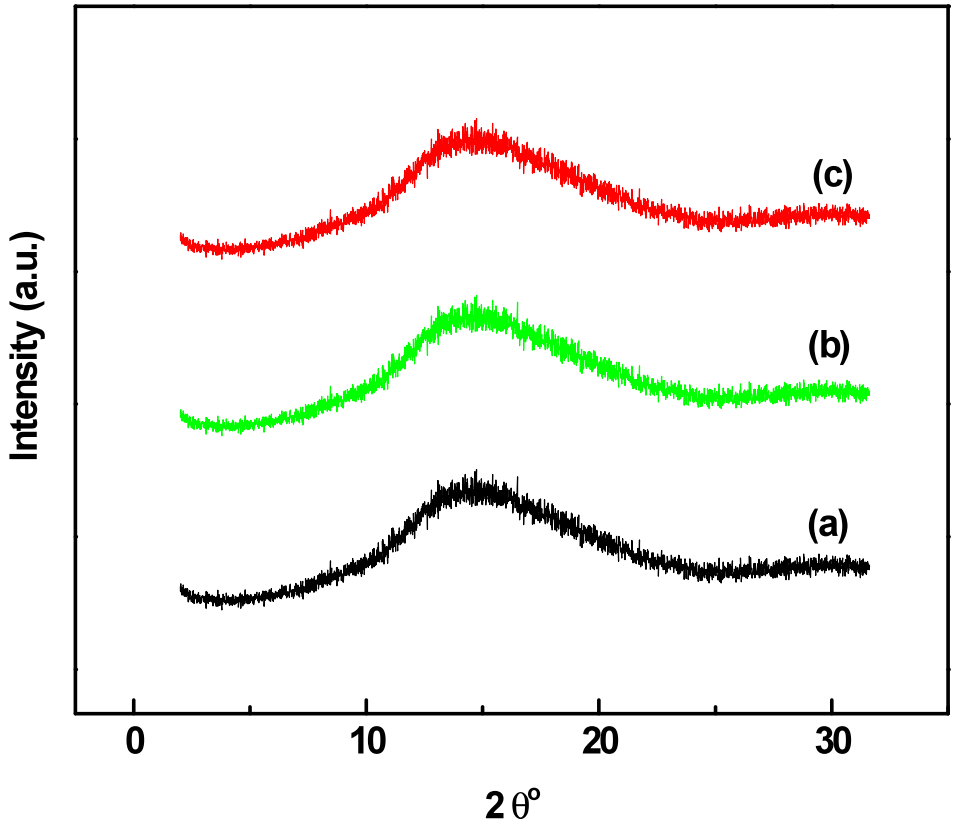

Figure 5.37 XRD results of (a) Eudragit® S100/ 20wt% TEC, (b) Eudragit® S100/ 20wt% TEC-4wt% DIK-Na^+, and (c) Eudragit® S100/ 20wt%TEC-15wt% DIK-Na^+ (Samples prepared by batch mixer).

5.5.3 Morphology Observation

Polarized light microscopy (Figure 5.38), SEM imaging and EDX chlorine mapping (Figure 5.39) confirmed the absence of crystalline particles and the uniform distribution of a fully dissolved DIK-Na^+ in the polymer matrix.

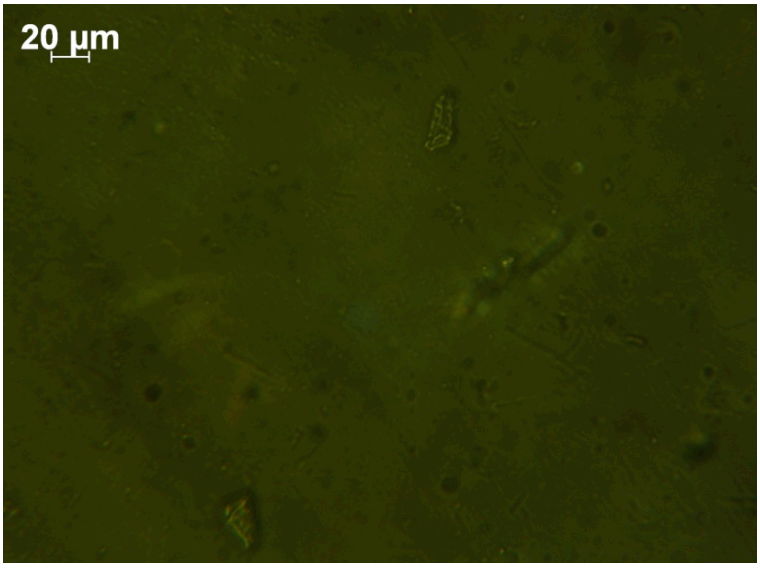

Figure 5.38 Polarized optical microscopy image of Eudragit® S100/ 20wt%TEC-15wt% DIK-Na^+.

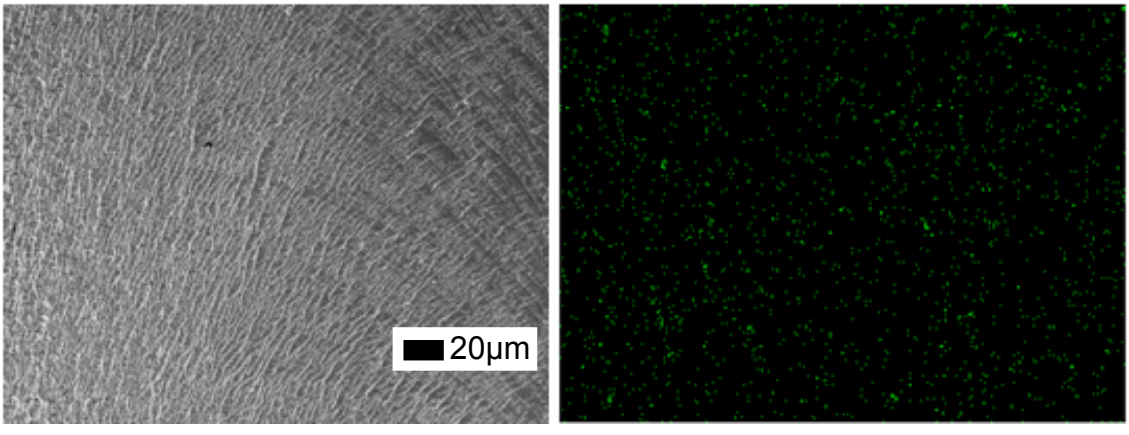

Figure 5.39 SEM image of Eudragit® S100/ 20wt%TEC-15wt% DIK-Na^+ (Left) and EDX chlorine mapping of the same region (Right).

5.5.4 Dissolution Test

Figure 5.40 shows the dissolution profiles of Eudragit® S100 blends in a pH 7.4 buffer solution. DIK-Na^+ dissolved quickly in the simulated body fluid, unlike its lack of dissolution under acidic conditions (Figure 5.12). Both Eudragit® S100/TEC (20wt%) with 4wt% and 15wt% DIK-Na^+ show sustained API release, which may be due to the slower dissolution rate of the polymer at this pH of 7.4 as compared to Eudragit® E100 at pH 1.2 (Figure 5.12). Dissolution of DIK from Eudragit® S100/ 4wt% DIK-Na^+ blend was tested at the pH 1.2 and pH was increased up to pH 7.4 (Appendix F) in order to confirm the stability of Eudragit® S100 at lower pH. The polymer excipient containing 15 wt% DIK-Na^+ shows slightly faster API release profile than the one containing 4 wt% DIK-Na^+. DIK-Na^+ has tendency to increase the pH of the medium, therefore the microenvironmental pH of blend containing 15wt% DIK-Na^+ can be higher than that of 4wt% blend. This could accelerate the DIK-Na^+ release. It should also be mentioned that according to literature data, higher plasticizer concentration can increase the API dissolution rate.

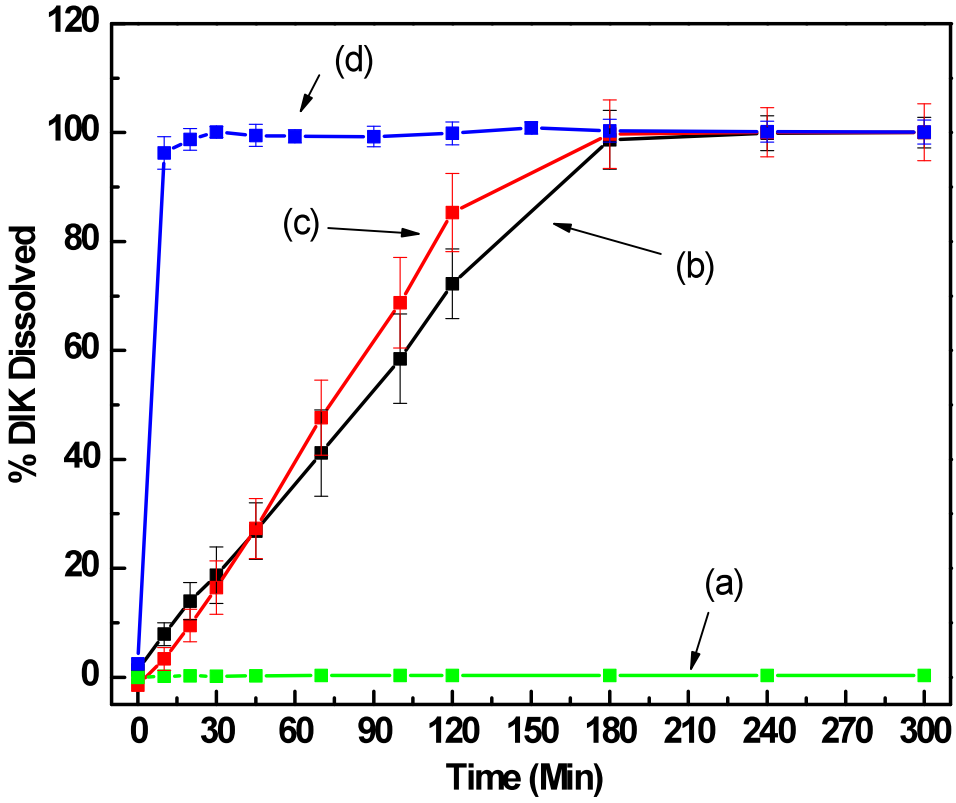

Figure 5.40 Dissolution profile of (a) Eudragit® S100/ 20 wt%TEC, (b) Eudragit® S100/ 20 wt% TEC- 4wt% DIK-Na^+, (c) Eudragit® S100/ 20wt% TEC/15wt% DIK-Na^+, and (d) DIK-Na^+ (in pH 7.4 phosphate buffer solution). (Samples prepared by batch mixer)

5.6 Conclusions

Eudragit® E100 was melt compounded with two different APIs, DIK-Na^+ and IND at 4 wt% and 15 wt% loadings. A miscible system was obtained with IND while DIK-Na^+ was not dissolved but dispersed in the polymer matrix. This miscibility difference was anticipated from calculations of solubility parameters. The immiscible system, Eudragit® E100/ DIK-Na^+, showed increased T_g and increased zero shear viscosity with increasing API loading.

Eudragit® E100/ DIK-Na^+ blends prepared by solvent casting could contain amorphous DIK-Na^+ in the matrix at low API concentration. This amorphous Eudragit® E100/ DIK-Na^+ system showed improved solubility of DIK-Na^+ up to 90% in a pH 1.2 buffer solution. The composites prepared by twin screw extrusion showed slightly finer API dispersion than the ones prepared by batch mixer. However, the apparent solubility of the API from these composites was similar to those of samples produced by the batch mixer. Enhanced solubility was more dependent on the state of API in the polymer rather than the preparation methods.

Eudragit® E100/IND blends showed decreased T_g and zero shear viscosity with increasing API loading. The increased apparent solubility of DIK-Na^+ from Eudragit® E100/DIK-Na^+ in 1.2 pH buffer solution was mainly attributed to increased wettablility due to the surfactant effect and increased microenvironmental pH due to the dissolved polymer. High DIK-Na^+ loadings resulted in API recrystallization in the medium. IND dissolved from Eudragit® E100/IND blends also showed increased apparent solubility

and this increased solubility was due to, not only to the increased wettabililty of the API by the polymer, but also to the IND transition from a crystalline to an amorphous state.

The Power law and the Peppas and Sahlin equations predicted the API dissolution mechanism from the polymer matrix. The results indicated that super case-II transport and erosion mechanisms are dominant. Therefore, API dissolution from the polymer matrix was better represented by the Hopfenberg surface erosion model.

Eudragit® S100/TEC also produced a miscible system with DIK-Na^+. This blend also showed reduced T_g and zero shear viscosity. In addition, Eudragit® S100/TEC blends showed sustained API release profile.

CHAPTER 6

API-FUNCTIONALIZED NANOCLAY/POLYMER COMPOSITES

Conventionally, nanoclays are used in order to increase thermal, barrier and mechanical properties of polymers. Studies on other polymer related applications are very rare. In this chapter, a novel application, namely the sustained API release from anionic nanoclays embedded in a water soluble polymer is studied and compared with the release from binary systems, which were discussed in previous chapters. To the best of our knowledge, this type of polymer/API/clay ternary system produced by melt mixing has not yet been reported in the literature.

6.1. Eudragit® E100 and DIK/Clay Compounds

In a previous chapter, a DIK/Clay hybrid was shown to have improved DIK apparent solubility due to the amorphous state of the API in the clay interlayer space. Therefore, it was anticipated that incorporation of the nanoclay hybrid may also increase the apparent solubility of the API released from the Eudragit® E100/ nanoclay hybrid composites.

6.1.1 XRD Analysis

Eudragit® E100 is an amorphous polymer showing no crystalline peaks in its XRD spectrum (Figure 6.1 (a)). However, Eudragit® E100 mixed with 15 wt% DIK-Na^+ shows a major peak at 6.67^o (Figure 6.1 (b)) and other minor peaks elsewhere. These peaks provide evidence that DIK-Na^+ is not dissolved during melt mixing but dispersed as crystalline particles. Eudragit® E100 compounded with DIK/Clay (10 wt%) (Figure 6.1 (c)) also shows crystalline peaks but these are not exactly the same as the ones of

Eudragit® E100 compounded with DIK-Na^+ but more closely correspond to those of the nanoclay hybrid DIK/Clay (Figure. 6.1(d)). This suggests that the API in the clay interlayer space did not undergo any changes during the melt mixing process. This is because the first peak in Figure 6.1(d) marked with a star corresponding to the intercalated API, does not shift to a higher 2θ angle but to a slightly lower 3.83° 2θ angle in Figure 6.1(c). The slightly increased basal spacing of DIK/Clay in the Eudragit® E100 matrix after hot melt processing may have resulted from a small amount of polymer migrated into the anionic clay interlayer space during melt compounding. Similar effects have been observed in other studies on nanoclay composites.[112,113]

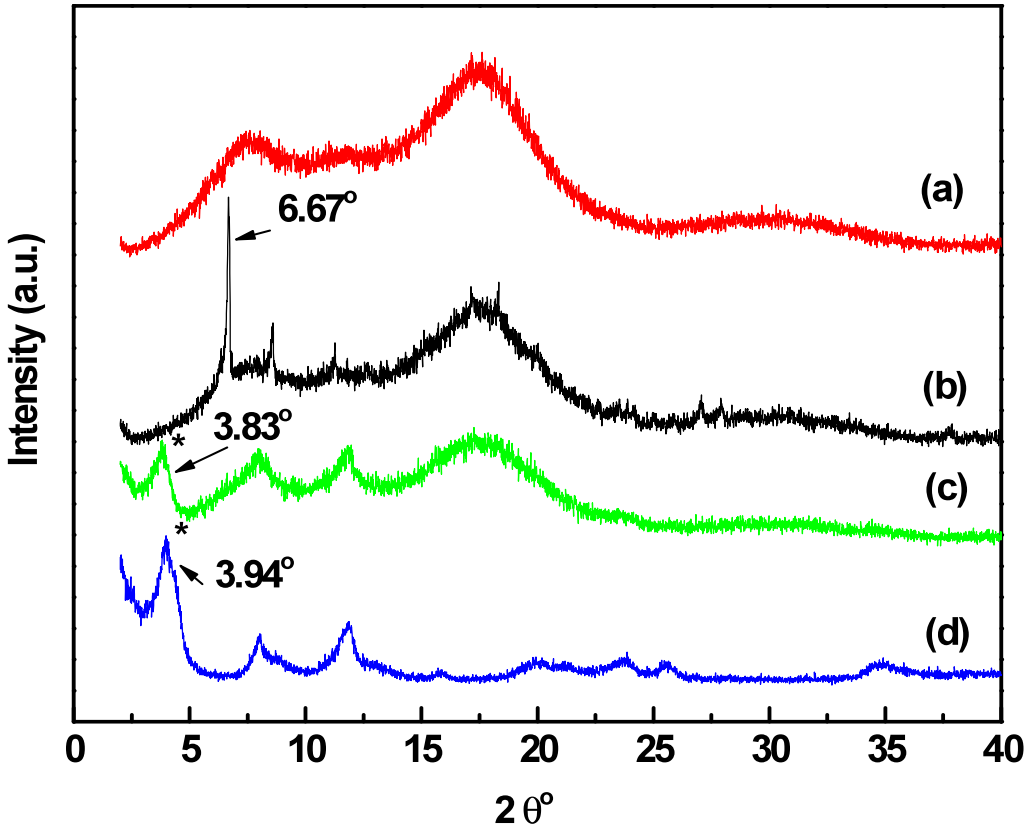

Figure 6.1 XRD results of (a) Eudragit® E100, (b) Eudragit® E100/ 15wt% DIK-Na^+, (c) Eudragit® E100-10wt% DIK/Clay, and (d) DIK/Clay (Samples prepared by batch mixer).

6.1.2 SEM and EDX Analysis

The fracture surfaces of Eudragit® E100 and its melt mixed compounds were examined by SEM. As discussed in previous chapters, Eudragit® E100 compounded with DIK-Na^+ shows agglomerated crystalline API particles (Figure 6.2 (top)). The size of the DIK/Clay hybrid particles shown in Figure 6.2 (bottom) is significantly smaller as compared to that of DIK-Na^+ particles and are more uniformly dispersed (average particle size 10 μm vs. 30 μm).

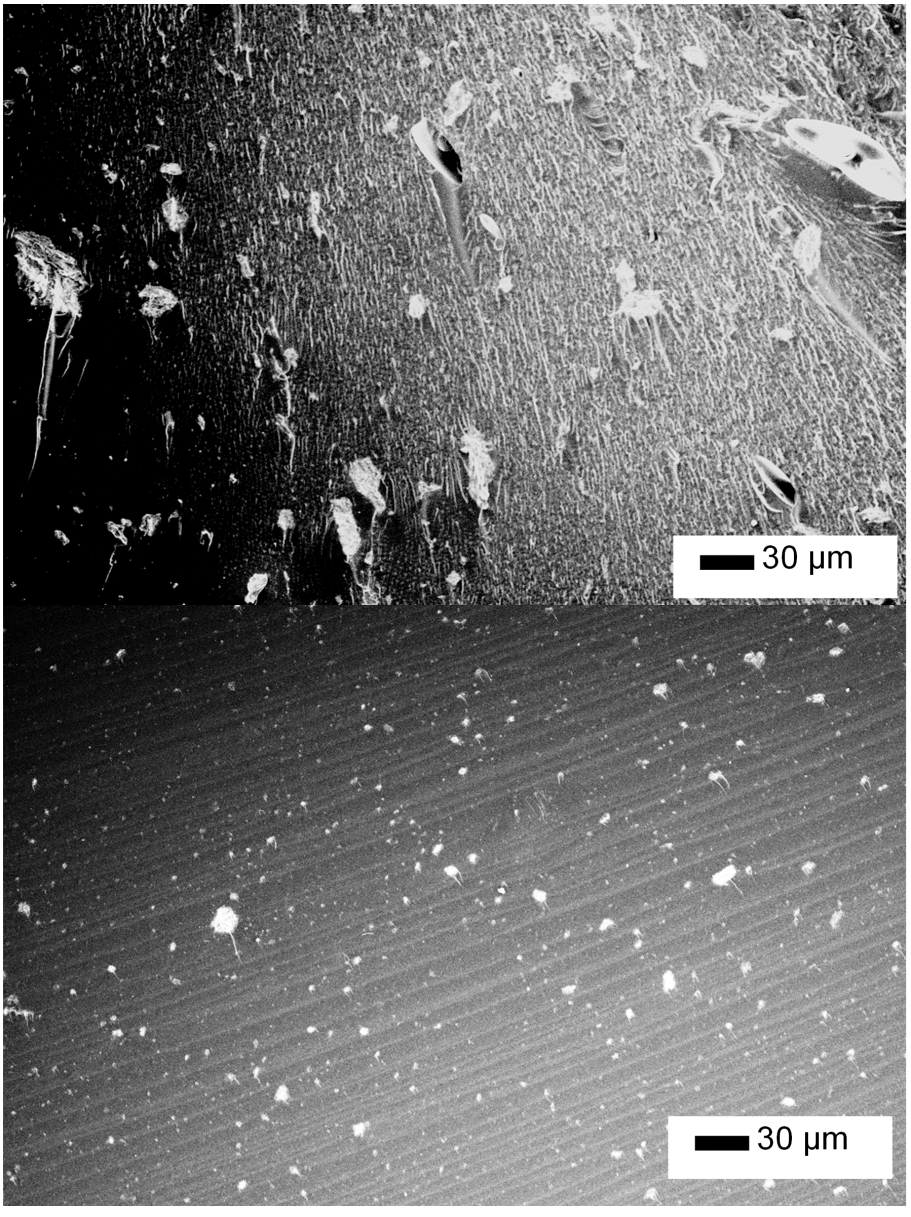

Figure 6.2 SEM images of fracture surface of (top) Eudragit® E100/ 4 wt% DIK-Na^+ and (bottom) Eudragit® E100-10wt% DIK/Clay (Samples prepared by batch mixer).

6.1.3 Dissolution Test

The data from the dissolution tests of Eudragit® E100 compounded with DIK-Na^+, DIK/Clay and physically mixed with DIK-Na^+ in SGF are shown in Figure 6.3.

The improved apparent solubility of DIK-Na^+ from Eudragit® E100/DIK-Na^+ compounds as compared to DIK-Na^+ from the Eudragit® E100/DIK-Na^+ physical mixture may be attributed to the less aggregated DIK-Na^+ particles in the matrix after hot melt mixing and the enhanced wettability due to the polymeric excipient. The API from the physical mixture was separated from the polymer powder and floated as segregated particles when the sample was immersed into the medium. As a result, the hydrophobic API (at low pH) tended to minimize its contacting surface with the medium, thereby reducing wettability. The API from the Eudragit® E100-DIK/Clay composite shows roughly 10% increased solubility as compared to the API from the Eudragit® E100/DIK-Na^+ compound. This increased apparent solubility can be explained as follows:

1. The crystalline DIK-Na^+ is at least partially present in an amorphous state in the anionic clay interlayer space and would therefore dissolve more efficiently in the medium.

2. The smaller size of the DIK/Clay as compared to the DIK-Na^+ agglomerates in the matrix would provide a larger contacting surface area, thereby affecting rate of dissolution and apparent solubility.

Along with the increased apparent solubility, it should be noted that the API dissolution results from Eudragit® E100-DIK/Clay have a relatively lower variability as compared to those from the Eudragit® E100/DIK-Na^+ compound due to the smaller and more uniformly dispersed DIK/Clay particles. However, the apparent solubility cannot reach 100 %, unlike the one in the case of API-polymer miscible systems[23] which confirms again that fully dissolved amorphous API in the polymer matrix is preferable in order to achieve the maximum apparent solubility.

By comparison to the difference in the API dissolution rate between the DIK/Clay and DIK-Na^+ shown in Figure 4.11, the API dissolution rates from the Eudragit® E100 compounds containing only API or nanoclay hybrid do not show significantly differences. This could be evidence that the surfactant effect of Eudragit® E100 in the earlier stages of the dissolution test was dominant and it prevailed over the effect of the clay hybrid. The physical mixture shows a slightly higher dissolution rate at the early stages. This is because the small size Eudragit® E100 powder (other samples were pressed to thin disks) dissolved faster and affected the overall mixture dissolution rate immediately.

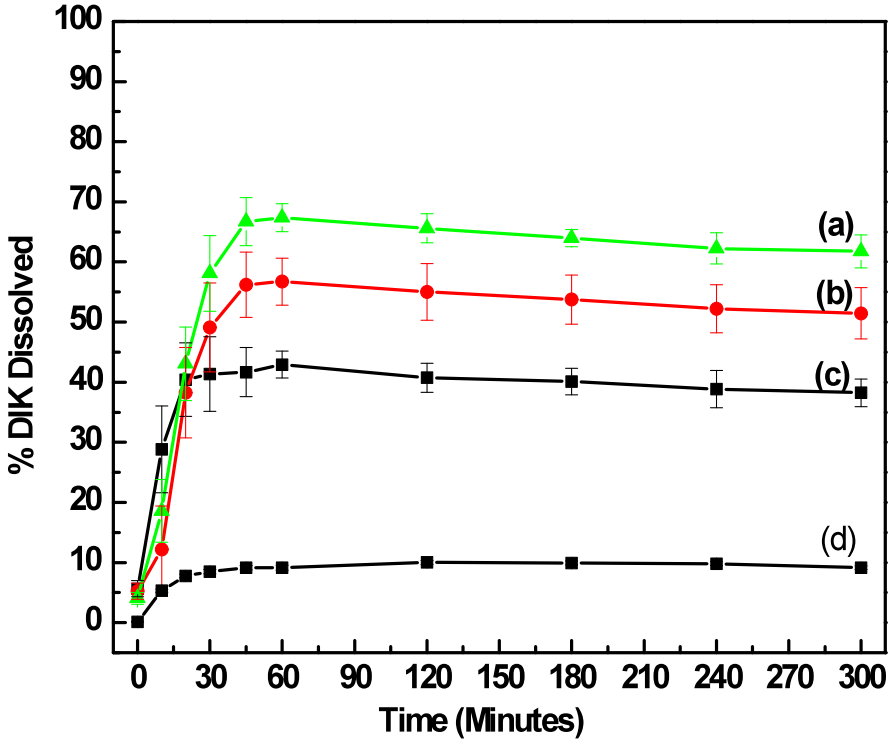

Figure 6.3 Dissolution results in SGF (pH 1.2) of: (a) Eudragit® E100-10 wt% DIK/Clay, (b) Eudragit® E100/ 4wt% DIK-Na^+, (c) physical mixture of Eudragit® E100 and 4 wt% DIK-Na^+ (Samples prepared by batch mixer) (Note: Data on DIK/Clay (d) added for comparison).

Dissolution test of the ternary system (Eudragit® E100-DIK/Clay) prepared by three different methods (batch melt mixing, solvent casting, and extrusion) showed similar dissolution patterns (i.e. similar dissolution rate and apparent solubility: see Appendix G). This is because each preparation method achieved micro rather than nano dispersion of the hybrid in the polymer matrix (Appendix H).

6.2 Eudragit® E100 Compound with IND/Clay

Eudragit® E100 and IND form a miscible system by melt mixing during which IND becomes amorphous. Therefore, maximum API release and apparent solubility are already expected for this system. In this section, binary and ternary Eudragit® E100 compounds containing respectively amorphous IND and IND at the clay interlayer space are compared.

6.2.1 XRD Analysis

In Figure 6.4 (d)**,** Eudragit® E100-IND/Clay shows a peak at 4.79^{o} due to the IND/Clay; this is absent in the spectra of the individual components. Recalling the data on DIK, Figures 6.1(c, d) contained similar spectra of DIK/Clay in Eudragit® E100 matrix and DIK/Clay. The interlayer spacing of DIK/Clay showed an increase from (2.24 nm → 2.31 nm) during melt mixing, from migration of polymer molecules into the clay layers by comparison to Figure 6.4 (d) that shows a slightly reduced interlayer space (1.91 nm → 1.84 nm) and a reduced peak intensity indicating reduced crystallinity. This decreased interlayer spacing of IND/Clay and reduced XRD intensity could be attributed to structural changes of IND during melt mixing at a temperature approaching its melting temperature of 162 ^{o}C and the high shear stresses involved.

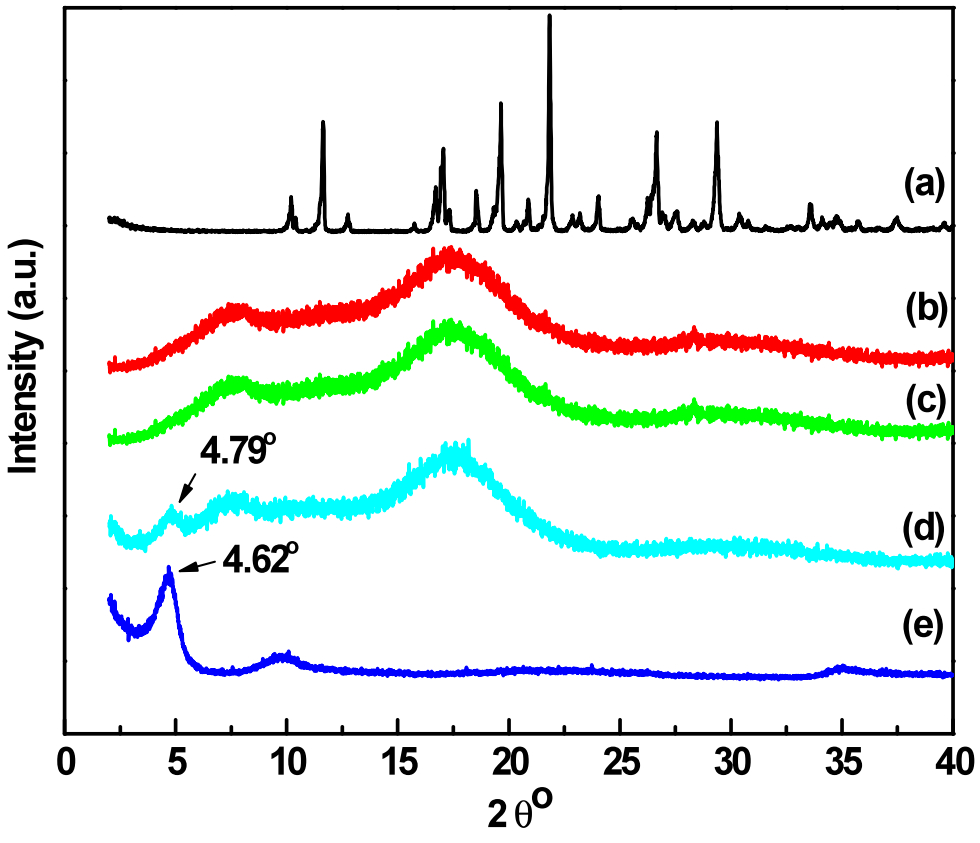

Figure 6.4 XRD results of (a) IND, (b) Eudragit® E100, (c) Eudragit® E100/4 wt% IND, (d) Eudragit® E100-10wt% IND/Clay, and (e) IND/Clay (Samples prepared by batch mixer).

6.2.2 SEM Analysis

While Eudragit® E100/ IND mixtures indicate a miscible system (Figure 6.5 top), the Eudragit® E100- IND/Clay system (Figure 6.5 bottom) shows particles in the polymer matrix, presumably corresponding to microsized poorly dispersed clay aggregates that should contain API. These morphological differences should affect the dissolution profiles as shown below.

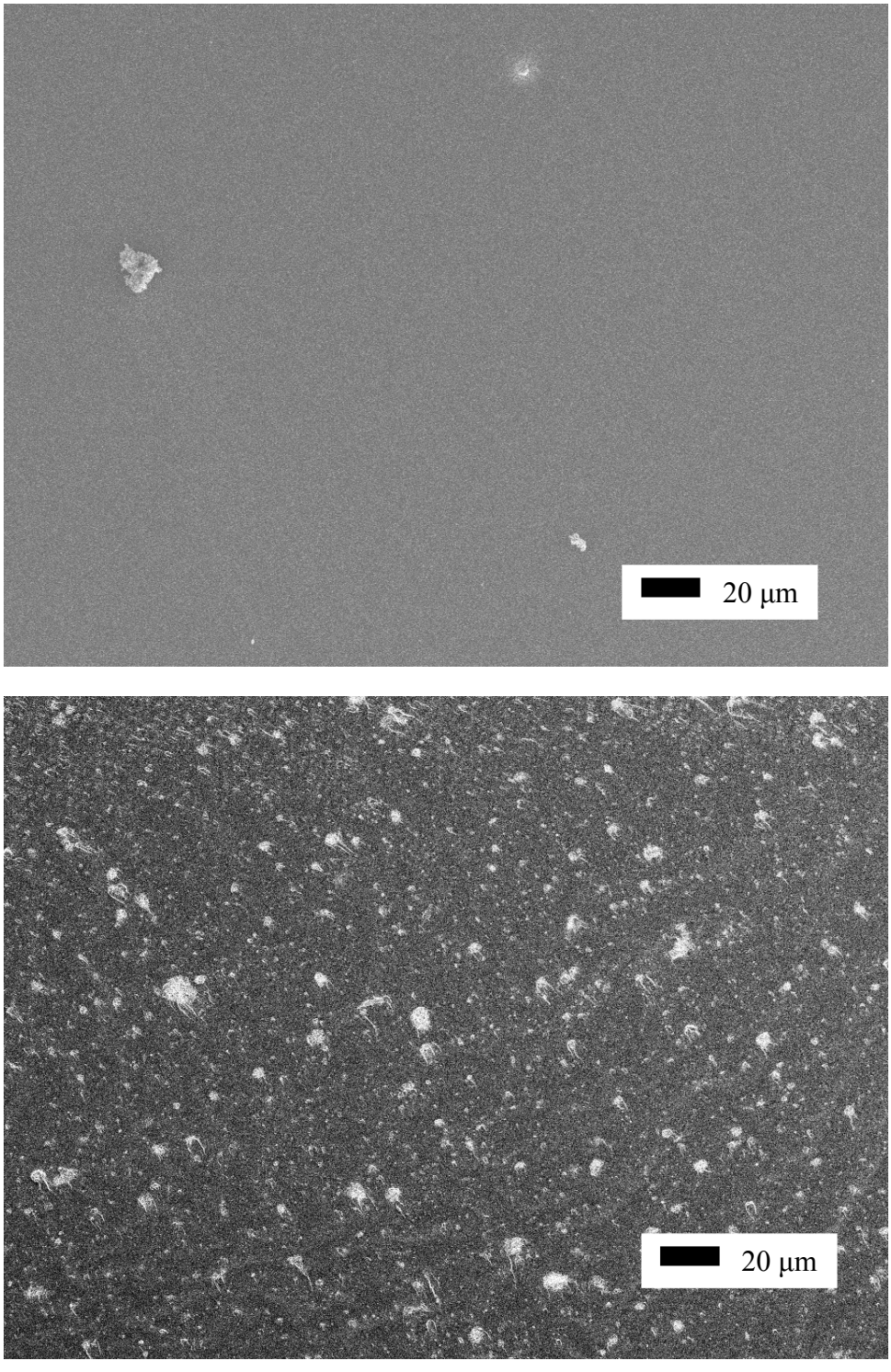

Figure 6.5 SEM images of the fracture surface of (top) Eudragit® E100/IND, and (bottom) Eudragit® E100-IND/Clay (Samples prepared by batch mixer).

6.2.3 Dissolution Results

Dissolution profiles of IND from Eudragit® E100/ 4wt% IND and Eudragit® E100-10wt% IND/Clay in the SGF (pH 1.2) are shown in Figure 6.6. Eudragit® E100 containing 10% IND/Clay shows approximately 70% of IND solubility while Eudragit® E100/ 4wt%IND shows almost 100 % IND apparent solubility. Therefore, it can be concluded that for this system API incorporation in the nanoclay is not as efficient as for the system containing amorphous API in the polymer matrix. Possible reasons can be strong interactions between IND and clay that retard dissolution and/or state of the API in the clay agglomerates (amorphous vs. crystalline).

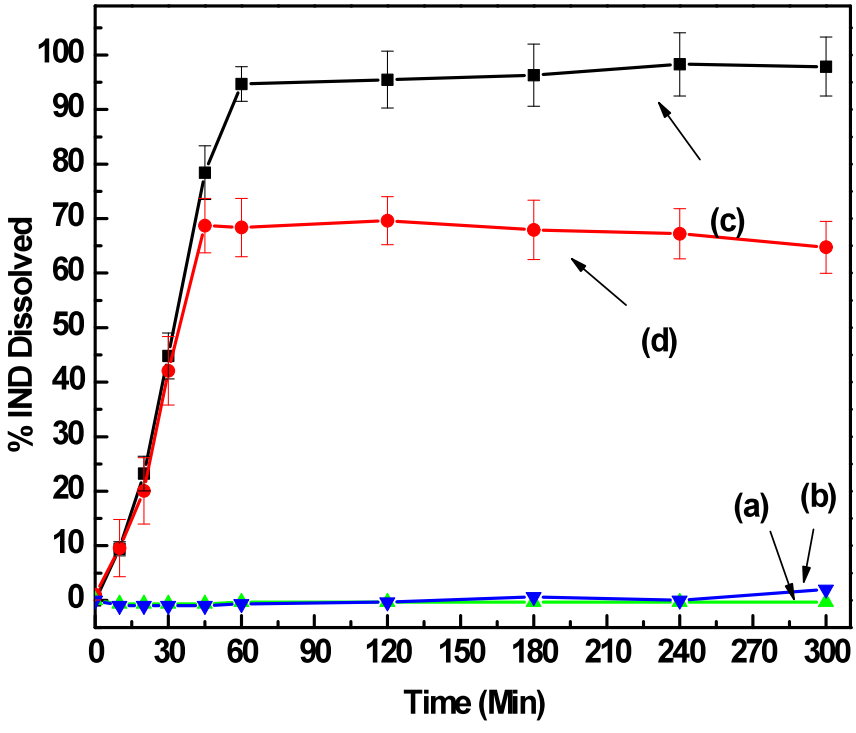

Figure 6.6 Dissolution profiles in SGF pH 1.2 of (a) Eudragit® E100, (b) IND, (c) Eudragit® E100/4wt% IND and (d) Eudragit® E100-10wt% IND/Clay (Samples prepared by batch mixer).

6.3 Eudragit® S100-Plasticizer Compounds with DIK/Clay

The quaternary system (polymer/plasticizer/API/clay) for this particular combination employs a different plasticized acrylic polymer and is intended to be used for sustained API delivery. In a conventional method employing a binary system of polymer /API, the API is directly released from the polymer matrix while the polymer is dissolved or eroded. In this quaternary system, API is not directly released but has to diffuse out from the clay interlayer in the presence of platelets that may control diffusion. Therefore, it is anticipated that API may be released slower than in a conventional binary system.

6.3.1 Thermal Analysis

Figure 6.7 contains TGA results of Eudragit® S100 plasticized with 20 % TEC and the blends/composites of the plasticized mixture with DIK-Na^+ and DIK/Clay. TGA curves of the unmodified polymer and its additives TEC and DIK-Na^+ are also shown for comparison. Figure 6.7 contains essentially the data shown and discussed earlier in Figure 5.32 with an additional curve for the composite Eudragit® S100/ 20% TEC- 10 wt% DIK/Clay. Thermal stability expressed as temperature at 20% weight loss provides the following ranking: Eudragit® S100 > DIK-Na^+ > Eudragit® S100/ 20 wt% TEC-10 wt% DIK/Clay > Eudragit® S100/ 20 wt% TEC-4 wt% DIK-Na^+ > Eudragit® S100/ 20 wt% TEC > TEC.

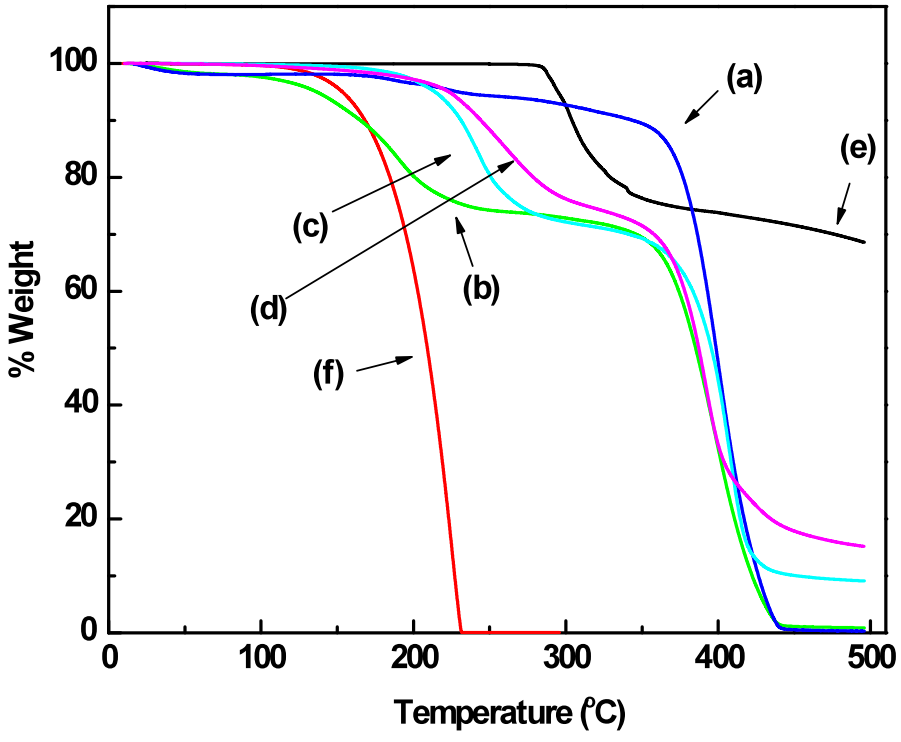

Figure 6.7 TGA results of (a) Eudragit® S100, (b) Eudragit® S100/ 20% TEC, (c) Eudragit® S100/ 20% TEC- 4 wt% DIK-Na^+, and (d) Eudragit® S100/ 20% TEC- 10 wt% DIK/Clay, (e) DIK-Na^+ and (f) TEC (Samples prepared by batch mixer).

Figure 6.8 contains glass transition temperature values for Eudragit® S100 plasticized with 20% TEC and the blends/composites of the plasticized mixture with DIK-Na^+ and DIK/Clay. Figure 6.8 includes essentially the data shown in Figure 5.31, and, in addition, the T_g of Eudragit® S100/ 20% TEC-10 wt% DIK/Clay. The glass transition temperature of composite (**e)** containing plasticizer and DIK/Clay was somewhat higher than that of Eudragit® S100 containing either only plasticizer (**b**) or plasticizer and DIK-Na^+ (**c** or **d)**. This increased T_g is a common phenomenon in clay

composites since the dispersed clay restricts the mobility of the polymer chains.[114] It can also be argued that during melt processing the API which could also be acting as a plasticizer was not released from the interlayer. Ha and Xanthos[115] reported that ionic liquids, which could be functioning as plasticizers, exerted a small plasticizing effect on PLA due to the barrier effect of the nanoclay layers.

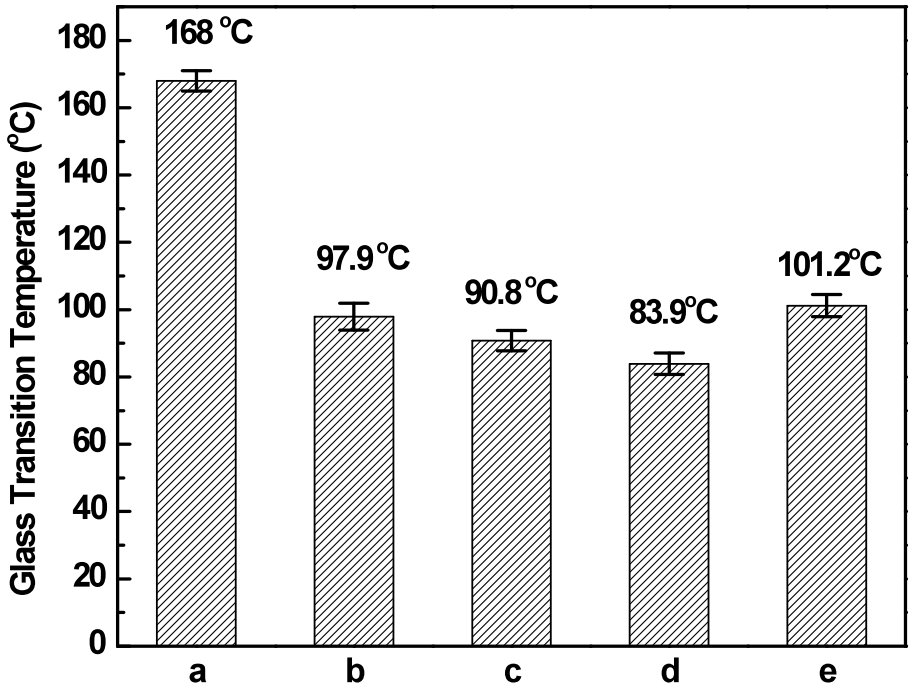

Figure 6.8 T_g of Eudragit® S100 composites of (a) Eudragit® S100, (b) Eudragit® S100/ 20wt% TEC, (c) Eudragit® S100/ 20 wt% TEC- 4 wt% DIK-Na^+, (d) Eudragit® S100/ 20wt% TEC-15 wt% DIK-Na^+, and (e) Eudragit® S100/ 20 wt% TEC-10 wt% DIK/Clay (Samples prepared by batch mixer).

6.3.2 SEM and EDX Analysis

Figure 6.9 shows a fracture surface of the Eudragit® S100 composite containing 20 wt% TEC and 10 wt% DIK/Clay. By rough approximation from the SEM images, the DIK/Clay particles are smaller than 5 μm (Figures 6.9 and 6.10) and the particles are more uniformly dispersed than in the Eudragit® E100 matrix (Figure 6.2 bottom). This suggests that Eudragit® S100 has better compatibility with DIK/Clay than Eudragit® E100.

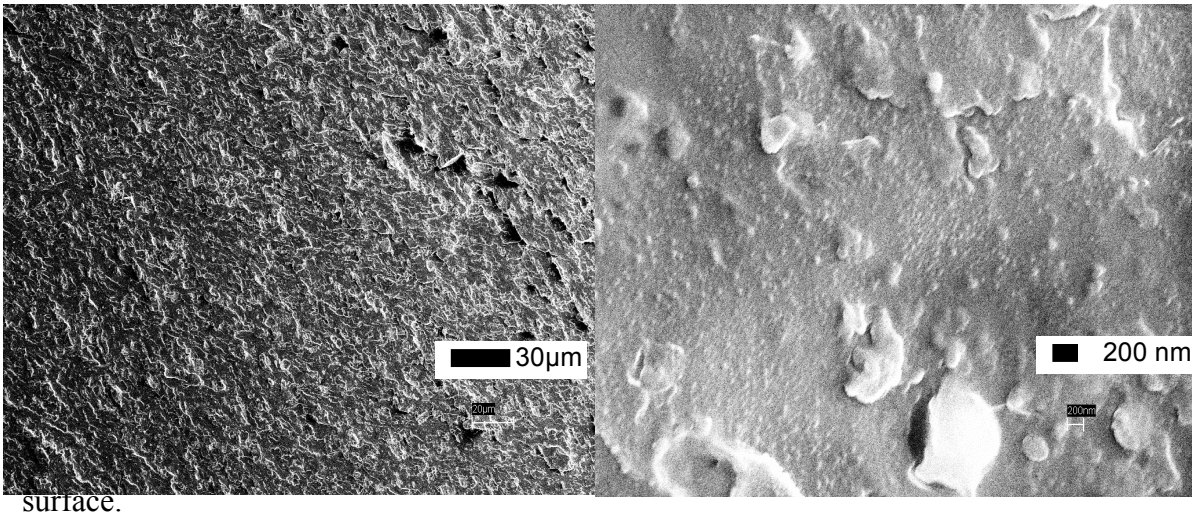

surface.

EDX mapping was carried out in order to identify the location of DIK/Clay in the matrix and the degree of dispersion of the hybrid. The shape and location of the DIK/Clay could be identified by EDX mapping of Mg, Al, and Cl mapping since HT contains magnesium and aluminum, and DIK contains chlorine. On the EDX images, dense bright dots indicate higher population of each individual element. The population of chlorine matched with magnesium and aluminum indicating that DIK is associated with nanoclay.

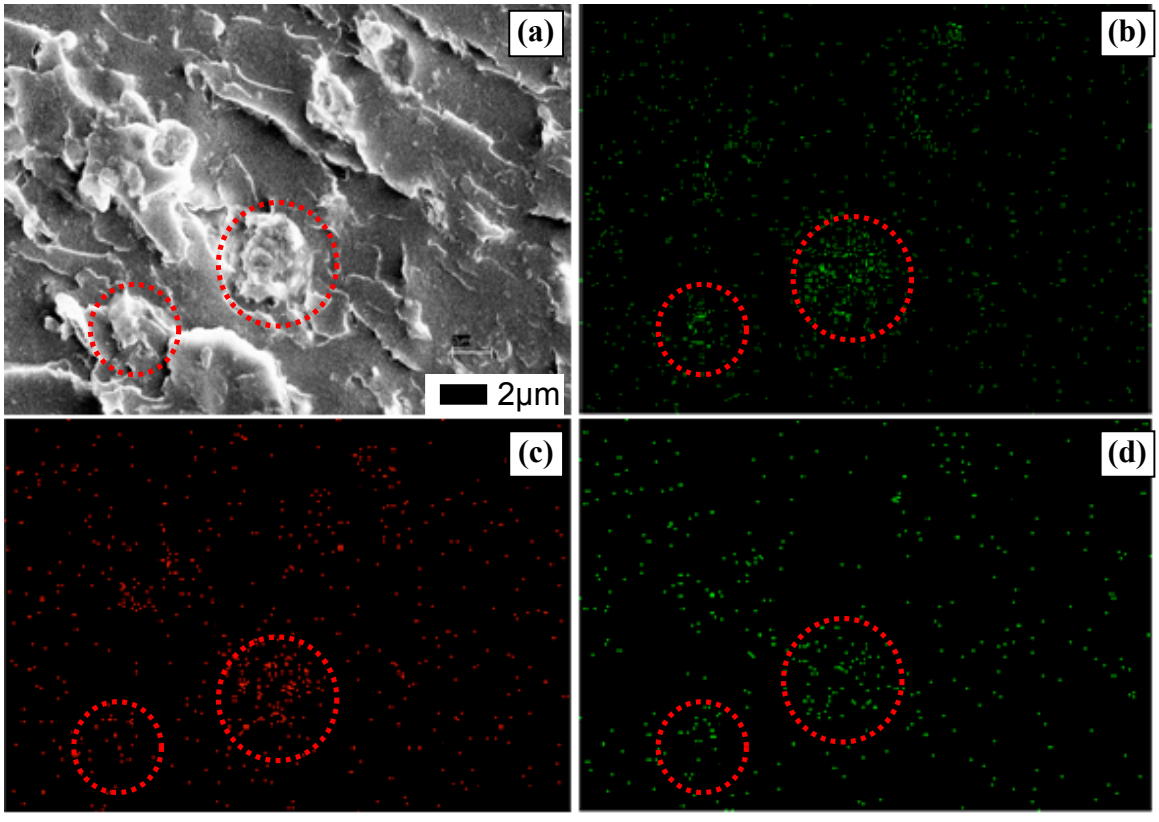

Figure 6.10 Images of Eudragit® S100/20 wt% TEC-10 wt% DIK/Clay by (a) SEM, (b) EDX Mg mapping, (c) EDX Al mapping, and (d) EDX Cl mapping (Samples prepared by batch mixer).

6.3.3 Rheological Study

The immiscible API-polymer system (Eudragit® E100/ DIK-Na^+) showed increased viscosity vs. the unfilled polymer since the API acted as a rigid filler (Figure 5.10). By contrast, based on their solubility parameters, it was expected that DIK-Na^+ and Eudragit® S100/TEC would be miscible; from the reduced T_g of the polymer in the Eudragit® S100/TEC-DIK-Na^+ compounds, it was also expected that DIK-Na^+ would act as an additional plasticizer. Figure 6.11 shows related RMS results where DIK-Na^+ reduced the zero shear viscosity of the matrix while DIK/Clay increased its viscosity. Thus, the systems can be classified respectively as polymer blends and polymer

composites. Unlike Eudragit® E100, Eudragit® S100 and its composites do not show a cross-over point between loss and storage modulus, and the storage modulus is always higher than the loss modulus indicating rubber like properties over the frequency range.

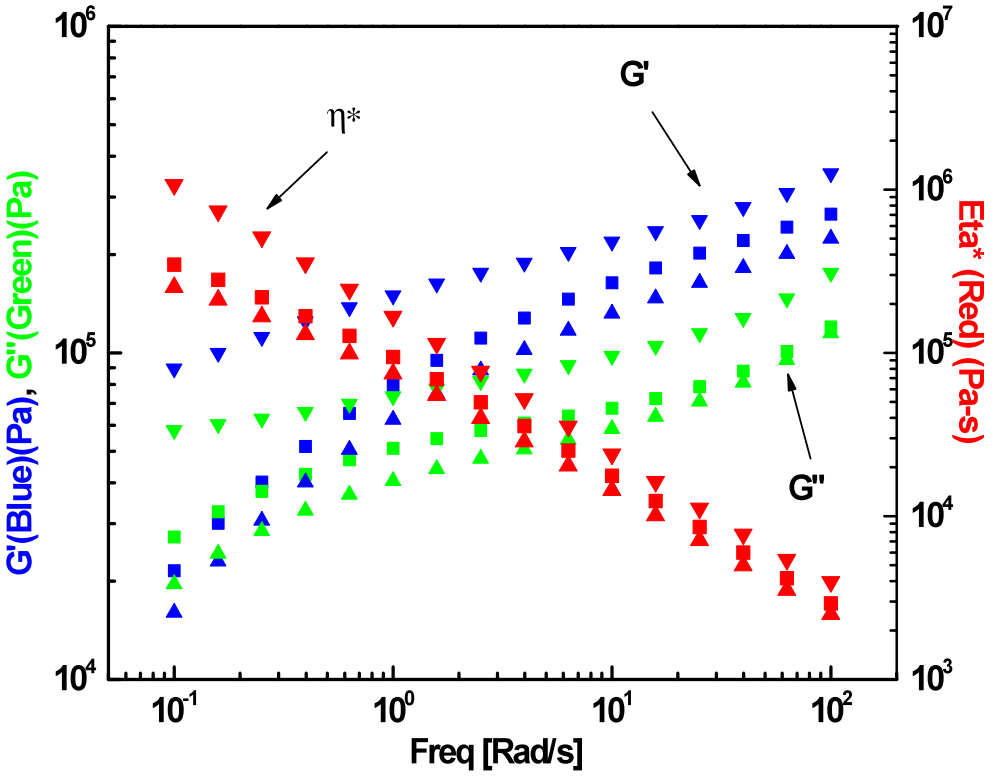

Figure 6.11 RMS results of (■) Eudragit® S100/20 wt% TEC, (▲) Eudragit® S100/20 wt%TEC-4 wt% DIK-Na^+, and (▼) Eudragit® S100/20 wt%TEC-10 wt% DIK/Clay (Samples prepared by batch mixer).

6.3.4 Dissolution Study

Initially, among the expected characteristics of the clay hybrid system was a sustained drug release. Since due to tortuosity reasons the intercalated API in the nanoclay interlayer space might have required more time to be released, sustained release seemed readily achievable. However, in the simulated gastric fluid acidic medium at pH 1.2, the anionic nanoclay was dissolved shortly after its immersion into the medium and the API in the clay interlayer would thus immediately be released. On the other hand, since HT is not soluble at a pH 7.4 simulated body fluid medium, sustained API release would be expected. Figure 6.12 shows the dissolution profiles of Eudragit® S100/ 20 wt% TEC containing 4 wt% DIK-Na^+ and 10 wt% DIK/Clay. Eudragit® S100 containing the API shows a relatively slow release profile while the one containing DIK/Clay shows an even slower API release. The different release behavior between the two compounds can be explained as follows:

1) DIK in the clay interspacing may experience one more step in its release path, which is diffusion from the clay interlayer space.

2) Nanoclay platelets may act as barriers and slow down the DIK release process in the polymer matrix and/or its buffer solution.

Note that Eudragit® S100/ 20wt% TEC containing 10wt% DIK/Clay achieved almost 100% DIK release, while DIK/Clay in Eudragit® E100 reached only 70% (Figure 6.3). This different apparent solubility is mainly due to the different water solubility of the API in the different pH media.

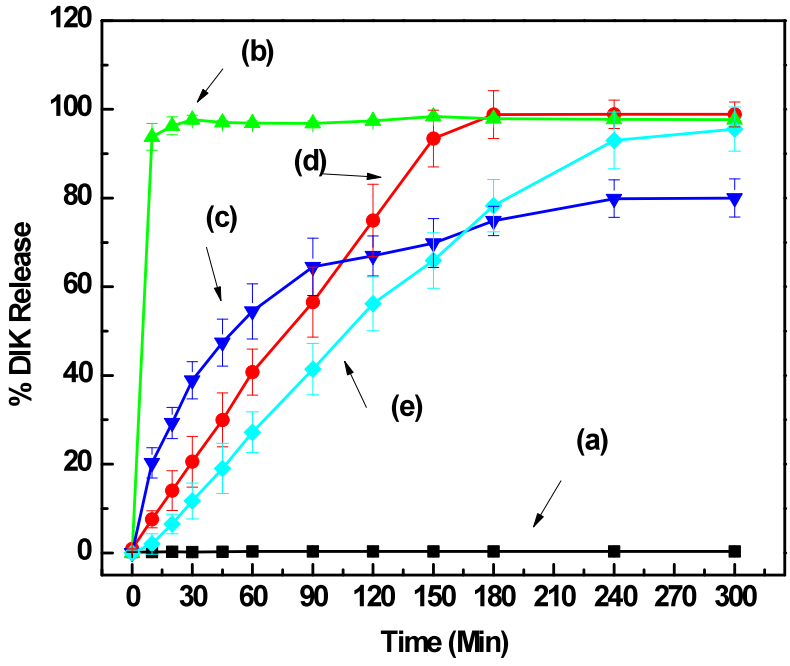

Figure 6.12 Dissolution results in pH 7.4 buffer of (a) Eudragit® S100, (b) DIK-Na^+, (c) DIK/Clay, (d) Eudragit® S100/ 20 wt% TEC- 4 wt% DIK-Na^+ and (e) Eudragit® S100/ 20 wt% TEC-10 wt% DIK/Clay (Samples prepared by batch mixer).

Dissolution results of Eudragit® S100 compounds were fitted with Equations 4.2 and 4.3 (ordinary least square regression, ± 95% confidence limits)[116] and results are listed in Table 6.1. It is to be noted that Eudragit® S100 compounds containing DIK/Clay have a larger "n" exponent value (Equation 4.2) as compared to the ones that do not contain clay. This is somehow indicating that the diffusion tendency of DIK vs. erosion was reduced due to the presence of the clay in the polymer matrix. Values calculated by Equation 4.3 also show interesting results that the sample containing nanoclay showed reduced diffusion constant while the erosion constant remains at a similar value as compared to the sample without the nanoclay. Therefore, it can be interpreted that DIK

release from the polymer matrix was either obstructed in the presence of nanoclay due to its barrier property, or the actual release mechanism was modified in the presence of the nanoclay.

Table 6.1 DIK dissolution fitting results of from Eudragit® S100/ TEC matrix for Equations 4.2 and 4.3

Sample	Power law, (Equation 4.2)	Peppas and Sahlin, (Equation 4.3)	
	n ± 95% CI	k_1 ($min^{-0.5}$) ± 95% CI	k_2 (min^{-1}) ± 95% CI
Eudragit® S100/20wt% TEC-4wt% DIK-Na^+	0.75 ± 0.02	0.75 ± 0.01	0.56 ± 0.05
Eudragit® S100/20wt% TEC-10wt% DIK/Clay	0.92 ± 0.03	0.02 ± 0.01	0.57 ± 0.04

6.4 Conclusions

Ternary polymer systems containing API modified nanoclay were compared with binary systems in which API was melt mixed with the polymer directly. Ternary systems showed several advantages. For example, the API from Eudragit® E100 melt mixed with DIK/Clay had higher DIK apparent solubility than from a binary system and less dissolution variation. However, use of this ternary system could not increase the API apparent solubility as much as an API-polymer miscible system did. As an example, Eudragit® E100 containing IND/Clay showed less apparent IND solubility than Eudragit® E100/IND system. Eudragit® S100 compounds containing plasticizer and DIK/Clay showed slower API release than in the absence of clay in pH 7.4 buffer solution. This slower release behavior due to the presence of the nanoclay platelets in the polymer matrix would be related to the formation of a more tortuous API diffusion path and/or modification of the release mechanism in the presence of the nanoclay. It remains to be seen whether a system containing exfoliated nanoclay and API separately mixed with the polymer would have different dissolution characteristic than our existing system.

CHAPTER 7

CONCLUDING REMARKS AND SUGGESTED FUTURE STUDIES

7.1 Summary

This dissertation contains the results of three related novel investigations in the field of structure-property-processing relationships of pharmaceutical polymer-based products. They are: a) modification of a pharmaceutical anionic nanoclay with two different APIs to produce nanohybrid API carriers intended to be used alone or in two, structurally different, acrylic polymer matrices, b) comparison of binary systems containing the above APIs in the selected acrylic polymers in terms of their miscibilities with the polymer, but in the absence of nanoclay, and c) comparison of the polymer/API binary systems with ternary polymer/API/Clay systems. Polymeric compounds were primarily produced by hot melt batch or extrusion mixing.

Hydrotalcite containing carbonate ions in its interlayer space is one of the most common types of anionic clays. However, due to the strong electrostatic forces between the carbonate anions in the interlayer space and the cationic metal layers of hydrotalcite, it is extremely difficult to replace the carbonate anions with foreign anions by ion exchange, including those anions present in anionic APIs. The co-precipitation method which involves synthesis of the clay in the presence of organic modifiers is generally used in order to produce the modified hydrotalcite containing foreign anions. Instead of the co-precipation method, the calcination method which can be directly applied to carbonated hydrotalcite was used in this work and successfully achieved API intercalations. During reconsitution of the clay, the crystalline API (DIK-Na^+ or IND) in the clay interlayer was apparently transformed in an amorphous state, and as a result it

showed increased apparent solubility in the simulated body fluids. The intercalated API was stable in the clay interlayer for several months. However, it should be noted that IND appeared to have degraded or structurally modified by the calcined hydrotalcite during the clay exchange reaction. Therefore, a particular combination of API and clay needs to be carefully selected.

The second study dealt with API-polymer miscible or immiscible systems prepared by different mixing methods. The selected APIs, DIK-Na^+ and IND, have low solubility at the low pH of the aqueous medium and different solubility parameters by comparison with the polymer. The Eudragit® E100/ DIK-Na^+ mixture produced by batch melt mixing showed an API solid dispersion whereas the Eudragit® E100/ IND system produced an API solid solution. These different morphologies were anticipated by calculating API and polymer solubility parameters and were confirmed by several analytical methods such as SEM, PLM, and XRD. Apparently, the API dissolved from the miscible API-polymer system showed better apparent solubility in the aqueous media. In order to confirm the effect on apparent solubility of the different API physical states differing in particle size or crystallinity, solvent casting and twin screw extruder mixing were compared with batch mixing. Solvent casting is a common method used in the pharmaceutical industry to provide good mixing since the API can be stirred in the low viscosity solution instead of a highly viscous molten polymer. Twin screw extruder can also provide better mixing due to the generation of higher shear stresses than in the batch mixer. The results for the twin screw extruder showed that DIK-Na^+ can be dispersed as a finer particle in the polymer matrix. As a result, the dissolution rate was slightly faster than the one from the batch mixer. At low DIK-Na^+ loading in the polymer matrix

prepared by solvent casting there were signs of DIK-Na^+/polymer miscibility attributed to the presence of residual solvent. The amorphous API in the polymer matrix showed improved apparent solubility as compared to its crystalline state. This confirmed that the state of API in the polymer matrix is the most important factor to increase its apparent aqueous solubility.

The third segment of this research focused on the API release from the ternary system (API/clay/polymer) produced by hot melt mixing (mostly batch mixing). In general, systems produced by hot melt mixing are binary systems that contain only APIs and polymers. In this work, a novel approach in order to have a sustained API release by utilizing the nanoclays was attempted. Since the API present in the clay interspacing may experience one more step in its release by diffusion as compared to the binary system, it was anticipated that the API from the ternary system would have a slower and more controlled release than the one from the binary system. At the pH of the simulated gastric fluid, the clay was dissolved in the acidic condition so that the sustained release was not observed while sustained released was shown in the simulated body fluid since the clay was not dissolved in the neutral pH and could function as a barrier controlling diffusion. Controlled API release from such a ternary system produced by hot melt mixing, to the best of our knowledge, has not been reported in the literature.

The mechanisms of APIs release in solution from the nanoclay and the polymer matrix were identified by using the Korsmeyer-Peppas (Power law) and Peppas-Sahlin models. The API dissolution from the nanoclay in different pH media showed diffusion predominant mechanism while from the polymer matrix at acidic conditions showed erosion predominant mechanism. Therefore, the API dissolution from the nanoclay and

from the polymer matrix showed good fitting with the Fickian diffusion and Hopfenberg surface-erosion models, respectively. By considering their characteristic dissolution mechanisms, it can be readily anticipated that the ternary system containing API/Clay/Polymer involves the diffusion and erosion combined mechanisms and may require more advanced and complex modeling in order to describe its release mechanism.

7.2 Future Studies

1. Study Possible Adverse Interactions (Degradation during Clay Intercalation) between API and Calcined Clay.

During the process of the clay modification, it was recognized that the pH of the solution (MeOH and H_2O) may affect the crystalline structure of the modified nanoclay. API modified nanoclays prepared in different pH solutions showed different XRD spectra. Particularly, the harmonic peaks identified as Miller indices of (*006*) and (*009*) were either shifted or removed. Therefore, it would be worthwhile to analyze the effects on the crystallinity of API modified nanoclays at different solution pH values. Since IND showed degradation or some structural modification while it reacted with the calcined hydrotalcite, it is possible that the highly alkaline solution may have caused these changes. Therefore, it would be worthwhile to identify the type of interaction that occurs during the reaction.

2. API/Clay Particles were not Dispersed in their Nanosize Dimensions.

This may be due to inappropriate screw configurations, poor compatibility between API modified clay and polymer, and poorly expanded interlayer due to the low MW API. Selection of proper screw configuration for TSE or applying gas such as super critical carbon dioxide during melt mixing may be helpful in order to achieve nanodispersion and break up agglomerates. Additional additives in the formulation, or APIs with higher MW and different structures could affect compatibility, wetting and dispersion.

3. Improve Controlled Release Characteristics by Combining Binary and Ternary Systems

It was clearly observed that the ternary system containing API modified nanoclay releases the API more slowly than the API-polymer binary system. This slower release from the ternary system is mainly due to the presence of the nanoclay which interferes with the API diffusion. Since release rates of binary and ternary systems are different, novel applications can be realized by using mixtures of the two systems. In the case of the same API in both systems, continuous API release can be achieved over a long time period. In the case of two different API systems, multifunctional API release can be achieved for example, API “A” from the binary system can be released at a designated time (earlier stage) and API “B” from the ternary system can be released at a later stage.

APPENDIX A

DIK/CLAY TGA ISOTHERMAL TEST

API modified clay may be exposed at a high temperature, higher than the mixing temperature (130 ^{o}C) which was used in this study, particularly in the case of a different polymer. In order to observe a possible thermal degradation, isothermal TGA tests of API modified clay were carried out at higher temperature. Figure A.1 shows isothermal TGA results of DIK/Clay at 180 ^{o}C and 200 ^{o}C for 10 minutes. The mixture does not show significant weight loss at both conditions, indicating good thermal stability (the initial weight loss is due to the presence of the moisture).

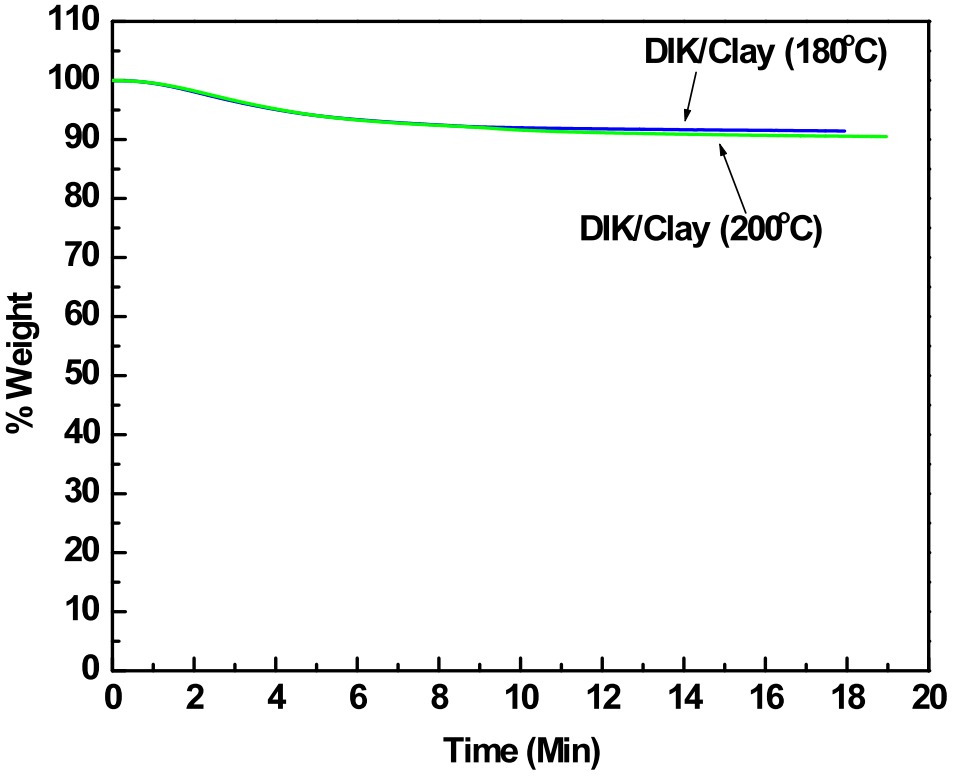

Figure A.1 Isothermal TGA results of DIK/clay at 180 ^{o}C and 200 ^{o}C in air.

APPENDIX B

CALCULATION FOR API CONTENT IN NANOCLAY

According to elemental analysis, DIK/Clay contains 22.68 wt% and 1.95 wt% of carbon and nitrogen respectively. Based on this information, the content of DIK in the clay can be calculated by the procedure below (Table B.1). IND content of IND/Clay is calculated as in Table B.2

Table B.1 Calculation of DIK Content

Element	Experimental element content, %	Calculated wt % of element based on API MW 296.1	Calculated API wt fraction (x) and Clay wt fraction (y)
Carbon	22.68 wt%	56.72 wt%	$\frac{0.5672x}{x+y} = 0.2268$, $x+y=1$, $x=0.399$
Nitrogen	1.95 wt%	4.72 wt%	$\frac{0.0472x}{x+y} = 0.0195$, $x+y=1$, $x=0.413$

Table B.2 Calculation of IND content

Element	Experimental element content, %	Calculated wt % of element based on API MW 357.7	Calculated API wt % (x) and Clay wt% (y)
Carbon	21.41 wt%	63.7 wt%	$\frac{0.637x}{x+y} = 0.2141$, $x + y = 1$, $x = 0.336$
Nitrogen	1.20 wt%	3.91 wt%	$\frac{0.0391x}{x+y} = 0.012$, $x + y = 1$, $x = 0.308$

APPENDIX C

DISSOLUTION OF HT IN SIMULATED GASTRIC FLUID

Hydrotalcite (HT) (0.5 g/*l*) was first dispersed and fully dissolved in SGF solution (pH 1.2) within 30 minutes as shown in Figure C.1

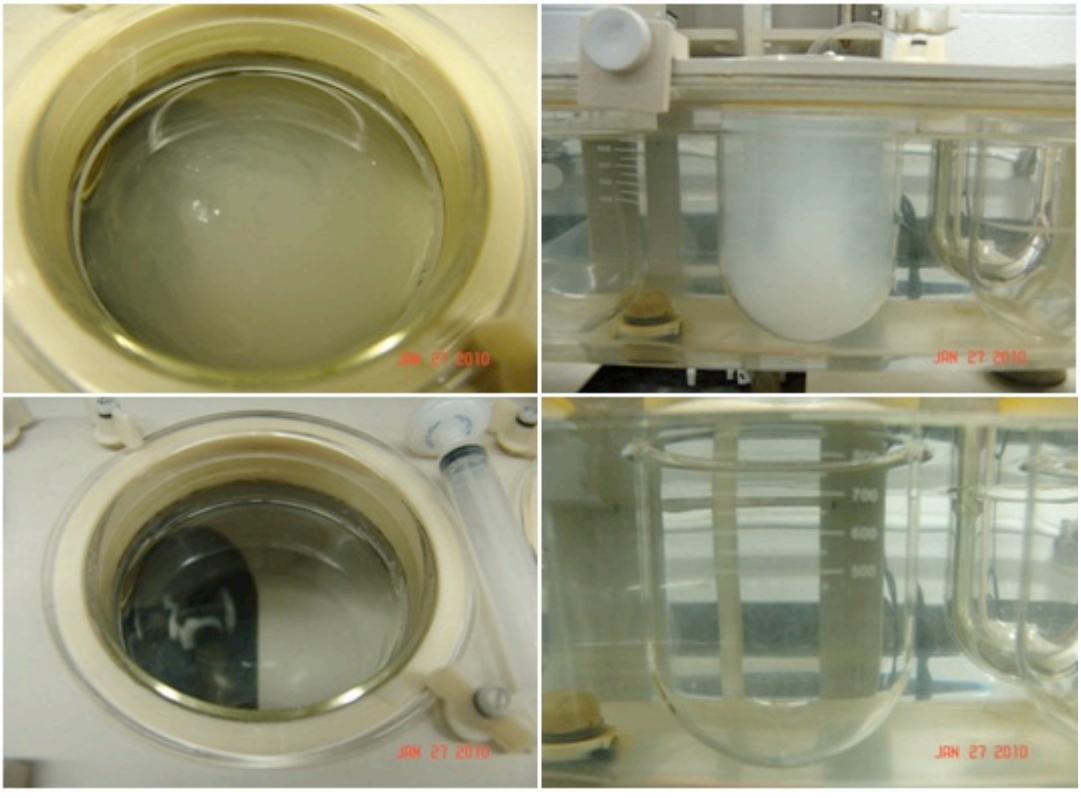

Figure C.1 HT dissolution in SGF (pH 1.2). (top) HT after being added into SGF (0 minute) and (bottom) HT after 30 minutes in the SGF.

APPENDIX D

ADDITIONAL INFORMATION FOR CALCULATING VISCOSITY RATIO OF DIK/CLAY COMPOSITES

In this section, additional information obtained from Nielson[100] for calculating viscosity ratios shown in Equations (5.3, 5.4, and 5.5) are listed.

k_E : 2.5 (dispersed spheres) in Equation 5.3
ϕ_{max} : 0.637 spheres (random closed packing) in Equation 5.4

In Equation 5.5
$$\psi \doteq 1+\left(\frac{1-\phi_{max}}{\phi_{max}^2}\right)V_f \qquad \text{(Equation D.1)}$$

In Equation 5.5 $A=k_E - 1=1.5$ (Equation D.2)

In Equation 5.5
$$B = \frac{\eta_c/\eta_m - 1}{\eta_c/\eta_m + A} \doteq 1 \text{ for rigid filler} \qquad \text{(Equation D.3)}$$

V_f: Volume fraction

Table D.1 Results of Viscosity Ratio

			Viscosity ratio, η_c/η_m			
API loading	Viscosity (Pa·s)	API V_f	Experimental	Mooney Eq. 5.3	D&K Eq. 5.4	Nielsen Eq. 5.5
0 wt%	17420	0	1.00	1.00	1.00	1.00
4 wt%	23190	0.03	1.33	1.10	1.09	1.09
15 wt%	29230	0.11	1.67	1.41	1.36	1.33
25 wt%	35670	0.19	2.04	2.01	1.78	1.67
40 wt%	52550	0.33	3.01	5.28	3.12	2.56

Densities of DIK-Na^+ and Eudragit® E100 are 1.5 g/cm^3 and 1.09 g/cm^3, respectively

APPENDIX E

THERMAL STABILITY OF EUDRAGIT® E100 /DIK-NA$^+$ COMPOSITES PREPARED BY VARIOUS METHODS

Figure E.1 shows the TGA results of Eudragit® E100/ 4wt% DIK-Na$^+$ prepared by different methods such as batch mixing, TSE, and solvent casting. At 500^{o}C the samples containing API show similar amount of residuals. This is an indication that all the samples contain the same amounts of API. Samples prepared by TSE and solvent casting show somewhat retarded onset degradation temperature. This may be due to the better dispersion of the API in the polymer matrix as compared to the one from batch mixer.

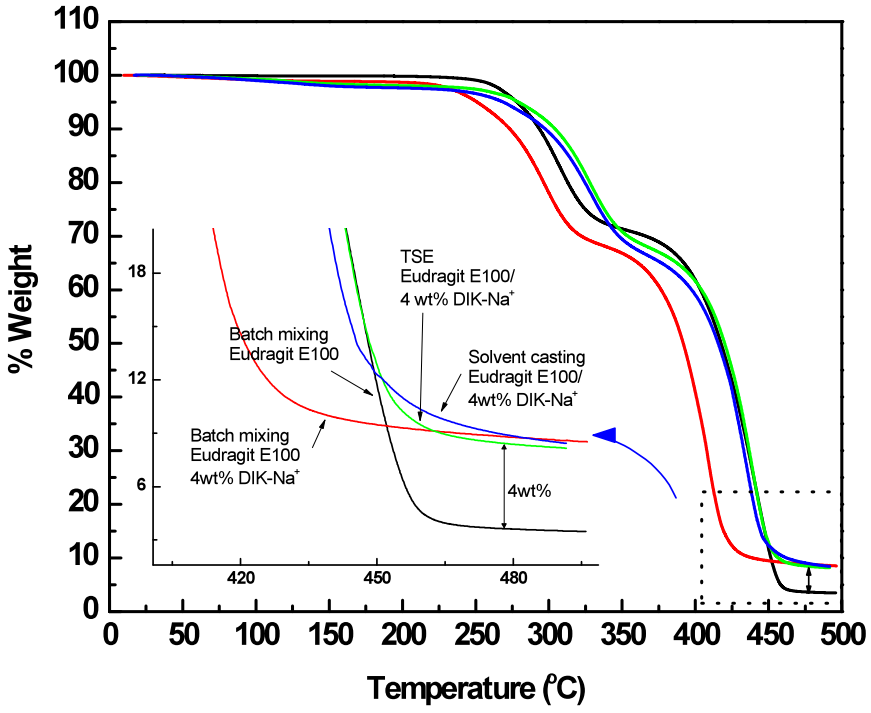

Figure E.1 TGA results of Eudragit® E100 and Eudragit® E100 containing 4 wt% DIK-Na$^+$ prepared by various methods (Batch mixing, TSE, and solvent mixing).

APPENDIX F

STABILITY TEST OF EUDRAGIT® S100 AT DIFFERENT pH

In order to confirm the stability of Eudagit® S100/ 20 wt% TEC- 4 wt% DIK-Na^+ at a low pH, the sample was immersed into the pH 1.2 SGF. The pH of the medium was increased by adding 0.5 N NaOH. Figure F.1 shows the amount of dissolved DIK from the blend to the medium. DIK-Na^+ was not detected at the pH lower than 7.4 due to the presence of Eudragit® S100 coating but it starts appearing when the pH of the medium reached 7.4.

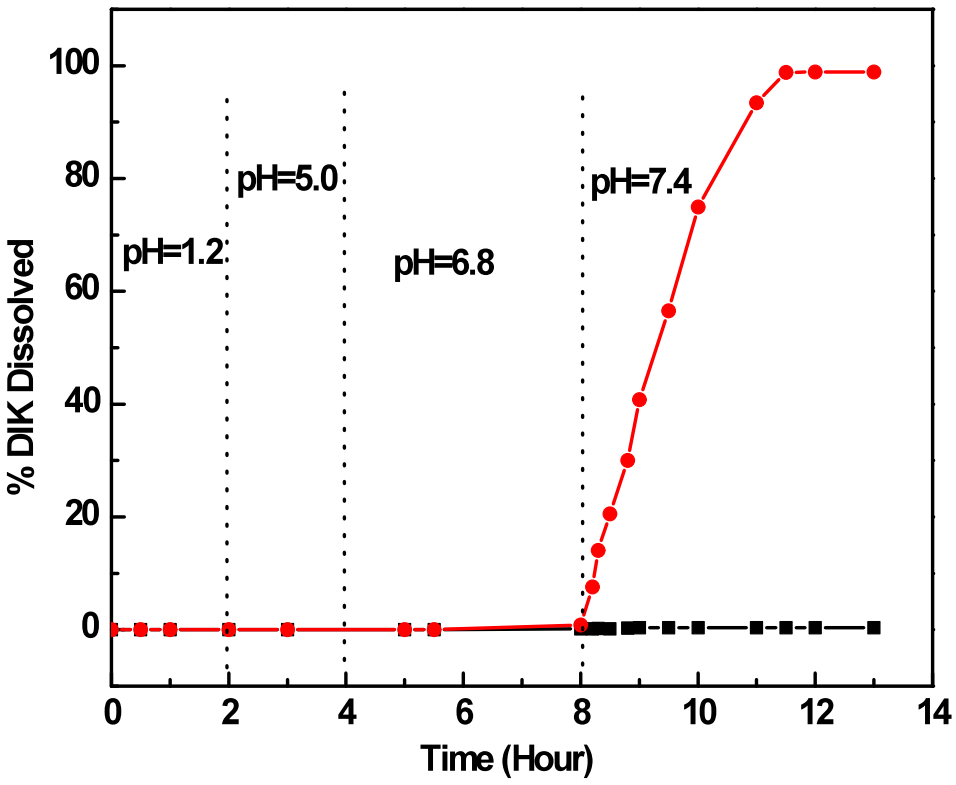

Figure F.1 Dissolution profile of DIK from Eudragit® S100/ 20 wt% TEC- 4wt% DIK-Na^+ at different pH.

APPENDIX G

DISSOLUTION TEST OF EUDRAGIT® E100-DIK/CLAY PREPARED BY DIFFERENT METHODS

Figure G.1 shows the dissolution profiles in SGF pH 1.2 of Eudragit® E100- DIK/Clay prepared by different methods. The dissolution results do not show much difference.

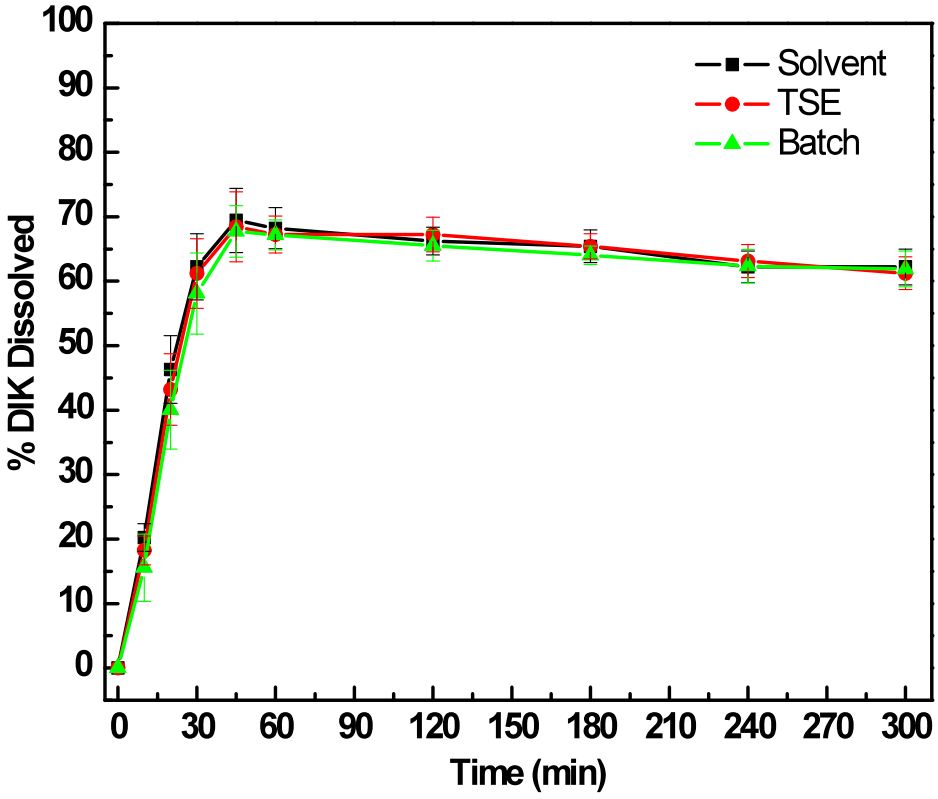

Figure G.1 Dissolution profile of DIK from Eudragit® E100- DIK/Clay prepared by TSE, batch mixing and solvent casting.

APPENDIX H

SEM IMAGES OF DIK/CLAY DISPERSION IN EUDRAGIT® E100 PREPARED BY VARIOUS METHODS

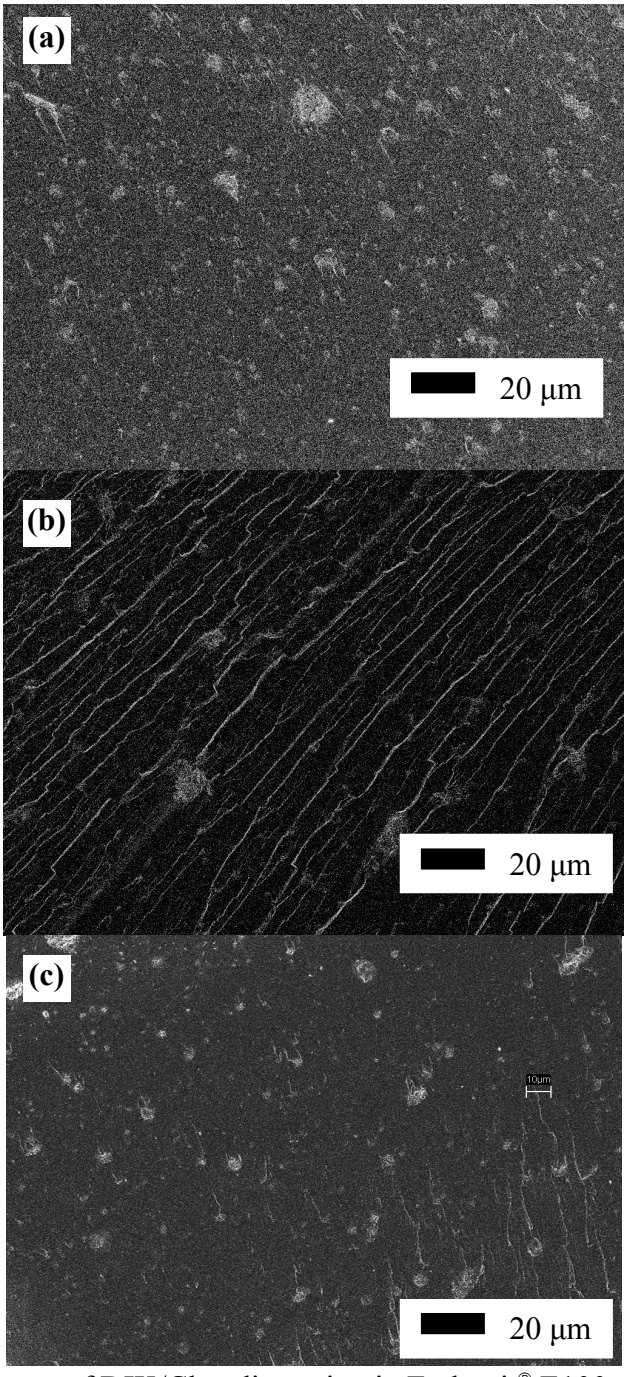

Figure H.1 SEM images of DIK/Clay dispersion in Eudragit® E100 matrix prepared by (a) TSE, (b) solvent casting, (c) batch mixing.

APPENDIX I

APIs CALIBRATION LINES IN pH 1.2 AND 7.4 BUFFER SOLUTIONS

In order to quantify the dissolved DIK-Na^+ and IND in the buffer solutions, the corresponding absorbance values were measured. Since DIK-Na^+ and IND have very low solubilities at the acidic conditions, two different methods were used in order to increase APIs solubility in the medium. The first method involves the addition of 5 g of surfactant (sodium dodecyl sulfate). The second method involves dissolution of APIs in 5 ml ethanol prior to the addition of the solution to the 1 L medium. UV absorbance of the API solutions prepared by both methods showed the same values and linear increases as shown in Figure H.1 and H.2.

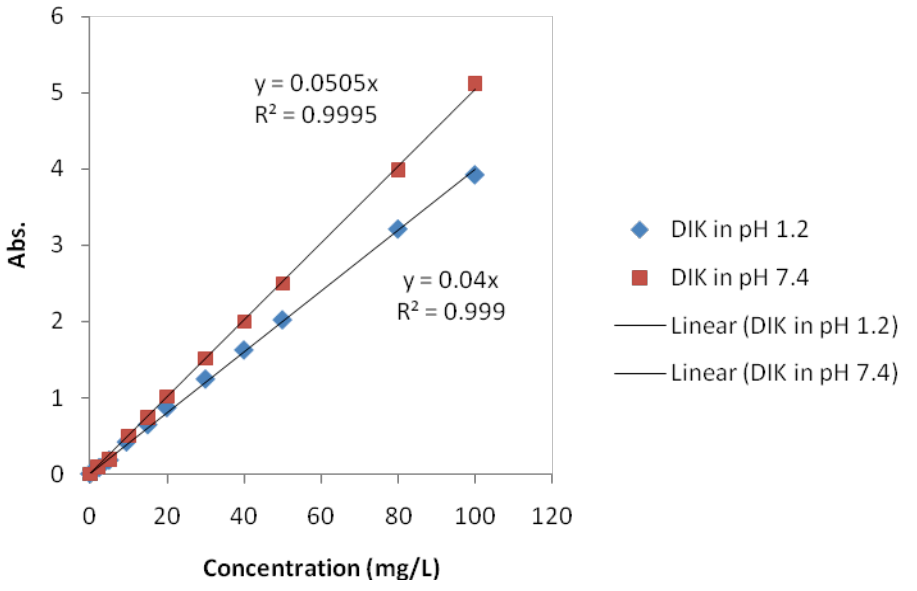

Figure I.1 DIK calibration line in pH 1.2 and 7.4 buffer solution.

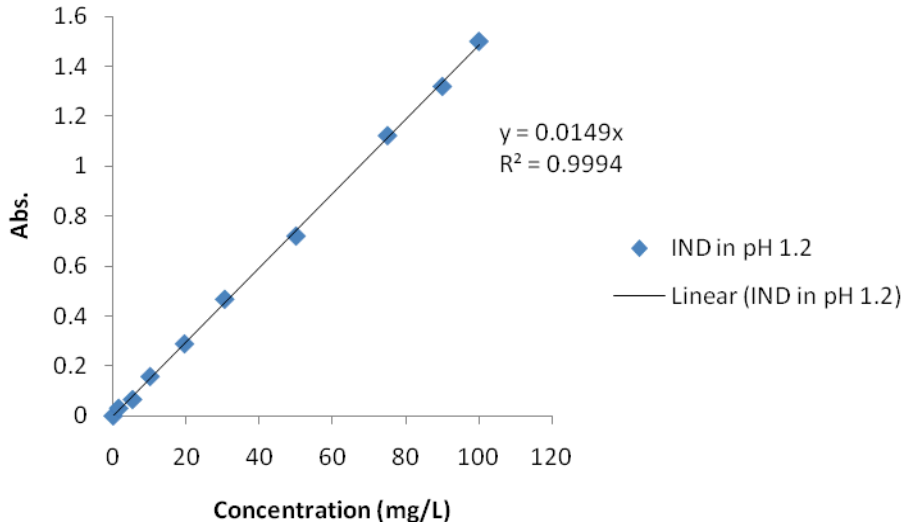

Figure I.2 IND calibration line in pH 1.2 buffer solution.

REFERENCES

1. Zhu, Y.; Shah, N. H.; Malick, A. W.; Infeld, M. H.; McGinity, J. W., Controlled release of a poorly water-soluble drug from hot-melt extrudates containing acrylic polymers. *Drug Development and Industrial Pharmacy* **2006**, 32, (5), 569-583.

2. Repka, M. A.; Gerding, T. G.; Repka, S. L.; McGinity, J. W., Influence of plasticizers and drugs on the physical mechanical properties of hydroxypropylcellulose films prepared by hot melt extrusion. *Drug Development and Industrial Pharmacy* **1999**, 25, (5), 625-633.

3. McGinity, J. W., Physical and chemical properties of Eudragit polymer influencing product performance in Eudragit matrix applications. In The 4th Advanced Workshop by Evonik Industries, Piscataway, NJ, 2008.

4. Villanova, J. C. O.; Orefice, R. L.; Cunha, A. S., Aplicacoes farmaceuticas de polimeros. *Polimeros* **2010**, 20, (1), 51-64 (written in Portuguese).

5. Kathuria, A., Matrix applications of polymethacrylate copolymer. In The 5th Advanced Workshop by Evonik Industries, Piscataway, NJ, 2009.

6. Kamena, K., Nanoclays and their emerging markets. *Functional fillers for plastics*. *2nd ed*.; Wiley-VCH Verlag GmbH & co. KGaA: Weinheim, Germany, 2010.

7. Schmidt, D.; Shah, D.; Giannelis, E. P., New Advances in polymer layered silicate nanocomposites. *Current Opinion in Solid State and Materials Science* **2002**, 6, (3), 205-212.

8. Aguzzi, C.; Cerezo, P.; Viseras, C.; Caramella, C., Use of clays as drug delivery systems: Possibilities and limitations. *Applied Clay Science* **2007**, 36, (1-3), 22-36.

9. Li, B.; He, J.; G. Evans, D.; Duan, X., Inorganic layered double hydroxides as a drug delivery system-intercalation and in vitro release of fenbufen. *Applied Clay Science* **2004**, 27, (3-4), 199-207.

10. Suzuki, N.; Nakamura, Y.; Watanabe, Y.; Yasushi, K., Intercalation compounds of layered materials for drug delivery use II. Diclofenac Sodium. *Chemical and Pharmaceutical Bulletin* **2001**, 49, (8), 964-968.

11. White, J. L.; Hem, S. L., Pharmaceutical aspects of clay-organic interactions. *Industrial and Engineering Chemistry Product Research and development* **1983**, 22, 665-671.

12. Dong, Y.; Feng, S.-S., Poly(d,l-lactide-co-glycolide)/montmorillonite nanoparticles for oral delivery of anticancer drugs. *Biomaterials* **2005**, 26, (30), 6068-6076.

13. Nhlapo, N.; Motumi, T.; Landman, E.; Verryn, S. M. C.; Focke, W. W., Surfactant assisted fatty acid intercalation of layered double hydroxides. *Journal of Materials Science* **2007**, 43, (3), 1033-1043.

14. Imaizumi, H., Stability and several physical properties of amorphous and crystalline forms of indomethacin. *Chemical and Pharmaceutical Bulletin* **1980**, 28, (9), 2565-2569.

15. Egawa, H.; Maeda, S.; Yonemochi, E.; Oguchi, T.; Yamamoto, K.; Nakai, Y., Solubility parameter and dissolution behaviour of cefalexin powders with different crystallinity. *Chemical and Pharmaceutical Bulletin* **1992**, 40, (3), 819-820.

16. Miyazaki, S.; Hori, R.; Arita, T., Physico-chemical and gastrointestinal absorption of some solid phases of tetracyline. *Yakugaku Zasshi* **1975**, 95, (6), 629-633.

17. Mullins, J. D.; Macek, T. J., Some pharmaceutical properties of novobiocin. *Journal of the American Pharmaceutical Association* **1960**, 49, (4), 245-248.

18. Hancock, B. C.; Parks, M., What is the true solubility advantage for amorphous pharmaceuticals? *Pharmaceutical Research* **2000**, 17, (4), 397-404.

19. Greenhalgh, D. J.; Williams, A. C.; Timmins, P.; York, P., Solubility parameters as predictors of miscibility in solid dispersions. *Journal of Pharmaceutical Sciences* **1999**, 88, (11), 1182-1190.

20. VanKrevelen, D. W., *Properties of polymers.* Elsevier Scientific Publishing Company: Amsterdam, Netherlands, 1976.

21. Chokshi, R. J.; Sandhu, H. K.; Iyer, R. M.; Shah, N. H.; Malick, A. W.; Zia, H., Characterization of physico-mechanical properties of indomethacin and polymers to assess their suitability for hot-melt extrusion processs as a means to manufacture solid dispersion/solution. *Journal of Pharmaceutical Sciences* **2005**, 94, (11), 2463-2474.

22. Brandrup, J.; Immergut, E. H., *Polymer Handbook. 3rd ed.*; Wiley: New York 1989.

23. Liu, H.; Wang, P.; Zhang, X.; Shen, F.; Gogos, C. G., Effects of extrusion process parameters on the dissolution behavior of indomethacin in Eudragit® E PO solid dispersions. *International Journal of Pharmaceutics* **2009**, 383, (1-2), 161-169.

24. Liu, H. Hot melt mixing/extrusion and dissolution of drug (indomethacin) in acrylic copolymer matrices. *Ph.D. Dissertation*, New Jersey Institute of Technology, Newark, NJ, 2010.

25. Forster, A.; Hempenstall, J.; Rades, T., Characterization of glass solutions of poorly water soluble drugs produced by melt extrusion with hydrophilic amorphous polymers. *Journal of Pharmacy and Pharmacology* **2001**, 53, (3), 303-315.

26. Nollenberger, K.; Gryczke, A.; Meier, C.; Dressman, J.; Schmidt, M. U.; Brühne, S., Pair distribution function X-ray analysis explains dissolution characteristics of felodipine melt extrusion products. *Journal of Pharmaceutical Sciences* **2009**, 98, (4), 1476-1486.

27. Schilling, S. U.; Shah, N. H.; Waseem Malick, A.; McGinity, J. W., Properties of melt extruded enteric matrix pellets. *European Journal of Pharmaceutics and Biopharmaceutics* **2010**, 74, (2), 352-361.

28. Bruce, L. D.; Shah, N. H.; Waseem Malick, A.; Infeld, M. H.; McGinity, J. W., Properties of hot-melt extruded tablet formulations for the colonic delivery of 5-aminosalicylic acid. *European Journal of Pharmaceutics and Biopharmaceutics* **2005**, 59, (1), 85-97.

29. Six, K.; Verreck, G.; Peeters, J.; Brewster, M.; Mooter, G. V. d., Increased physical stability and improved dissolution properties of itraconazole, a class II drug, by solid dispersions that combine fast- and slow-dissolving polymers. *Journal of Pharmaceutical Sciences* **2004**, 93, (1), 124-131.

30. Forster, A.; Hempenstall, J.; Tucker, I.; Rades, T., The potential of small-scale fusion experiments and the Gordon-Taylor equation to predict the suitability of drug/polymer blends for melt extrusion. *Drug Development and Industrial Pharmacy* **2001**, 27, (6), 549-560.

31. Qi, S.; Gryczke, A.; Belton, P.; Craig, D. Q. M., Characterisation of solid dispersions of paracetamol and EUDRAGIT® E prepared by hot-melt extrusion using thermal, microthermal and spectroscopic analysis. *International Journal of Pharmaceutics* **2008**, 354, (1-2), 158-167.

32. Guarino, A.; Bisceglia, M.; Castellucci, G.; Iacono, G.; Casali, L. G.; Bruzzese, E.; Musetta, A.; Greco, L., Smectite in the Treatment of Acute Diarrhea: A Nationwide Randomized Controlled Study of the Italian Society of Pediatric Gastroenterology and Hepatology (SIGEP) in Collaboration With Primary Care Pediatricians. *Journal of Pediatric Gastroenterology and Nutrition* **2001**, 32, (1), 71-75.

33. Linares, C. F.; Brikgi, M., Interaction between antimicrobial drugs and antacid based on cancrinite-type zeolite. *Microporous and Mesoporous Materials* **2006**, 96, (1-3), 141-148.

34. Vatier, J.; Harman, A.; Castela, N.; Droy-Lefaix, M. T.; Farinotti, R., Interactions of cimetidine and ranitidine with aluminum-containing antacids and a clay-containing gastric-protective drug in an artificial stomach-duodenum model. *Journal of Pharmaceutical Sciences* **1994**, 83, (7), 962-966.

35. Grim, R. E., *Clay mineralogy*. McGraw-Hill Book Co. Inc.: New York, NY, 1968.

36. Reijchle, W. T., Synthesis of anionic clay minerals. *Solid State Ionics* **1986**, 22, (1), 135-141.

37. Choy, J.; Park, M., *Cationic and anionic clays for biological applications*. Elsevier: Oxford, U.K., 2004.

38. Drits, V. A.; Sokolova, T. N.; Sokolova, G. V.; Cherkashin, V. I., New members of the hydrotalcite-manasseite group. *Clays and Clay Minerals* **1987**, 35, (6), 401-417.

39. Ambrogi, V.; Fardella, G.; Grandolini, G.; Perioli, L.; Tiralti, M. C., Intercalation compounds of hydrotalcite-like anionic clays with anti-inflammatory agents, II: Uptake of diclofenac for a controlled release formulation. *AAPS PharmSciTech* **2002**, 3, (3), 1-6.

40. Costantino, U.; Ambrogi, V.; Nocchetti, M.; Perioli, L., Hydrotalcite-like compounds: Versatile layered hosts of molecular anions with biological activity. *Microporous and Mesoporous Materials* **2008**, 107, (1-2), 149-160.

41. Park, J. K.; Choy, Y. B.; Oh, J.-M.; Kim, J. Y.; Hwang, S.-J.; Choy, J.-H., Controlled release of donepezil intercalated in smectite clays. *International Journal of Pharmaceutics* **2008**, 359, (1-2), 198-204.

42. McGinity, J. W.; Lach, J. L., Sustained release applications of montmorillonite interaction with amphetamine sulfate. *Journal of Pharmaceutical Sciences* **1977**, 66, (1), 63-66.

43. McGinity, J. W.; Harris, M. R., Increasing dissolution rates of poorly soluble drugs by adsorption to montmorillonite. *Drug Development and Industrial Pharmacy* **1980**, 6, (1), 35-48.

44. Choy, J.-H.; Kwak, S.-Y.; Park, J.-S.; Jeong, Y.-J.; Portier, J., Intercalative nanohybrids of nucleoside monophosphates and DNA in layered metal hydroxide. *Journal of the American Chemical Society* **1999**, 121, (6), 1399-1400.

45. Del Arco, M.; Fernandez, A.; Martin, C.; Sayalero, M. L.; Rives, V., Solubility and release of fenamates intercalated in layered double hydroxides. *Clay Minerals* **2008**, 43, (2), 255-265.

46. Del Arco, M.; Cebadera, E.; Gutierrez, S.; Martin, C.; Montero, M. J.; Rives, V.; Rocha, J.; Sevilla, M. A., Mg, Al layered double hydroxides with intercalated indomethacin: Synthesis, characterization, and pharmacological study. *Journal of Pharmaceutical Science* **2004**, 93, (6), 1649-1658.

47. Carriazo, D.; del Arco, M.; Martín, C.; Ramos, C.; Rives, V., Influence of the inorganic matrix nature on the sustained release of naproxen. *Microporous and Mesoporous Materials* **2010**, 130, (1-3), 229-238.

48. Monkhouse, D. C.; Lach, J. L., Use of adsorbents in enhancement of drug dissoluton I. *Journal of Pharmaceutical Science* **1968**, 61, (9), 1430-1435.

49. Das, S. K.; Kapoor, S.; Yamada, H.; Bhattacharyya, A. J., Effects of surface acidity and pore size of mesoporous alumina on degree of loading and controlled release of ibuprofen. *Microporous and Mesoporous Materials* **2009**, 118, (1-3), 267-272.

50. Li, B.; He, J.; Evans, D. G.; Duan, X., Enteric-coated layered double hydroxides as a controlled release drug delivery system. *International Journal of Pharmaceutics* **2004**, 287, (1-2), 89-95.

51. Bugatti, V.; Costantino, U.; Gorrasi, G.; Nocchetti, M.; Tammaro, L.; Vittoria, V., Nano-hybrids incorporation into poly([epsilon]-caprolactone) for multifunctional applications: Mechanical and barrier properties. *European Polymer Journal* **2010**, 46, (3), 418-427.

52. Bhaskar, R.; Murthy, R. S. R.; Miglani, B. D.; VIswanathan, K., Novel method to evaluate diffusion controlled release of drug from resinate. *International Journal of Pharmaceutics* **1986**, 28, (1), 59-66.

53. Cypes, S. H.; Saltzman, W. M.; Giannelis, E. P., Organosilicate-polymer drug delivery systems: controlled release and enhanced mechanical properties. *Journal of Controlled Release* **2003**, 90, (2), 163-169.

54. Korsmeyer, R. W.; Gurny, R.; Buri, E. M.; Peppas, N. A., Mechanism of solute release from porous hydrophilic polymer. *International Journal of Pharmaceutics* **1983**, 15, (1), 25-35.

55. Campbell, K.; Craig, D. Q. M.; McNally, T., Poly(ethylene glycol) layered silicate nanocomposites for retarded drug release prepared by hot-melt extrusion. *International Journal of Pharmaceutics* **2008**, 363, (1-2), 126-131.

56. Forni, F.; Iannuccelli, V.; Coppi, G.; Bernabei, M. T., Effect of Montmorillonite on Drug Release from Polymeric Matrices. *Archiv der Pharmazie* **1989**, 322, (11), 789-793.

57. Lee, W.-F.; Chen, Y.-C., Effect of bentonite on the physical properties and drug-release behavior of poly(AA-co-PEGMEA)/bentonite nanocomposite hydrogels for mucoadhesive. *Journal of Applied Polymer Science* **2004**, 91, (5), 2934-2941.

58. Sallmann, A. R., The history of diclofenac. *The American Journal of Medicine* **1986**, 80, (4, Supplement 2), 29-33.

59. Kincl, M.; Meleh, M.; Veber, M.; Vrecer, F., Study of physicochemical parameters affecting the release of Diclofenac sodium from lipophilic matrix tablets. *Acta Chimica Slovenica* **2004**, 51, 409-425.

60. Ivic, B.; Ibric, S.; Betz, G.; Djuric, Z., Evaluation of diclofenac sodium release from matrix pellets compressed into MUPS tablets. *Yakugaku Zasshi* **2009**, 129, (11), 1375-1384.

61. Accelrys Inc. Materials Studio, 4.4; San Diego, Ca, 2009.

62. Reijers, H. T. J.; Valster-Schiermeier, S. E. A.; Cobden, P. D.; van den Brink, R. W., Hydrotalcite as CO2 Sorbent for Sorption-Enhanced Steam Reforming of Methane. *Industrial & Engineering Chemistry Research* **2005**, 45, (8), 2522-2530.

63. Six, K.; Leuner, C.; Dressman, J.; Verreck, G.; Peeters, J.; Blaton, N.; Augustijns, P.; Kinget, R.; Mooter, G. V. d., Thermal properties of hot-stage extrudates of itraconazole and Eudragit E100. *Journal of Thermal Analysis and Calorimetry* **2002**, 68, (2), 591-601.

64. Nollenberger, K., Hot melt extrusion with Eudragit Polymers. In Eudragit Matrix Applications The 4th Advanced Workshop, Piscataway, NJ, 2008.

65. Budavari, S.; O'Neil, M. J.; Smith, A.; Heckelman, P. E.; Kinneary, J. F., *The Merck Index*. 12th ed.; Merck & Co., Inc: Whitehouse Station, NJ, 1996.

66. Dodds, W. S.; Stutzman, L. F.; Sollami, B. J., Carbon Dioxide Solubility in Water. *Industrial & Engineering Chemistry Chemical & Engineering Data Series* **1956**, 1, (1), 92-95.

67. Manahan, S. E., *Environmental Chemistry. 8th ed.*; CRC Press LLC: Boca Raton, FL, 2004.

68. Iyi, N.; Matsumoto, T.; Kaneko, Y.; Kitamura, K., Deintercalation of carbonate ions from a hydrotalcite-like compound: Enhanced decarbonation using acidic salt mixed solution. *Chemistry of Materials* **2004**, 16, (15), 2926-2932.

69. Tichit, D.; Coq, B., Catalysis by hydrotalcites and related materials. *CAT TECH* **2003**, 7, (6), 206-217.

70. Colthup, N. B.; Daly, L. H.; Wiberley, S. E., *Introduction to Infrared and Raman Spectroscopy*. 2nd ed.; Academic Press Inc.: New York, NY, 1975.

71. Cullity, B. D.; Stock, S. R., *Elements of X-ray diffraction. 3rd ed.*; Prentice Hall: Upper Saddle River, NJ, 2001.

72. Kuk, W.-K.; Huh, Y.-D., Preferential intercalation of isomers of anthraquinone sulfonate ions into layered double hydroxides. *Journal of Materials Chemistry* **1997**, 7, (9), 1933-1936.

73. Crepaldi, E. L.; Tronto, J.; Cardoso, L. P.; Valim, J. B., Sorption of terephthalate anions by calcined and uncalcined hydrotalcite-like compounds. Colloids and Surfaces A: *Physicochemical and Engineering Aspects* **2002**, 211, (2-3), 103-114.

74. Gago, S.; Dias, A. S.; Monteiro, B.; Pillinger, M.; Valente, A. A.; Santos, T. M.; Gonçalves, I. S., Synthesis and characterization of layered double hydroxides intercalated by an oxomolybdenum complex. *Journal of Physics and Chemistry of Solids* **2006**, 67, (5-6), 1011-1015.

75. Li, C.; Wang, G.; Evans, D. G.; Duan, X., Incorporation of rare-earth ions in Mg-Al layered double hydroxides: intercalation with an [Eu(EDTA)]- chelate. *Journal of Solid State Chemistry* **2004**, 177, (12), 4569-4575.

76. Costa, F. R.; Leuteritz, A.; Wagenknecht, U.; Jehnichen, D.; Häußler, L.; Heinrich, G., Intercalation of Mg-Al layered double hydroxide by anionic surfactants: Preparation and characterization. *Applied Clay Science* **2008**, 38, (3-4), 153-164.

77. Gago, S.; Pillinger, M.; Valente, A. A.; Santos, T. M.; Rocha, J.; Goncalves, I. S., Immobilization of Oxomolybdenum Species in a Layered Double Hydroxide Pillared by 2,2'-Bipyridine-5,5'-dicarboxylate Anions. *Inorganic Chemistry* **2004**, 43, (17), 5422-5431.

78. Meyn, M.; Beneke, K.; Lagaly, G., Anion-exchange reactions of layered double hydroxides. *Inorganic Chemistry* **1990**, 29, (26), 5201-5207.

79. Tammaro, L.; Costantino, U.; Bolognese, A.; Sammartino, G.; Marenzi, G.; Calignano, A.; Tetè, S.; Mastrangelo, F.; Califano, L.; Vittoria, V., Nanohybrids for controlled antibiotic release in topical applications. *International Journal of Antimicrobial Agents* **2007**, 29, (4), 417-423.

80. Xanthos, M., *Functional fillers for plastics 2nd ed*.; Wiley-VCH Verlag GmbH& Co KGaA: Weinheim, Germany, 2010.

81. Noyes, A. A.; Whitney, W. R., The rate of solution of solid substances in their own solutions. *Journal of the American Chemical Society* **1897**, 19, (12), 930-934.

82. Wurster, D. E.; Taylor, P. W., Dissolution rates. *Journal of Pharmaceutical Sciences* **1965**, 54, (2), 169-175.

83. Yang, M.; Wang, P.; Huang, C.-Y.; Ku, M. S.; Liu, H.; Gogos, C., Solid dispersion of acetaminophen and poly(ethylene oxide) prepared by hot-melt mixing. *International Journal of Pharmaceutics* **2010**, doi: 10.1016/j.ijpharm.2010.04.033.

84. Langer, R.; Peppas, N., Chemical and physical structure of polymers as carriers for controlled release of bioactive agents: A review. *Polymer Reviews* **1983**, 23, (1), 61-126.

85. Siepmann, J.; Peppas, N. A., Modeling of drug release from delivery systems based on hydroxypropyl methylcellulose (HPMC). *Advanced Drug Delivery Reviews* **2001**, 48, (2-3), 139-157.

86. Peppas, N. A.; Sahlin, J. J., A simple equation for the description of solute release. III. Coupling of diffusion and relaxation. *International Journal of Pharmaceutics* **1989**, 57, (2), 169-172.

87. Costa, P.; Sousa Lobo, J. M., Modeling and comparison of dissolution profiles. *European Journal of Pharmaceutical Sciences* **2001**, 13, (2), 123-133.

88. Bettini, R.; Colombo, P.; Massimo, G.; Catellani, P. L.; Vitali, T., Swelling and drug release in hydrogel matrices: polymer viscosity and matrix porosity effects. *European Journal of Pharmaceutical Science* **1994**, 2, (3), 213-219.

89. Hassan, M. M.; Durning, C. J., Effects of polymer molecular weight and temperature on case II transport. *Journal of Polymer Science Part B: Polymer Physics* **1999**, 37, (22), 3159-3171.

90. Rathbone, M. J.; Hadgraft, J.; Roberts, M. S., *Modified Release Drug Delivery Technology*. Marcel Dekker, Inc: New York, NY, 2003.

91. Delafuente, J. C., Understanding and preventing drug interactions in elderly patients. *Critical Reviews in Oncology/Hematology* **2003**, 48, (2), 133-143.

92. Calabrese, E. J., Toxicological consequences of multiple chemical interactions: a primer. *Toxicology* **1995**, 105, (2-3), 121-135.

93. Wiberley, S. E.; Bunce, S. C.; Bauer, W. H., Carbon-Hydrogen Stretching Frequencies. *Analytical Chemistry* **1960**, 32, (2), 217-221.

94. Ambrogi, V.; Fardella, G.; Grandolini, G.; Nocchetti, M.; Perioli, L., Effect of hydrotalcite-like compounds on the aqueous solubility of some poorly water-soluble drugs. *Journal of Pharmaceutical Sciences* **2003**, 92, (7), 1407-1418.

95. Rowe, J. S.; Carless, J. E., The influence of the microcapsule wall on the assay of indomethacin microcapsules in the presence of antacids--implications for product stability. *International Journal of Pharmaceutics* **1983**, 13, (3), 313-320.

96. Gogos, C. G.; Wang, P., Hot melt extrusion as a drug manufacturing technology. In Eudragit 3-Day Workshop, Hot melt extrusion & modified release applications, Piscataway, NJ, 2009.

97. Chang, T. C.; Wang, Y. T.; Hong, Y. S.; Chen, H. B.; Yang, J. C., Organic-inorganic hybrid materials 7: characterization and degradation of polyvinylimidazole-silica hybrids. *Polymer Degradation and Stability* **2000**, 69, (3), 317-322.

98. Marras, S. I.; Tsimpliaraki, A.; Zuburtikudis, I.; Panayiotou, C., Morphological, thermal, and mechanical characteristics of polymer/layered silicate nanocomposites: The role of filler modification level. *Polymer Engineering & Science* **2009**, 49, (6), 1206-1217.

99. Nielsen, L. E., *Mechanical properties of polymers and composites*. Marcel Dekker, Inc: New York, 1974; Vol. 2.

100. Nielsen, L. E., *Polymer Rheology*. Marcel Dekker, Inc: New York, NY, 1977

101. Tadmor, Z.; Gogos, C. G., *Principles of polymer processing 2nd ed.*; Wiley Interscience: Hoboken, NJ, 2006.

102. Todd, D. B., *Plastics compounding - Equipment and processing*. Hanser/Gardner Publications, Inc.: Cincinnati, OH, 1998.

103. Craig, D. Q. M., The mechanisms of drug release from solid dispersions in water-soluble polymers. *International Journal of Pharmaceutics* **2002**, 231, (2), 131-144.

104. Yamamoto, H., 1-Acyl-indoles. II. A New Syntheses of 1-(pchlorobenzoyl)-5-methoxy-3-indolylacetic acid and its polymorphism. *Chemical and Pharmaceutical Bulletin* **1968**, 16, (1), 17-19.

105. Taylor, L. S.; Zografi, G., Spectroscopic characterization of interactions between PVP and indomethacin in amorphous molecular dispersions. *Pharmaceutical Research* **1997**, 14, (12), 1691-1698.

106. Lin, S. Y.; Perng, R. I., Solid state interaction studies of drugs/polymers I. Indomethacin/ Eudragit E, RL or S resins. *STP Pharma Sciences* **1993**, 3, 465-471.

107. Tong, P.; Zografi, G., A study of amorphous molecular dispersions of indomethacin and its sodium salt. *Journal of Pharmaceutical Sciences* **2001**, 90, (12), 1991-2004.

108. Aitken-Nichol, C.; Zhang, F.; McGinity, J. W., Hot melt extrusion of acrylic films. *Pharmaceutical Research* **1996**, 13, (5), 804-808.

109. Crowley, M. M.; Zhang, F.; Koleng, J. J.; McGinity, J. W., Stability of polyethylene oxide in matrix tablets prepared by hot-melt extrusion. *Biomaterials* **2002**, 23, (21), 4241-4248.

110. Crowley, M. M.; Fredersdorf, A.; Schroeder, B.; Ucera, S.; Prodduturi, S.; Repka, M. A., The influence of guaifenesin and ketoprofen on the properties of hot-melt extruded polyehylene oxide films. *European Journal of Pharmaceutical Science* **2004**, 22, (5), 409-418.

111. Simha, R.; F., B. R., General relation involving the glass transition temperature and coefficient of expansion of polymers. *Journal of Chemical Physics* **1962**, 37, (5), 1003-1007.

112. Ha, J. U.; Xanthos, M., Functionalization of nanoclays with ionic liquids for polypropylene composites. *Polymer Composites* **2009**, 30, (5), 534-542.

113. Kawasumi, M.; Hasegawa, N.; Kato, M.; Usuki, A.; Okada, A., Preparation and Mechanical Properties of Polypropylene−Clay Hybrids. *Macromolecules* **1997**, 30, (20), 6333-6338.

114. Uhl, F. M.; Davuluri, S. P.; Wong, S.-C.; Webster, D. C., Organically modified montmirillonites in UV curable urethane acrylate films. *Polymer* **2004**, 45, (18), 6175-6187.

115. Ha, J. U.; Xanthos, M., Novel modifiers for layered double hydroxides and their effects on the properties of polylactic acid composites. *Applied Clay Science* **2010**, 47, (3-4), 303-310.

116. PolymathSoftware Polymath version 6.1, Willimantic, CT, 2010.